

KYAMBOGO UNIVERSITY
GRADUATE SCHOOL
DEPARTMENT OF MECHANICAL AND MANUFACTURING
ENGINEERING

MASTERS THESIS

**CHARACTERISATION OF RESISTANCE SPOT WELDING
ELECTRODES WITH ANNULAR RECESS DESIGN**

BY

APORA JAMES

**A Master's Thesis submitted to the Graduate School in Partial Fulfillment of the
Requirements for the Award of the Master of Science Degree in Advanced Manufacturing
Systems Engineering of Kyambogo University**

NOVEMBER 2018

KYAMBOGO



UNIVERSITY

**DEPARTMENT OF MECHANICAL AND MANUFACTURING
ENGINEERING**

**CHARACTERISATION OF RESISTANCE SPOT WELDING ELECTRODE
WITH ANNULAR RECESS DESIGN**

BY

APORA JAMES

(16/U/13977/GMEM/PE)

SUPERVISORS

DR. CATHERINE WANDERA

DR. TITUS B. WATMON

NOVEMBER 2018

ABSTRACT

This study investigated the characteristics of resistance welding electrode with annular recess design for supplying an electric current to metallic workpieces for welding two workpieces together. It comprises cylindrical body of an electrically conductive material (copper) having an annular recess tip for contacting workpiece. The tip is formed with a recess which gave the tip annular workpiece contacting surface. The recess was filled with an electrical and heat resistant material containing ceramic cement known as kaolin mixed with clay. The novel idea of the tool design is to enable formation of molten material pool which forms weld nuggets with even strength around the joints. The beginning facts about the recess design tool is that the annular recess minimizes current and voltage concentration in the middle of the tool tips, thereby; causing molten materials to flow both to the centre and onto the perimeter of the spot welded joint where the welding pressure is applied. Studies have shown that conventional spot welding tools produce joints which are stronger on the edges but weaker in the centre of the nuggets which presumably experience high voltage concentration. The data collection was done through RSW welding experiments where welding of sheet metal materials with same thickness was carried out; alloy steel materials cut from a salvage vehicle were used to make the sample strips measuring 50mm by 175mm each. The design and manufacture of annular recess was carried. The welded joints were subjected to different tests to characterize the weldability and integrity of the welded joints. The tests involved destructive testing and non-destructive tests of the joints. Magnetic Particle Inspection (MPI) was used to test the weld joint integrity beside the visual inspection. In this research study, effect(s) of electrode tip geometry on the tensile-shear strength in resistance spot welded joints of metal steel sheet (body panel) cut out from an old salvage vehicle of similar thickness (1mm) was studied. The outcome of this study showed remarkable improvement on the tensile-shear strength of RSW joint with a nugget diameter about 8.1mm by approximately 11.4KN using the annular recess electrodes compared to 5.7KN at nugget diameter of 7.8mm using the conventional electrode. The annular recess electrode provided an enhanced joint strength by approximately 2 times than the conventional electrode. Therefore application of this new technique creates a new tool that can enhance RSW joints strength in metal fabrications and also improvement on the crash worthiness of the vehicle.

Keywords: Current, Electrode, Nuggets, Resistance, Spot-welding,

DECLARATION

I humbly declare that this research thesis is my original work piece and that it has never been submitted to this University or elsewhere for academic purpose.

Signature:

APORA JAMES

(16/U/13977/GMEM/PE)

APPROVAL

This research thesis has been submitted to the Graduate School, Department of Mechanical and Production Engineering solely for academic purpose by **APORA JAMES (13/U/13977/GMEM/PE)**, a 2nd year student of MSc.AMS. Eng, under our supervision and we do acknowledge that this is his original work piece.

Principal Supervisor

Second Supervisor

Signature:

Signature.....

Dr Titus B. Watmon

Dr Catherine Wandera

Date.....

Date.....

DEDICATION

To my wife Mrs Achen A. Rose, sons Otim Filbert, Lengomoi James Apora and daughters Akello Angel, Kimara Bethany Lindah.

ACKNOWLEDGMENT

This research thesis was made with the protracted support of my family especially my wife Mrs Achen Rose, A., and in the wisdom of many contributors. At this juncture, the author would like to acknowledge the contribution and guidance of Management and staffs of the following institutions, namely Makerere University-Department of Mechanical Engineering – Materials laboratory especially Mr Okello for his technical guidance, Nakawa Vocational Institute especially the Principal Mr Muwanga G., Head of welding Section-Ms Mirembe E. and not forgetting the Technician Mr Abas for being helpful in carrying out the welding experiments, and Buhimba Technical College especially the deputy principal Mr Elaru and the head of welding section Mr Okeny who guided me on the usage of the magnetic particle inspections.

The Dean Faculty of Engineering Kyambogo University, Dr. Sakula for his parental and academic guidance during the onset of the research study, the head of department mechanical and production engineering Dr. Watmon Titus for protracted support and continued guidance, the graduate coordinator Dr. Wandera Catherine for professional guidance on the subject of research writing and publication, Mr Okumu L. in the materials laboratory, and all the staff of the Department of Mechanical and Production Engineering for being supportive but not forgetting all my course mates Mr. Batia, Mr Matende, Ms Atima, Mr Omara and Mr. Mafabi with whom we shared the same class for the two years.

Finally to my late father Mr. Alengo Nekomia (RIP) and late mother Mrs Akello Alice Alengo (RIP) for their guidance, support and all they have endured to make me what I am today. While you rest in peace, be assured I am following all you taught me.

Table of Contents

ABSTRACT	i
DECLARATION.....	ii
APPROVAL.....	iii
DEDICATION	iv
ACKNOWLEDGEMENT.....	v
LIST OF FIGURES.....	ix
LIST OF TABLES	xi
ABBREVIATIONS /ACRONYMS	xiii
CHAPTER ONE	1
1.0 INTRODUCTION.....	1
1.2 Background to the study	2
1.3 Problem Statement	3
1.4 Purpose of the Study.....	4
1.5.0 Main Objective	4
1.5.1 Specific Objective	4
1.6 Research Questions	4
1.7 Rationale of the Study	5
1.8 Conceptual Framework	6
CHAPTER TWO	8
2.0.0 LITERATURE REVIEW	8
2.1.0 Introduction to RSW	8
2.2.0 Overview of RSW Parameters	12
2.2.1 Welding Current.....	14
2.2.2 Welding time	16
2.2.3 Electrode force	17
2.2.4 Squeeze time.....	19
2.2.5 Hold time.....	19
2.2.6 Nugget Growth.....	19
2.3.0 Characteristics of RSW electrodes	23
2.3.1 Types of RSW electrodes	26
2.3.2 RSW electrode design	27
2.3.3 Classification of RSW electrode materials.....	30
2.4.0 Classification of RSW Materials	31
2.5.0 Characterization of Mechanical Properties of RSW Joints	32
2.5.1 Testing methods used in RSW	33
2.5.2 Tensile Shear Testing	36
2.5.3 Mechanical Performance of RSW joints	38

2.6.0 Evaluating Failure modes in RSW	39
CHAPTER THREE	44
3.0 METHODOLOGY	44
3.1.0 Types of Materials.....	44
3.2.0 Determination of the mechanical properties of the 1mm Sample Metal Sheet (SMS). ...	45
3.2.1 Determination of surface hardness of the 1mm Sample Metal Sheet	45
3.2.2 Determination of the chemical composition of the sample metal sheets	46
3.2.3 Determination of the chemical composition of the sample copper electrodes.....	46
3.3.0 Welding Parameters	47
3.3.1 Surface Preparation	50
3.4.1 Detailed Description of the Drawings	51
3.5.0 Equipment for the Welding	52
3.5.1 Welding Operations.....	54
3.6.0 Testing the Weld Strengths and Reliability.....	55
3.6.1 Non-destructive Testing of the Weld Nuggets Integrity	55
3.6.2 Information required prior to testing	55
3.6.3 Magnetic Particle Inspection	56
3.6.4 Destructive Testing of the Weld Nugget Integrity	58
3.6.5 Determination of tensile shear strength of the welded joints under the two welding schedules.	58
3.6.6 Peel Test for welded joints under conventional and annular recess electrodes.....	60
3.6.7 Micro-structural analysis on the cross sectional view of the welded joints using the conventional and annular recess electrodes respectively.....	61
3.7.0 Data Processing	62
CHAPTER FOUR	65
4.0 RESULTS AND ANALYSIS	65
4.1 Mechanical Properties of the 1mm Sample Metal Sheet (SMS).....	65
4.2 Chemical Composition of 1mm Sample Metal Sheet (SMS).....	66
4.3 Chemical Composition of the 3 Ø16mm Sample Copper Rods (SCR)	66
4.4.0 Design of Annular Recess Electrode	67
4.4.1 Mass Properties of Annular Recess Electrode Material	68
4.4.2 The Costing Report for the Manufacture of the New Novel Electrode.....	69
4.5.0 Machining to Spec. the New Novel Electrode.	69
4.5.1 Machining to Spec. the Conventional Electrode.	70
4.6 Results of RSW Experiments with Conventional Electrodes and Annular Recess Electrodes.....	71
4.7 Analysis of RSW Results when Conventional and Annular Recess Electrodes were used respectively.....	73
4.8 Results of Magnetic Particle Inspection	73

4.9 Analysis of the Magnetic Particle Inspection Test Results	75
4.9.1 Results of the Tensile Shear Strength of Welded Joints made under Conventional and Annular Recess Electrode	76
4.9.2 Analysis of Effect of Weld Current on Tensile Shear Strength for Weld Joint made using Conventional and Annular Recess Electrodes respectively	76
4.9.3 Analysis of Effect of Weld Time on Tensile Shear Strength for Weld Joint made using Conventional and Annular Recess Electrodes respectively.	78
4.9.4 Analysis of Effect of Electrode Force on Tensile Shear Strength of Weld Joint using Conventional and Annular Recess Electrodes respectively.	80
4.9.4 Analysis of Effect of Weld Current on Nugget Diameter of Weld Joint using Conventional and Annular Recess Electrodes respectively.	82
4.9.4 Analysis of Effect of Weld Time on Nugget Diameter of Weld Joint using Conventional and Annular Recess Electrodes respectively.	84
4.9.5 Analysis of Effect of Electrode Force on Nugget Diameter of Weld Joint using Conventional and Annular Recess Electrodes respectively.	86
4.9.7 Analysis of Failure Mode observed on Peel Test.....	90
4.9.9 Analysis of Micrographs obtained from Microstructure Test	93
CHAPTER FIVE	95
5.0 Conclusion and Recommendation	95
5.1 Recommendations	98
6.0 References	99

LIST OF FIGURES

Figure 1.1 Conceptual framework for characterization of annular recess electrode design.	6
Figure 2.1 Schematic diagram of Resistance Spot Welding (www.subtech.com)	11
Figure 2.2 Descriptions of Resistances Acting on RSW(Aslanlar, S. 2006)	12
Figure 2.3 Simple schematic showing the four phases making up the total weld time for the resistance spot welding process (Andrea Jane Peer, 2017)	14
Figure 2.4 Schematic of the dynamic resistance developed during spot welding of uncoated steel(N. Williams and J. Parker, 2004)	20
Figure 2.5 (a) State of matter comparing zinc & steel, (b) Exaggerated drawing of the zinc layers	22
Figure 2.6 Schematic diagram for the dynamic resistance developed during spot welding of coated steel (N. Williams and J. Parker, 2004)	22
Figure 2.7 Electrode Sizing for Dissimilar Thickness (www.resistanceweldsupplies.com, 2016)	23
Figure 2.8 Secondary Heat Balance Vs. Electrode Selection (www.resistanceweldsupplies.com, 2016)	24
Figure 2.9 Current Density (www.resistanceweldsupplies.com, 2016)	26
Figure 2.10 Resistance Spot Welding Electrode Geometries (A. Subramanian, 2017)	27
Figure 2.11 Electrode designs in various configurations 1-8 (www.tuffaloy.com-catalog.html)	29
Figure 2.12 Example stress versus strain curve of a metallic material, pointing out characteristic features	33
Figure 2.13 Example of how to measure the weld button size post destructive testing (AWS Standards, 2007)	35
Figure 2.14 Loading configuration for tensile shear testing(AWS D8.1M, 2007)	37
Figure 2.15 Loading versus elongation of single spot weld steel specimens subjected to tensile shear loading[1]	38
Figure 2.16 Pullout failure mode during peel test	40
Figure 2.17 Common fracture modes seen in the automotive industry (worldauto steel)	41
Figure 3.1 Tensile Testing machine (KYU, 2018)	46
Figure 3.2 Hardness testing machine, Super Rockwell-Duplex 713-SR, Maquina. No.1233/94 (KYU, 2018)	47
Figure 3.3 Sample Metal Sheet, 1mm thick, 50mm by 175mm, stacked to 5 pairs each and 3 bundles per label 1- 4	51
Figure 3.4 Illustrative design of the Study set-up and operations	52

Figure 3.5 (a) Electrode force control Unit, (b) UTO Spot Welder, and (C) Weld Current and time control unit respectively (Nakawa Voc. Inst., 2018).	54
Figure 3.6 Magnetic Yoke, Y-7 AC/DC (Buhimba Tech. Col., 2018)	57
Figure 3.7 Magnetic Strength Tests (1), Magnetic Flux Strength Test (2), Magnetic Test of Sample (3), Minimum Light Intensity Test (4) (Buhimba Tech. Col., 2018)	58
Figure 3.8 Preparation of the metal sheets (a) to form lap joint (b) ready for RSW	60
Figure 3.9 Specimen descriptions for the tensile shear test.	60
Figure 3.10 Peel Testing Process (Zhang,H.and Senkara,J., 2006)	61
Figure 3.11 Measurement of Nugget diameter after peel test (Zhang,H.and Senkara,J., 2006)	61
Figure 3.12 Metallurgical Microscopes (a) and Grinder Polisher (b) (KYU, 2018)	62
Figure 3.13 Metallurgical Microscopes (MUK, 2018)	62
Figure 4.1 3D View of Annular Recess Electrode, (b) cross sectional view	69
Figure 4.2 Annular Recess Electrode, filled with kaolin and mixed with clay	71
Figure 4.3 Conventional Electrodes	71
Figure 4.4 Analysis of Effect of Weld Current on Tensile Shear Strength	78
Figure 4.5 Analysis of Effect of Weld Time on Tensile Shear Strength	80
Figure 4.6 Analysis of Effect of Electrode Force on Tensile Shear Strength	82
Figure 4.7 Analysis of Weld Current on Nugget Diameter	84
Figure 4.8 Analysis of Weld Time on Nugget Diameter	85
Figure 4.9 Analysis of Electrode Force on Nugget Diameter	87
Figure 4.10 Large Sheet Separation, - using conventional electrodes	91
Figure 4.11 Small Sheet Separation, - using annular recess electrodes	91
Figure 4.12 Weld joint microstructures, for joints welded using conventional electrodes	92
Figure 4.13 Weld joint microstructures, for joints welded using annular recess electrodes	92
Figure 4.14 (1) Longitudinal joint cracks - under conventional electrodes, and (2) Circular joint cracks at the base of weld bead – under annular recess electrodes	92

LIST OF TABLES

Table 3.1 Welding Schedule for Conventional Electrode – under varied welding current; 1cycle = 0.02seconds, 50HZ.....	48
Table 3.2 Welding Schedule for Conventional Electrode – under varied Welding time; 1cycle = 0.02seconds, 50HZ	48
Table 3.3 Welding Schedule for Conventional Electrode – under varied Electrode force; 1cycle = 0.02seconds, 50HZ.....	48
Table 3.4 Welding Schedule for Annular Recessed Electrode (6mm-2.5mm) – under varied Welding Current; 1cycle = 0.02seconds, 50HZ	49
Table 3.5 Welding Schedule for Annular Recessed Electrode (6mm-2.5mm) – under varied Welding Time; 1cycle = 0.02seconds, 50HZ	49
Table 3.6 Welding Schedule for Annular Recessed Electrode (6mm-2.5mm) – under varied Electrode Force; 1cycle = 0.02seconds, 50HZ.....	49
Table 4.1 RSW Results when Conventional and Annular Recess Electrodes were used respectively.	72
Table 4.2 Photographic Magnetic Test (MT) results for Conventional and Annular Recess Electrodes respectively	74
Table 4.3 Results of Tensile Shear Strength of Welded Joint Vs Weld Current	76
Table 4.4 Regression Analysis of Weld Current Vs Tensile Shear Strength of RSW joint - when Conventional and Annular Recess Electrodes were used respectively.	77
Table 4.5 Results of Tensile Shear Strength of Welded Joint Vs Weld Time.....	78
Table 4.6 Regression Analysis of Weld time Vs Tensile Shear Strength of RSW joint - when Conventional and Annular Recess Electrodes were used respectively.....	79
Table 4.7 Results of Tensile Shear Strength of Welded Joint Vs Electrode Force	80
Table 4.8 Regression Analysis of Electrode Force Vs Tensile Shear Strength of RSW joint - when Conventional and Annular Recess Electrodes were used respectively.	81
Table 4.9 Results of Nugget Diameter of Welded Joint Vs Weld Current.....	82
Table 4.10 Regression Analysis of Weld Current Vs Nugget Diameter of RSW joint - when Conventional and Annular Recess Electrodes were used respectively.....	83
Table 4.11 Results of Nugget Diameter of Welded Joint Vs Weld Time.....	84
Table 4.12 Regression Analysis of Weld Time Vs Nugget Diameter of RSW joint - when Conventional and Annular Recess Electrodes were used respectively.....	85
Table 4.13 Results of Nugget Diameter Vs Electrode Force.....	86
Table 4.14 Regression Analysis of Electrode Force Vs Nugget Diameter of RSW joint - when Conventional and Annular Recess Electrodes were used respectively.....	87

Table 4.15 Failure Mode when Conventional and Annular Recess Electrodes were used..... 89

ABBREVIATIONS /ACRONYMS

RSW	– Resistance Sport Welding
MPI	– Magnetic Particle Inspection
RWMA	- Resistance Welder Manufacturers Association
FSS	– Ferrite Stainless Steel
HSSS	– High Strength Steel Sheet
HAZ	– Heat Affected Zone
FZ	– Fusion Zone
IF	– Interfacial Failure
PF	– Pullout Failure
BM	– Base Metal
FEM	– Finite Element Method
CFW	– Conceptual Frame Work
AWS	– American Welders Society
AC	– Alternating Current
DC	– Direct Current
D	– Diameter
t	– Time
Q	– Heat
I	– Current
AHSS	– Advance High Steel Strength Steel
MFDC	– Mid Frequency Direct Current

CHAPTER ONE

This chapter discussed in detail the general background to the study, the motivation for the study, specific tasks to enable achievement of the desired goals, scope and limitation to the study.

1.0 INTRODUCTION

Resistive spot welding (RSW) is a joining process in which contacting metal surfaces are joined by the heat obtained from resistance by the electric current. Spot welding is carried out on a machine which may be fixed on the factory floor (automated or non automated) or by hand-operated portable equipment.

In process, the joint is placed in the machine between two copper electrodes which can be interchanged for different applications. The electrodes close, squeezing the sheets together. Current is then automatically switched on for a pre-set time during which melting occurs at the interface. The current is supplied through a transformer and may be as high as 50,000 Amperes at a low voltage of about 4 to 25 Volts. The time for current flow is extremely short anywhere between 0.06 millisecond to 3 seconds. Force is maintained by the electrodes until the weld solidifies. The electrodes are then opened, and the workpiece is removed.

According to Pouranvari M. *et al*, 2012 and Hernandez, 2010 the resistance spot welding is defined as important metal joining process, used mainly in metal fabrications, automobile and railcar manufacturing industries. The study conducted by Goodarzi, M. *et al*, 2009, on the overload performance on the “dependence on weld attributes for resistance spot welded galvanized low carbon steel”, the process has been categorized as cheap, quite easily done and can be automated compared to other metal joining processes.

The resistance to the flow of current when an electric current is passed through the faying metal sheets generates heat at their interface. The temperature increases at the interface of the worksheets and when the melting point of the metal is reached, the metal will begin to melt, and a nugget starts to form out of the fused metal. Consequently, solidification occurs as the current supply is cut off, and with electrode force still acting, as stated by

Feng, J.C, *et al*, 2006, and Zhange H. et al , 2006 in their study of Nugget growth characteristic for AZ31B magnesium alloy during spot welding and resistance welding fundamentals and applications respectively. However, the formation and growth of the weld nugget is, determined by the variables, such as welding current, weld time, electrode force and electrode tip geometry, Thakur, A.G, et al, 2010 and Charde, N, *et al*, 2013. Chao, Y.J. 2003, observed that a modern vehicle typically contains approximately 2000 to 5000 spot welds. Unlike other welding processes, no filler metal or fluxes are used in the resistance spot welding.

The commonly used material in the resistance spot welding is Ferritic Stainless Steel (FSS) which accounts for nearly half of the AISI400 series stainless steels, Mohandas, T, *et al*, 2005. The characteristic feature of this material is that it does not contain nickel and hence it is considered as cheaper substitutes to austenitic stainless steels. Moreover, ferritic stainless steels are widely used for structural applications in metal fabrications, automobile and rail coaches manufacturing, Pouranvari, M, *et al*, 2015.

According to Mohandas, T, *et al*, 2005 and Shanmugan, K., *et al*, 2009, FSS steels are highly resistant to pitting and crevice corrosion, which contains 10% to 30%Cr along with other alloying elements, notably molybdenum. Ferritic stainless steels show excellent resistance to stress corrosion cracking. Although Taban, E., *et al*, 2008, observed that the toughness of ferritic stainless steel welds to be low due to the large grain size of the fusion zone. However, among FSS itself, low chromium content ferritic stainless steels, such as AISI409 comes in handy to fill the gap between austenitic stainless steel and low carbon steels, which has merits of both, Taban, E., *et al*, 2008. The AISI409 provides the basic advantages of the stainless steel such as corrosion resistance and engineering properties of carbon steel (M. Li, *et al*, 2014).

1.2 Background to the study

Resistance spot welding is typically used to provide spot welds between overlying sheet metal members, which is popular in the manufacturing industries of automobile industry, washing machines, refrigeration and freezer cabinets, central-heating radiators, steel office furniture, and storage cabinets.

According A. J. Peer, 2017, attempts by numerous researchers to explicitly analyze the process formation of the nugget during the resistance spot welding have been difficult. Still research is going on analyzing the nugget formation since 1984 (H. Neid, 1984, C. Tsai *et al*, 1992, S. Na and S. Park, 1996, and Y. Cho *et al*, 2003). While Y. Cho *et al*, 2003 during experimental measurement of nugget formation only observed initial temperature differences at the workpiece interface as a rounded shape using high speed photography.

This therefore called for an in-depth study into the characteristics of the nugget formed. Eisazadeh. H *et al*, 2010, while researching on new parametric study of nugget size in resistance spot welding process using finite element method (FEM), observed that the most critical parameters in the process were; current intensity, welding time, workpiece thickness and material, electrode geometry, electrode force and current shunting. Although the influence of the electrode geometry was not vividly detailed in this nugget formation, G. Watanabe *et al*, 2016 in their study on “Improvement of cross-tension strength using a concave electrode in resistance spot welding of high-strength steel sheets (HSSS),” observed an improvement in joint strength by 8.5KN for the nugget diameter of 6.5mm i.e., approximately 1.5 times greater than the joint strength of 5.5KN obtained by conventional electrodes. In this particular experiment carried out by G. Watanabe *et al*, 2016, the concave shape of 2mm diameter was only applied on the lower electrode while the upper used conventional electrode.

1.3 Problem Statement

Nugget diameter in resistance spot welding depends on current intensity, weld time, electrode force and electrode geometry. The integrity (impact strength, vibration noise and harshness) of resistance spot welded structures (vehicles, railcars, aero-plane and other fabricated items) depends on the nugget strength. The comfort and safety of passengers traveling in the resistance spot welded vehicles depends largely on the nugget strength. The influence of the current intensity, weld time and electrode force have been extensively researched as reviewed in the literature, little research has been done on the electrode geometry. This study will address this knowledge gap.

1.4 Purpose of the Study

The purpose of this research is to investigate in-depth the effect of electrode tip geometry change on the weld joints strength of sample metal sheet extracted from an old range rover with comparison to using the conventional electrodes. According to Zuniga, S.M., 1994 and Pouranvari, M. et al, 2008, the integrity and the mechanical performance of the spot welds, as resistance spot welding process is one of the main welding processes used in the manufacturing of vehicle structures. The major fault types identified during a vehicle crash is the resistance spot weld joint failure, Pouranvari, M, et al, 2011. Donders, S., et al, 2006 and Pouranvari, M., 2017, in their study observed that at a global perspective, failure of spot welded joints may affect the vehicle's structural integrity through noise, vibration, and harshness performance.

Therefore the sustainable safety of the passenger and equipment would require improvement in the mechanical performance of the spot welded joints in a vehicle, fabricated machines or rail coach will certainly improve its structural integrity and crash worthiness. The quest for the current research study was therefore to enhance structural integrity and the crash worthiness of fabricated equipment, vehicles and rail coaches, hence improving safety of the passengers and operators.

1.5.0 Main Objective

To investigate the characteristics of resistance spot welding electrodes with annular recess design configurations.

1.5.1 Specific Objective

1. To evaluate the performance characteristics of the annular recess electrode.
2. To analyze the performance of the recess annular electrode in comparison with the conventional electrode.
3. To conduct the integrity test on the welded joints of the metal sheets.

1.6 Research Questions

1. What is the effect of annular recess electrode tip (s) geometry change when used on both lower and upper electrodes on the weld current, weld time and joint strength?

2. What performance characteristics of the annular electrodes are distinguishable from the conventional electrodes?
3. What is the effect of using recessed electrodes on the integrity of the resistance spot welded joints?

1.7 Rationale of the Study

Resistance spot welding principally comprises of two conductive electrodes, power transformer and the mechanism for pressing the work pieces together for proper weld joining.

Due to its simplicity and ease of adoptability to any tool arms at varying positions, RSW machines have been incorporated into the robot arms and this has tremendously improved the production capacity in the automobile industries, railcar manufacturing, and other subsidiary industries in the recent times, besides the excellent quality finishes and RSW joint strength.

Therefore the current research study was meant to improve on the strength of RSW joints, create product safety reliability to the automobile customers worldwide and enhance the crashworthiness of the vehicles by use of the annular electrodes at work-piece –tool interface during the manufacturing processes.

1.8 Conceptual Framework

This conceptual framework covered step by step formulated investigative flow chart that dissected the dependent variables (such as the peak load, and nugget diameter) and independent process variables (such as current, weld time, electrode force and electrode geometry) that enabled accomplishment of the objectives mentioned above: (Study the CFW diagram shown in figure 1.1).

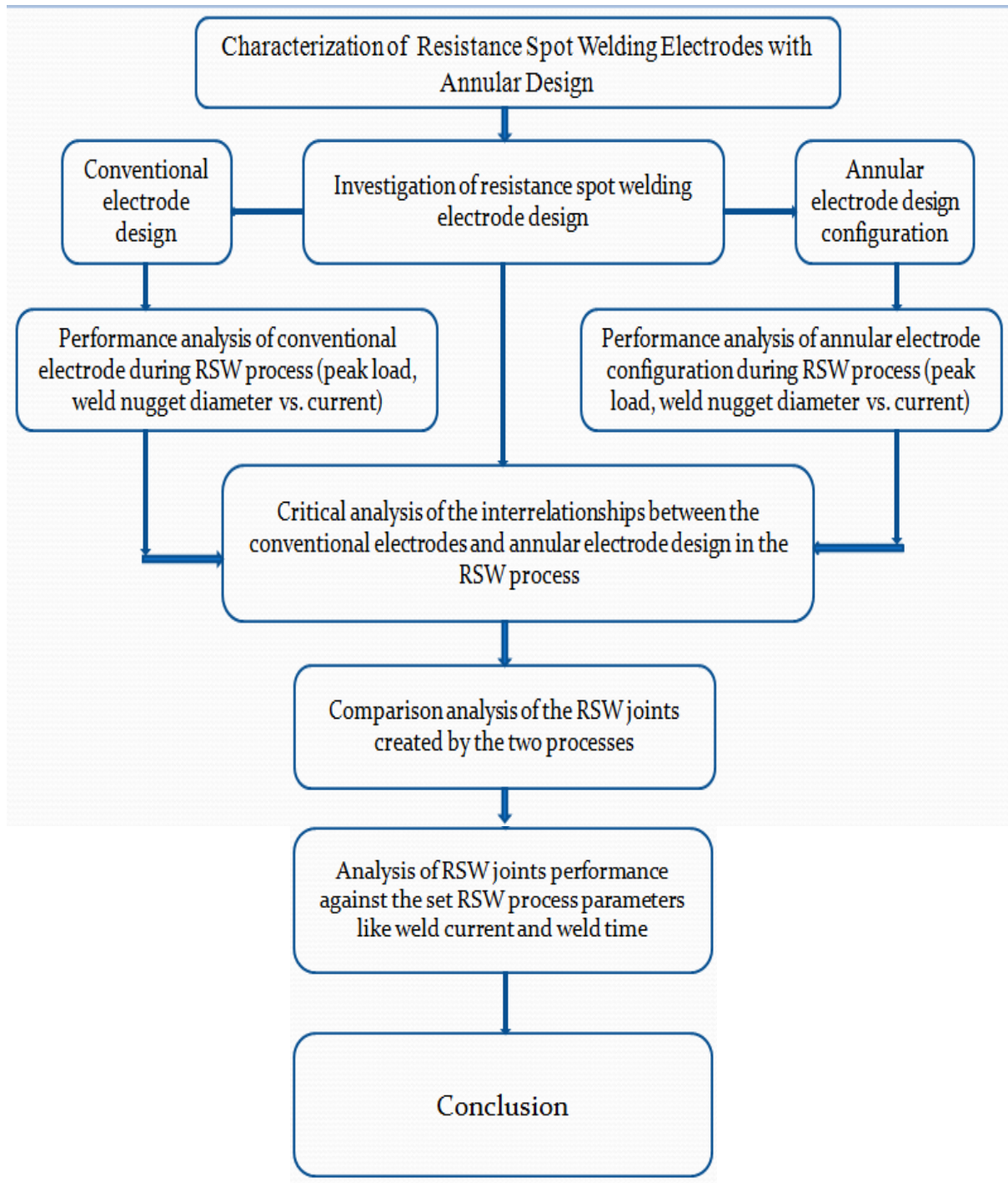


Figure 1.1 Conceptual frameworks for characterization of annular recess electrode design.

1.9 Scope and Limitation of the Research

The mechanical properties of resistance spot welded joints of the sample steel sheets were investigated in this research study, with the sole aim on its load bearing capacity and the energy absorption capacity. However, the major limitations of this study are as given below.

- a) The mechanical behavior of the resistance spot welded joint of sample metal sheets extracted from an old range rover metal steel sheet under fatigue load condition was not discussed in this study.
- b) Corrosion behavior of the resistance spot welded joint of the sample stainless steel was also not covered in this study.
- c) In this study, an attempt was made to improve the mechanical performance of the resistance spot welded joint of the sample steel by using electrodes with annular recess design. However the optimum welding conditions to achieve maximum mechanical performance parameters was not covered in this study.
- d) Ductile to brittle transient transformation of the welded joint due to decrease in temperature was not covered in this study.

CHAPTER TWO

This chapter covered the basic theory behind resistance spot welding, RSW process parameters, and works and contributions of other scholars on similar subject matter.

2.0.0 LITERATURE REVIEW

The literature review covered all aspects of resistance spot welding with emphasis on parameters that affect the functioning of the electrodes.

2.1.0 Introduction to RSW

Resistance welding is one of the simplest, cheapest and reliable means of joining metals. The resistance welding process was discovered over 120 years ago and its definition has never changed (www.resistanceweldsupplies.com). It is therefore defined as a method of joining two or more metals by clamping under pressure and passing through them an electric current for a specific time. The electric resistance to the flow of current in the circuit generates heat that is sufficient to initiate a plastic state or molten state on the workpieces and produces fusion at the interface surfaces.

Much as resistance spot welding is now over 120 years old, the process of metal fusion by application of heat and pressure commenced over 1000years, ago. Blacksmith and Phoenician artisan welded metals or joined metals together with forge and hammer over 3000years ago under heat and pressure (www.resistanceweldsupplies.com). However, over time, the technology and flexibility used in the resistance welding controls and control systems changed dramatically.

The process of resistance welding was discovered in 1877 by Mr. Elihu Thomson while conducting a class in electricity at Central High School, Philadelphia, demonstrating the operation of spark coil. The first practical demonstration of the of the resistance welding was performed at Franklin Institute in Philadelphia in 1879 and perfected in 1886 and

subsequently the first production of resistance welding machine code named, Thomson – Gibb machine was realized (www.resisnaceweldsupplies.com)

The science behind the operation of resistance welding process is governed by two laws of physics. These are Ohm’s law and Joules law. Ohm’s law states that the current flowing through a conductor between two points is directly proportional to the voltage across the two points. Mathematically this is expressed as shown below;

$$E \propto I \dots\dots\dots 2.1(i)$$

$$E = IR \dots\dots\dots 2.1(ii)$$

Where E = the voltage across the two points,

I = current flowing through the conductor and,

α = Proportionality sign

R = resistance to the flow of current, and in equation (ii) R is treated as a constant independent of the current.

Note that the “R” in Ohm’s law is the same “R” in the resistance welding. Thus resistance welding therefore works on the principle of Ohm’s law.

While, Joules law, a unit of energy, is the energy expended by an electric current of 1 ampere flowing through a 1 ohm resistance for 1 second.

This is expressed mathematically as shown below;

$$H = I^2RT \dots\dots\dots 2.1(iii)$$

Where H = the heat energy,

I^2 = Current squared,

R = Resistance in the circuit,

T = Time current is allowed to flow.

The resistance welding control, only regulate current (I) and time (T), R however, is a variable dependent on the machine set up, materials being welded, force applied, metallurgy and thickness of the material as shown in figure 2.1.

According to J.B. Shamsul, *et al*, 2007, Marashi, S.P.H., 2016 and Habib, L., *et al*, 2016, resistance spot welding (RSW) is a commonly used sheet metal joining process in various manufacturing industries. It is considered a simple process where, high current is made to pass through the work sheets under squeeze pressure to make the joint. The major input parameters observed by researchers affecting the growth of resistance spot weld are welding current, welding time and electrode force, Thakur, A.G., *et al*, 2010 and Ozyurek, D., 2008.

RSW is the most widely used type of all the resistance welding processes. Both electric current and mechanical force are applied simultaneously to make joints in this process. Force is applied to the electrodes to ensure sufficient contact between the parts to be welded. The holding force and welding current are applied to the work piece via copper alloy electrodes, as shown in figure 2.1. According to Habib, L., *et al*, 2016, the volume of the metal from the work pieces that have undergone heating, melting, fusion and re-solidification is called the weld nugget. Pouranvari, M., *et al*, 2007, considered RSW process as being simpler, faster and cheaper compared with most of the other welding processes. RSW can be used to weld both materials of different chemical composition such as stainless steel, high strength low alloy steel, advanced high strength steel and low carbon steel and different material thicknesses, J.B. Shamsul, *et al*, 2007. However, Pouranvari, M., 2011 and Thakur, A.G., *et al*, 2010 in their study observed that the quality of the joint is best judged by nugget size and joint strength.

In RSW, high welding currents are usually used to generate heat energy to make the weld. The heat energy generated is affected by three factors such as current, resistance at the sheets interface and the time during which current flows through the workpieces

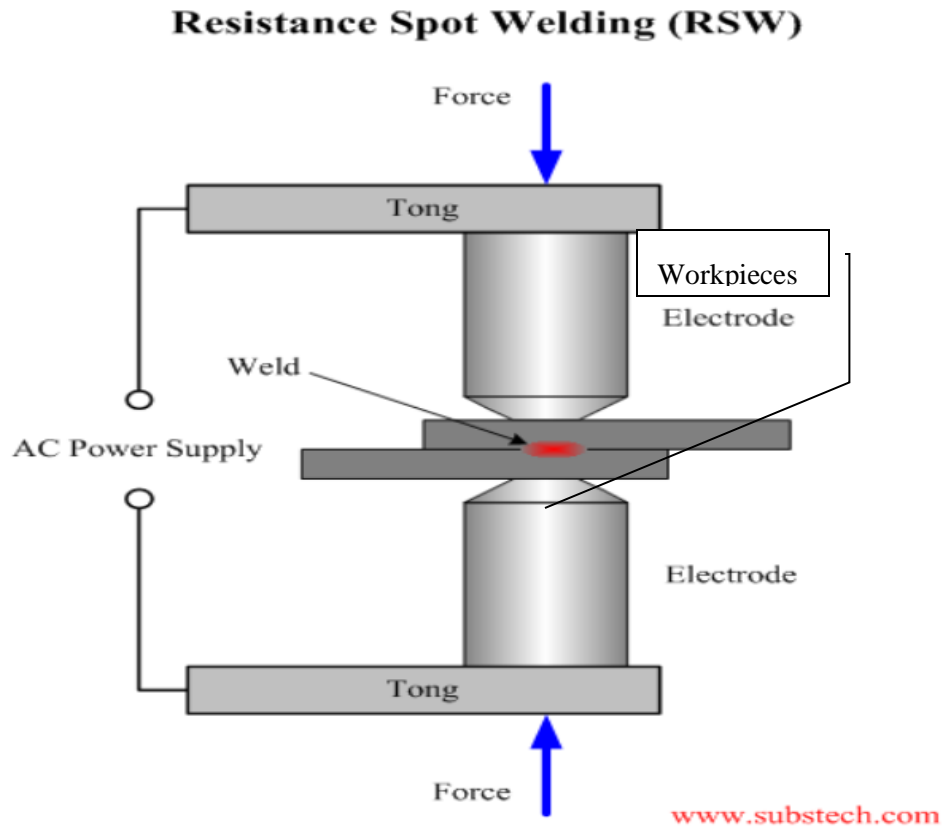


Figure 2.1 Schematic diagram of Resistance Spot Welding (www.substech.com)

A research study by Aslanlar S., 2006 and Pouranvari, M., *et al*, 2013, indicated that the heat generated is given by the formula 2.1(iii), where H is the heat generated (in joules), I the current (in ampere), R the resistance of the work (in ohms), t is the duration of current (in seconds).

The secondary circuit of a resistance welding machine and the metal sheets being welded form a series of resistances in effect, as shown in figure 2.2. By analysis of the circuit the total resistance as stated by Aslanlar, S., 2006 is the sum of all the individual resistance as they are connected in series. The most critical resistance value in the circuit is R_3 because, it influences the formation of weld nugget in a positive way.

$$R = R_1 + R_2 + R_3 + R_4 + R_5 \dots \dots \dots (iv).$$

In fact, Zhang, H., *et al*, 2006 and Aslanlar, S., 2006, observed that the higher the value of R_3 , the higher will be the spot weld ability.

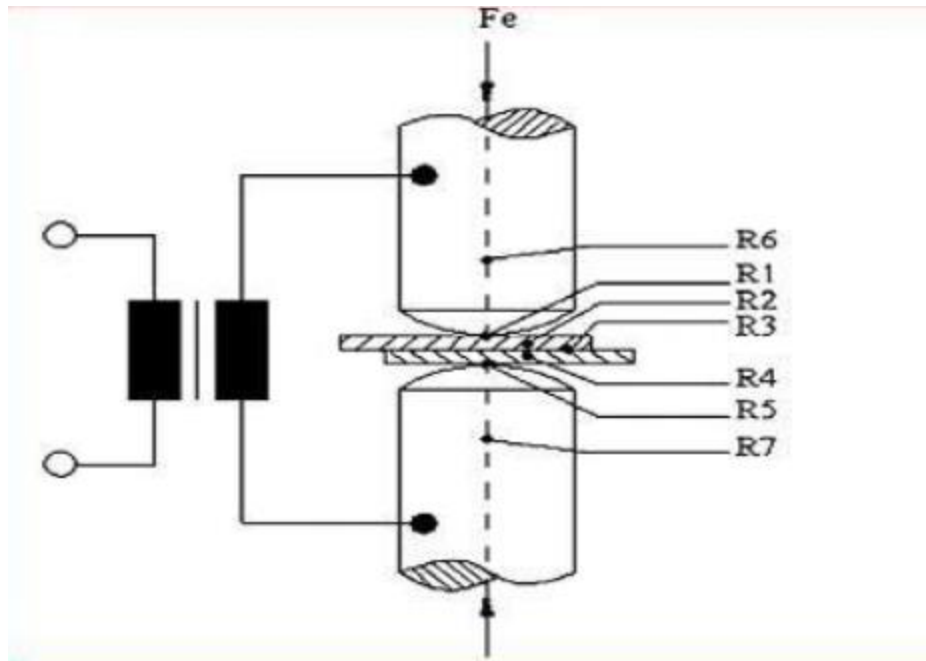


Figure 2.2 Descriptions of Resistances Acting on RSW (Aslanlar, S. 2006)

Where,

Fe = Electrode Force,

$R1$ = Specimen Resistance,

$R2$ = Upper Specimen – Upper Electrode contact Resistance,

$R3$ = Upper Specimen – Bottom Electrode contact Resistance,

$R4$ = Bottom Specimen Resistance,

$R5$ = Bottom Specimen – Bottom Electrode contact Resistance,

$R6$ = Upper Electrode Resistance, and

$R7$ = Bottom Electrode Resistance as shown in figure 2.2 above.

The heat is generated by a relatively short-time flow of low voltage with high density electric current across the intended joint location, and the pressure being supplied by contacting electrodes to the workpiece. Both electric current and pressure are closely regulated and controlled all the time.

There are some of the sub-classifications of electrical resistance welding include 'spot welding', 'seam welding', and 'butt welding'. 'spot welding' is a resistance process of welding in which coalescence is produced by the heat obtained from resistance to the flow of an electric current through the workpieces pressed together by pointed electrodes. The electrodes are brought to and removed from the workpieces at predetermined times and rates, and a clamping force is applied through the electrodes by some suitable means. The most widely used electrode material is pure copper, as it gives optimum results.

In general, relatively high conductivity electrodes should be used to weld low conductivity materials and low conductivity electrodes would be used on high conductivity materials. Moreover it should have enough compressive strength to withstand the applied welding pressures. In seam welding, electrodes in the form of rolls are used to transmit pressure and to send current through the overlapping sheet being moved between them. Interrupted current control is usually necessary since it provides better control of the heat, allows each successive increment in the seam to cool under pressure, and minimizes distortion, flashes and burns. Butt welding is used to join lengths of rods and wire. The ends are pressed together and an electric current passed through the work so that the ends are heated to a plastic state due to higher electrical resistance existing at the point of contact. The pressure is sufficient to form a weld.

2.2.0 Overview of RSW Parameters

The welding schedule as observed by Williams *et al*, 2004, involves the mainly four successive steps; namely initial squeeze, application of current, hold, and electrode release as shown in figure 2.3. The heat generated under the electrodes from the concentration of current creates a molten weld nugget, due to a combination of contact resistance and bulk resistance. The molten weld nugget solidifies once the current ceases and cooling commences. The equation below, known as Joule's first law, generally represents how to

calculate the amount of heat generated during the RSW process, Zhange H. and Senkara. J, 2011.

$$Q = I^2RT \dots \dots \dots 2.1(V)$$

The total heat, Q , is calculated by multiplying the squared weld current (I), total circuit resistance (R), and weld time (T). The main variable parameters for heat generation are the current, resistance, and time. Thus the process variables that can easily be controlled with the RSW equipment are weld current and time. However, resistance value is majorly influenced by the electrode diameter ($D = 4\sqrt{t}$, where t = thickness of the metal sheet) making the contact resistance at the faying interface and is dependent on the material thickness t , temperature, and welding force exerted by the two water cooled electrodes. Therefore, weld current, time in milliseconds or cycles (DC or AC power source respectively), and electrode force are the three important variables specified in Resistance Welder Manufacturers' Association (RWMA) that can be manually controlled. Recommended values for different material compositions and thicknesses can be found in RSW standards. The sequence of the RSW operations defining the total weld time is shown in figure 2.3.

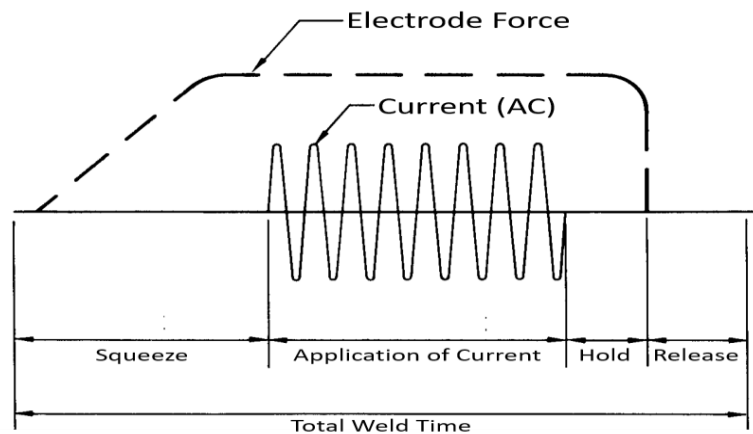


Figure 2.3 Simple schematic showing the four phases making up the total weld time for the resistance spot welding process (Andrea Jane Peer, 2017)

The input process parameters employed during the RSW determines the quality of the weld joint. According to Karci, *et al*, 2009, welding current, welding time and electrode force are

the predominant process parameters influencing the quality of weld joint in resistance spot welding.

2.2.1 Welding Current

The welding current is the most significant variable for generating heat during resistance spot welding. A region of high current density is created through the water cooled electrodes to cause localized heating and melting of the clamped workpieces at the electrode tips. Too low current will not be able to generate adequate heat energy to the melting of the material at the faying interface to form nugget. On the other hand too high current will cause splashing of molten metal from the fusion zone. Such splashing of molten metal is commonly known as expulsion and it leads to weakness of the weld joint. In addition high current also leads to porosity in the weld and very large indentations on the metal surface. The current level also affects the distortion of the base metal and the size of the heat affected zone (HAZ). Aslanlar, S., 2006 and Pouranvari, M., *et al*, 2013 reiterated that welding current value depends on sheet thickness, other input parameters and weld quality requirements.

The current profiles may range from simple pulses to more complexes up slopes and down slopes. However, depending on the material and its weld ability, a current profile is selected to widen the process scope to create a more robust process. The use of sloping can be used in advanced high strength steels (AHSS) to localize heating at the faying interface. Thus I. Khan *et al*, 2007, during their study presupposed that weld formation is based not only on the heat input, but also how the heat is applied, which has been a driving force in creating more complex current profiles for spot welding.

Not long ago, single phase alternating current (AC) welding processes had been the main equipment used for automotive welding. However, W. Li *et al*, 2005 and Hofman *et al*, 2005 both observed that newer methods like mid- frequency direct current (MFDC) inverters are being more widely employed for their high precision control, improved reliability, and reduced power demands. Researchers also compared the performance of AC and DC output

during resistance spot welding of different material gauges with different thicknesses. Hofman *et al*, 2005, in their study noted that AC versus DC had little effect on welding of thin gauge dual phase steels, but with thicker material the DC inverter gave larger weld nuggets and better mechanical properties. While W. Li *et al*, 2005, on the other hand premised their discussions on low welding currents; there was a discrepancy in weld sizes between AC and DC processes but that variation was reduced as current level increased to the expulsion point. Thus a comparative analysis of AC and DC processes by W. Li *et al*, 2004 and 2005, showed characteristic difference in each of the processes respectively, and this was linked to the contact resistance breakdown occurring separately as a result of the change in heating patterns.

2.2.2 Welding time

Welding time is the time period in milliseconds or cycles depending on the source of the power, during which the welding current is permitted to pass through the metal sheets. The weld time is usually chosen based on the material composition, coating, and thickness. During squeeze time, only pressure is applied to hold the workpieces together firmly and current is not applied. According to Aslanar, S., 2006, welding current is applied at the end of squeeze time, when electrode force has reached the desired level. Similar to welding current, the Resistance Welder Manufacturers' Association, 1961 specified that a too short weld time generates insufficient heat to form the nugget. While on the other hand, a long welding time results in overheating and expulsion. In manufacturing environment, it is a common practice to keep short welding time to the extent possible to lower the cost of production. Thus, A. Subrammanian *et al*, 2017, in their study observed that a shorter weld time is desirable and is more likely to be compensated by higher weld current to give sufficient results. In production environment, Aslanar, S., 2006, stated that typical traditional weld times range between 200 - 700 milliseconds depending on material configuration, other process parameters and weld requirements. Han *et al*, 1993, stated that welding time along with welding current are the most sensitive parameters to control expulsion in RSW.

The mechanical performance of the weld joint is basically dependent on the quality of the weld joint formed; Z. Mikno *et al*, 2016. The hold, or cooling, time is another important variable post-current in resistance spot welding. The water-cooled electrodes facilitate conduction of heat away from the workpieces during the hold time. D. Dickinson, 1981, in showed welding in the automotive industry noted that faster solidification of the molten weld nugget to gain sufficient strength is facilitated by the water cooled electrodes. However, W. Chuko and J. Gould, 2002, while studying the development of appropriate resistance spot welding practice for transformation-harden steels emphasized that adequate hold time is required to solidify the weld nugget and subsequently form martensite as preceding low current temper pulse is applied to the weldment.

For AC welding supplies, time is measured by cycles which are $1/60^{\text{th}}$ second for a 60 Hz North American machine and for DC welding supplies, time is measured in milliseconds. In manufacturing facilities, the weld time is most importance because it can directly affect the cost and cycle time of production. In the cases of thicker or more advanced material compositions, more complicated multi-pulse welding conditions are used to create larger or tempered weld nuggets. While these conditions can enhance the quality of the weldment, N. Williams and J. Parker, 2004, noted they are often undesirable compared to a single pulsed weld condition due to the increased time. Therefore time setting in resistance spot welding is very critical as it affects the quality of the weld joints.

2.2.3 Electrode force

Electrode force is most commonly provided by either pneumatic or hydraulic systems. This force is the result of pressure applied to the piston of a cylinder connected directly to the welding head. The actual amount of electrode force depends on the effective line pressure, weight of the head, and the piston diameter. Most welders, however, have electrode force charts on the side of the machine, tabulating air pressure vs. electrode force. If there is no chart available for the machine, the following formula may be used to calculate the approximate total weld force:

Electrode Force is given by;

$$F = \pi \times D^2/4 \times P \text{ or } .78 \times D^2 \times P \text{ (.78 is approximately equal to } \pi/4 \text{)} \dots \dots \dots 2.2.3 \text{ (i)}$$

D = the Piston Diameter in inches

P = the Line Pressure in pounds per square inch

Electrode Force (F) is in pounds.

To calculate the line pressure required to produce a desired electrode force, this formula can be reconfigured as follows:

$$\frac{\text{Electrode Force}}{0.78 \times D^2} = \text{Line Pressure (P)} \dots \dots \dots 2.2.3 \text{ (ii)}$$

However the above formulas significantly do not allow for dead weights and friction in the cylinder or ram of the machine. Thus it is advisable, when changing electrode force on air operated machines, from one value to a greatly different value, it may be wise to readjust the speed control valve on the welder also. Too slow an approach wastes time and may require a longer squeeze time. Too fast an approach impacts the electrodes on the workpiece and shortens the electrode life. The impact force may also damage the electrode holders or head and can damage the workpieces as well.

To effect control of the electrode force, a solenoid valve is used to actuate the piston in the weld cylinder. The solenoid valve is typically an electrically operated valve in the compressed air or hydraulic line connected to the cylinder on the welding machine. When the welding control applies voltage to the valve, it opens, allowing compressed air or hydraulic fluid to enter the cylinder to develop the electrode force.

Electrode force is required primarily to press firmly the workpieces to be joined together. Sufficient amount of electrode force is required to guarantee good weld quality. The contact resistance between workpieces usually reduces as the electrode force increases, which in turn lower the amount of heat energy generated. In order to compensate this, larger amount of current will have to be used. When very low electrode force is used, it fails to

initiate the required contact between workpieces and also between the electrode and the workpiece. In such a scenario, sparking, splashing and rapid wear of electrodes may tend to occur. Excessively high electrode force will lead to plastic deformation on the surface, leading to indentation. According to Pouranvari, *et al*, 2010 and Zhang, *et al*, 2006, higher level of indentation is not desirable as it lowers the strength of the weld. Based on the study by Pouranvari and Ranjbasnoodeh, 2013, an increase in electrode force resulted in the reduction in strength and failed at lower load. Excessive electrode force during RSW causes molten metal flow, thus reducing the joint cross sectional area upon which the load will act, hence facilitating failure at lower load

2.2.4 Squeeze time

Squeeze time is the first stage in the operating sequence of RSW, followed by weld time, hold time and off time. According to RWMA Bulletin#5, 2016, squeeze time has no direct effect on the technical properties of the weld. However, it must be significantly long enough to allow the electrode force to reach the required level before welding current is switched on. According to the Aslanlar, S., 2006, while performing a research study on “the effect of nucleus size on mechanical properties in electrical resistance welding of sheets used in automotive industry”, observed that too short a squeeze time may result in expulsions from the nugget or expulsions from the area between the electrode and work piece surface. Adequate squeeze is the key to successful joint quality during resistance spot welding process.

2.2.5 Hold time

During hold time, the welding current ceases, whereas electrode force or pressure is maintained on the workpieces till last cycle of the welding current. It provides the cooling time for the nugget, as the water cooled electrode is still in contact with the sheets. The hold time must be long enough for the molten metal to solidify and also to ensure enough weld strength. Therefore, increased thickness of the work piece and longer weld time require longer hold time. It is quite acceptable to use short hold time for materials which

have a tendency to become brittle during cooling (about 10-20 cycles). Long hold time may lead to increased wear of the electrodes as stated by Aslanlar, S., 2006.

2.2.6 Nugget Growth

Basing on the reviews of the above process variables i.e, weld current, weld time and electrode force, manual or semi automatic controls can be applied to create an optimized condition suitable for sufficient heat generation for the weld. Welds are formed at the interface between the workpieces as the contact resistances are much higher than the bulk resistances of the materials (figure 2.4). High resistance is created at the surface due to asperities that create uneven profiles. Sufficient contact to enable development of the nugget is only possible once the asperities are broken down and subsequent reduction in contact resistance. The resistance of heating increases the temperature as shown by stage 3 in figure 2.4, until the liquidus temperature is surpassed. Slight decreases in resistivity are seen once the molten nugget is formed

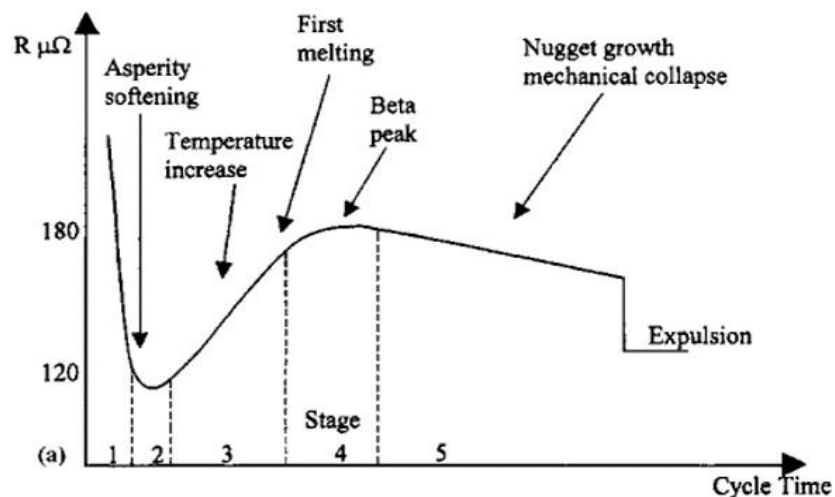


Figure 2.4 Schematic of the dynamic resistance developed during spot welding of uncoated steel (N. Williams and J. Parker, 2004)

In the review of the available literature, Tsai *et al*, 1992, S. Na and S. Parker, 1996 and H. Neid, 1984, have all successfully completed physic based numerical analysis on nugget growth and temperature distribution. Since the resistance welding process is electrically and thermal-mechanically coupled, it is intricate to analyze the results without comparison to

actual testing samples. For experimental measurement, Y. Cho and S. Rhee, 2003 used high speed photography to analyze the nugget formation during welding. They observed initial heating in a rounded shape at the interface. The heating profile expands into a square shape, encompassing the area under the electrode and concluded that as temperatures continue to rise; a molten nugget begins to form in the center of the heated region and expands in all directions.

In the manufacturing industries especially automotive industry, materials are often coated for corrosion protection. The major problem eminent when attempting to weld galvanized steel is the phase difference in melting points of the two metals, i.e., steel and zinc. Further the zinc coatings usually change the surface resistivity and behavior of the workpieces during RSW. In figure 2.5, the dynamic resistance curves of zinc-coated steels shows a more complex profile and significantly differ from that of uncoated steels (figure 2.3). During resistance welding process, the layer of zinc coating must be displaced to allow for intimate contact of the steel substrate. The soft, conductive nature of zinc allows for the coating to be melted and pushed to the edge of the contact interface. The change in the dynamic resistance profile alters the nugget formation. Basing on the findings of M. Khan, 2007, the added cycle time due to temperature and time increases the heat generation and creates a more spherical weld nugget after solidification. However, N.J. Den Uijl, 2015, on the other hand observed that other coatings, like the AlSi coating often found on boron steels, facilitate reduction in the conductivity at the surface and give dissimilar results during spot welding. Therefore to weld steel to steel through the zinc coating, the temperature of the zinc will be raised beyond its boiling point, and thus zinc literally evaporates to the atmosphere leaving behind white powder forming zinc oxide ([www. resistanceweldssupplies.com](http://www.resistanceweldssupplies.com)). Figure 2.5 may offer a better appreciation of the above processes.

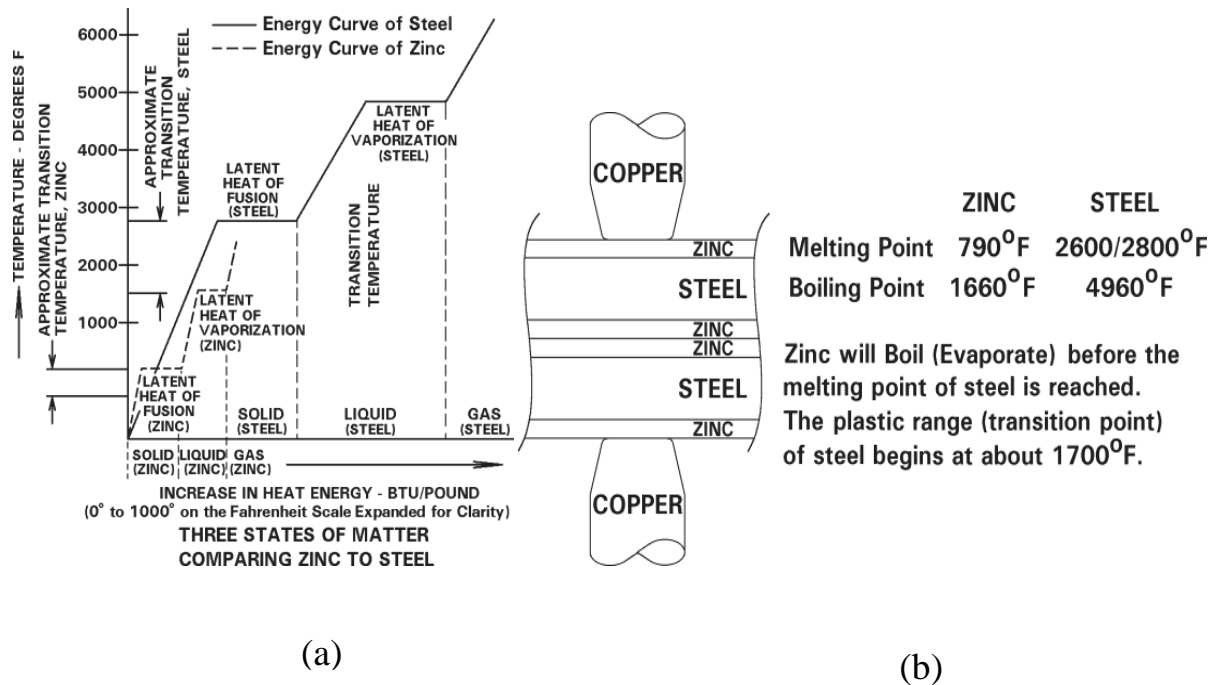


Figure 2.5 (a) State of matter comparing zinc & steel, (b) Exaggerated drawing of Zinc Layers (www. Resistanceweldsupplies.com, 2016)

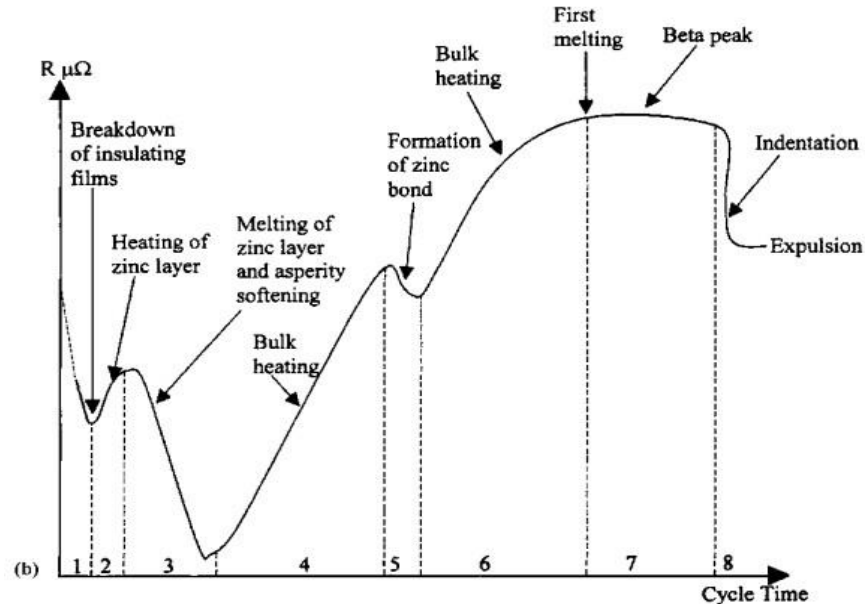


Figure 2.6 Schematic diagram for the dynamic resistance developed during spot welding of coated steel (N. Williams and J. Parker, 2004)

2.3.0 Characteristics of RSW electrodes

The basic “rule of thumb” as adopted by AWS provides a simple guide lines used by welders to determine the size of the face of the electrodes to be used to weld dissimilar thicknesses of material. Figure 2.7 provide illustrations that best explain the rule of the thumb. If similar sized electrodes are used, the weld nugget will not form at the interface of the two materials.

To employ this “rule of thumb,” a sketch line drawn to scale, of the two workpieces in a horizontal position. A vertical line is also drawn through the two workpieces, at the centerline of the electrodes to be used. Hence join the two lines at a 45° angle to the center line of the electrodes, passing through the interface between the two workpieces. Thus the point at which the two 45° angle lines intersect the outer surfaces of the workpieces will indicate the relative diameters of the two electrodes. The larger electrode will be against the thicker workpiece as shown in figure 2.7.

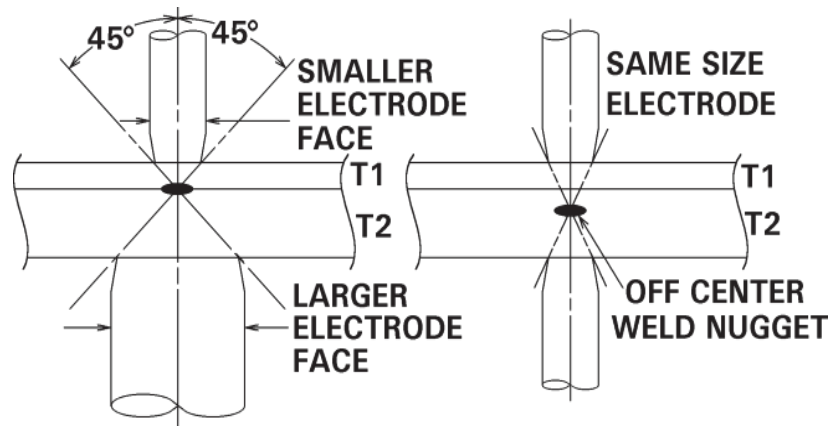


Figure 2.7 Electrode Sizing for Dissimilar Thickness (www.resistanceweldsupplies.com, 2016)

This “rule of thumb” will only work well where the ratio of the thin to thick material, $T1/T2$, does not exceed $1/3$ as stated in AWS. Changing the electrode material of one electrode can also move the weld nugget. Placing an electrode of higher resistance (i.e., lower conductivity) against the thicker workpiece and an electrode of lower resistance (high conductivity) against the thinner piece will move the weld nugget toward the interface of the two workpieces.

Mismatching electrode face diameter and materials can also cause an imbalance when welding same thicknesses of material. As a matter of strategies to control and achieve quality, electrodes should be properly stocked such that alloys and sizes cannot be mixed involuntarily. Replacement of used up electrodes during production should always be done as a pair so that the proper diameter to the workpiece can be maintained. To adequately manage RSW processes that involve working on the same thickness and dissimilar thickness materials respectively, and materials of different alloys, figure 2.8 may be used to provide a better guide.

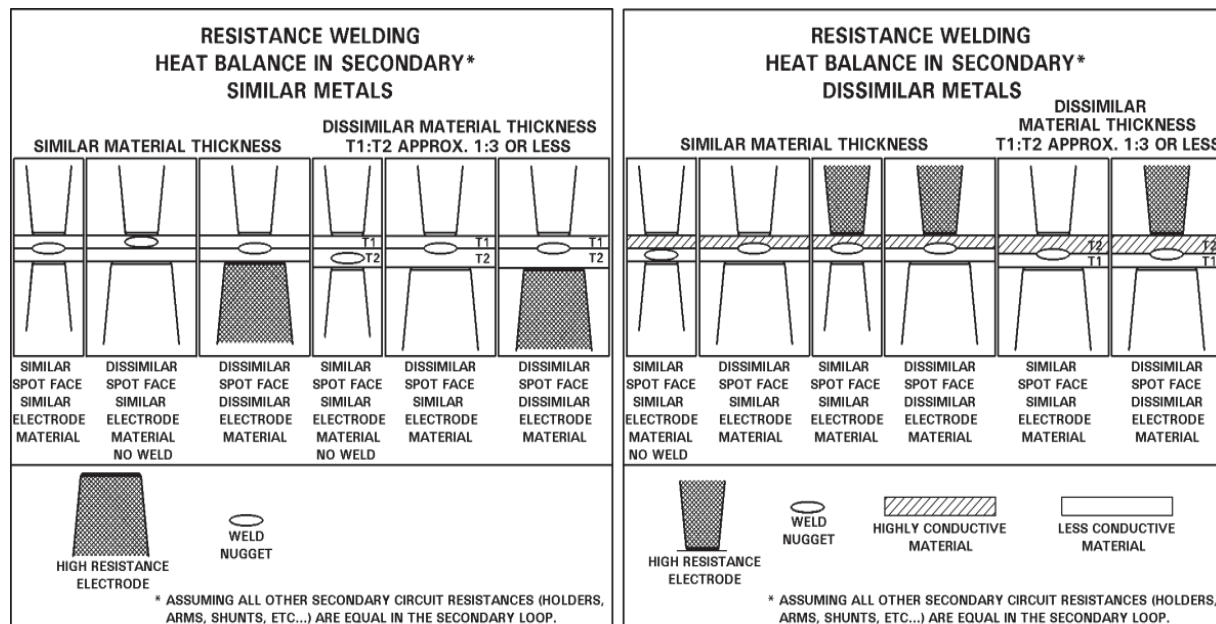


Figure 2.8 Secondary Heat Balance Vs Electrode Selection
(www.resistanceweldsupplies.com, 2016)

The industrial practice employed to maintain consistency in quality resistance spot weld emphasizes that electrodes should be machined to shape, not filed. This practice averts the problem of faulty welds due to improper selection, preparation and maintenance of electrodes. The size and shape of the electrode also has a bearing to the welding current requirements. An electrode too small may “produce” a hot weld, while an electrode too large may “produce” a cold weld. Therefore, some adjustment in the control setting of welding current or timing and the electrode force may seem to alleviate this problem momentarily, but

proper electrode selection is the correct remedy to maintaining good weld quality as seen in figure 2.8.

The condition of the electrode, type, shape, or material can also significantly affect the weld parameters to the extent that changes in the weld control settings cannot fully overcome the weld problem created by the condition of the electrodes. The size and shape of the face of the electrode is related to current density which should be maintained constant in order to make welds of consistent quality. Electrode wear contributes dramatically to current density. An increase in electrode diameter of about 25% can reduce the current density by about 40% (www.resistanceweldsupplies.com, 2016). Even though the control is maintaining the current constant, the weld nugget strength and size will be reduced. Figure 2.9 graphically demonstrates the result of electrode “mushrooming” on current density. The result is weld quality degradation.

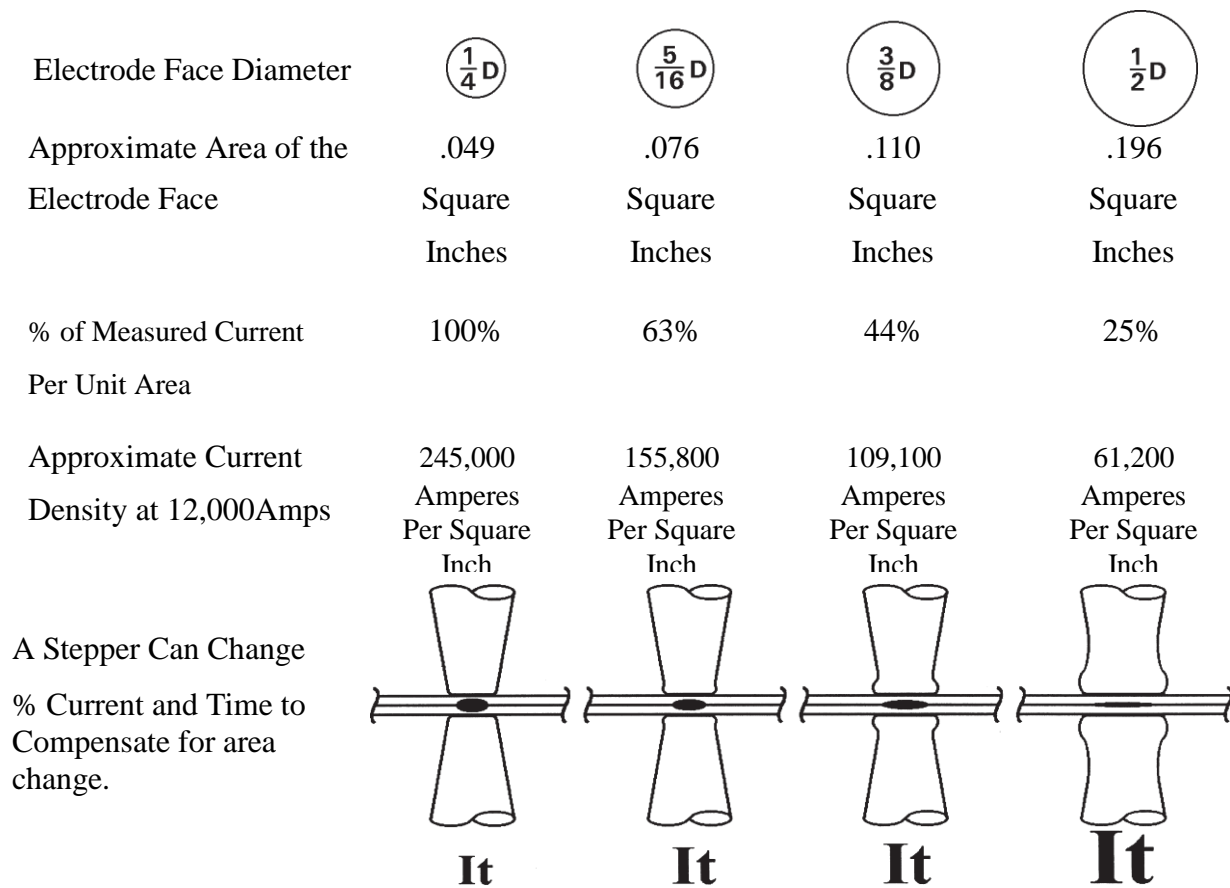


Figure 2.9 Current Density (www.resistanceweldsupplies.com, 2016)

2.3.1 Types of RSW electrodes

“Copper alloys are mainly used as electrode material in RSW”, Zhange H. and Senkara J., 2006. In RSW, electrodes hold the workpieces firmly together, provide passage for current with sufficient intensities, and also do the job of post-weld cooling. Typical electrode geometries are shown in figure 2.10. Truncated cone electrodes are commonly used in industrial applications due to their limited contact tip growth. Alignment of truncated cone electrodes is significant to be specially taken care off as the weld quality can be adversely affected with misalignment.

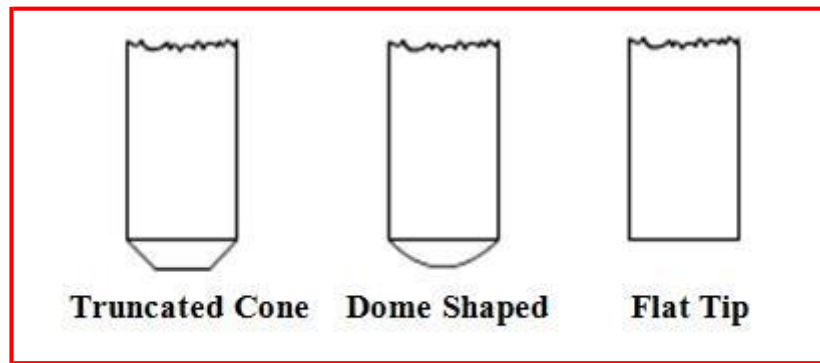


Figure 2.10 Resistance Spot Welding Electrode Geometries (A. Subramanian, 2017)

2.3.2 RSW electrode design

Available literature indicates that aspect of electrode force life (Simons, W. P. 1967) and electrode geometry (Nadkarni, A. V., and Weber, E. P. 1977) have been extensively studied. The non uniform heating condition spread over the electrode tip surface was identified as one of the factor that facilitated the increased rate of electrode tip deformation (Friedman, L. M and Mc Clay, R. C. 1969). This was further explained in terms of surface resistance variation as a result of non uniformities in the steel coating. Other literature available indicates that, electrode geometry and its effect on current distribution were considered as the main source of an even heating across the electrode face.

The non uniform distribution in the region of the electrode tip was suspected to give rise to the irregular heating which would otherwise promote localized heating. Green Wood, J.S. 1961, observed that the current distribution in the resistance spot welding does not flow straight across the material being welded, but spread into the worksheet through the electrode tip circumference causing current constriction at the location, while Holm R, 1967, noted that a current constriction occurs at the electrode face with unbalance amount of current flowing through the circumference of the electrode tip. However, Kaiser *et al*, 1982 observed an annular molten zone around the circumference of some welds, which was corroborated by Lane C.T. *et al*, 1987.

The initial temperature patterns as observed by Greenwood, 1961, indicated a maximum value in a ring around the circumference of the electrode tip that catapulted to the assertion that “ if current is so high enough to produce weld in such a short time, a ring weld will form.” The same phenomenon was also corroborated by Neid, H. a, 1984, while studying “the finite element modeling of the resistance welding process. Thus the prevalence of uniform current distribution at the outer circumference of the electrode tip is indeed with the fact that current constricts around corners such as angle between the tapered end of a truncated cone electrode and the workpiece.

The most important parameter in the electrode geometry is the contact area between the electrode and the metal sheet. In general, the tip diameter should be slightly larger than the nugget diameter. If the tip diameter is too small for the application, the nugget formed will be small and weak. On the contrary, if the tip diameter is too large, over heating can occur, resulting in formation of voids. Figure 2.11, illustrates the various electrode design configurations commonly used in the manufacturing industries.

Despite after various reviews of numerous literatures, information regarding annular recess electrode design configuration is still limited except attempt made by Watanabe *et al*, 2016 while studying “Improvement of cross-tension strength using a concave electrode in resistance spot welding of high-strength steel sheets (HSSS),” revealed an improvement in joint strength by 8KN for the nugget diameter of 6.5mm i.e., approximately 1.5 times greater than the joint strength of 5.5KN obtained by conventional electrodes as earlier mentioned in section 1.2. The current study however, exploits the application of two annular recessed electrode design 2.5mm diameter, 4mm deep mounted on both upper and lower jaws of the RSW machine. The electrode tip diameter was fixed to 6mm. The parameters to be tested ranges from weld joint integrity, microstructures and the joint strength.

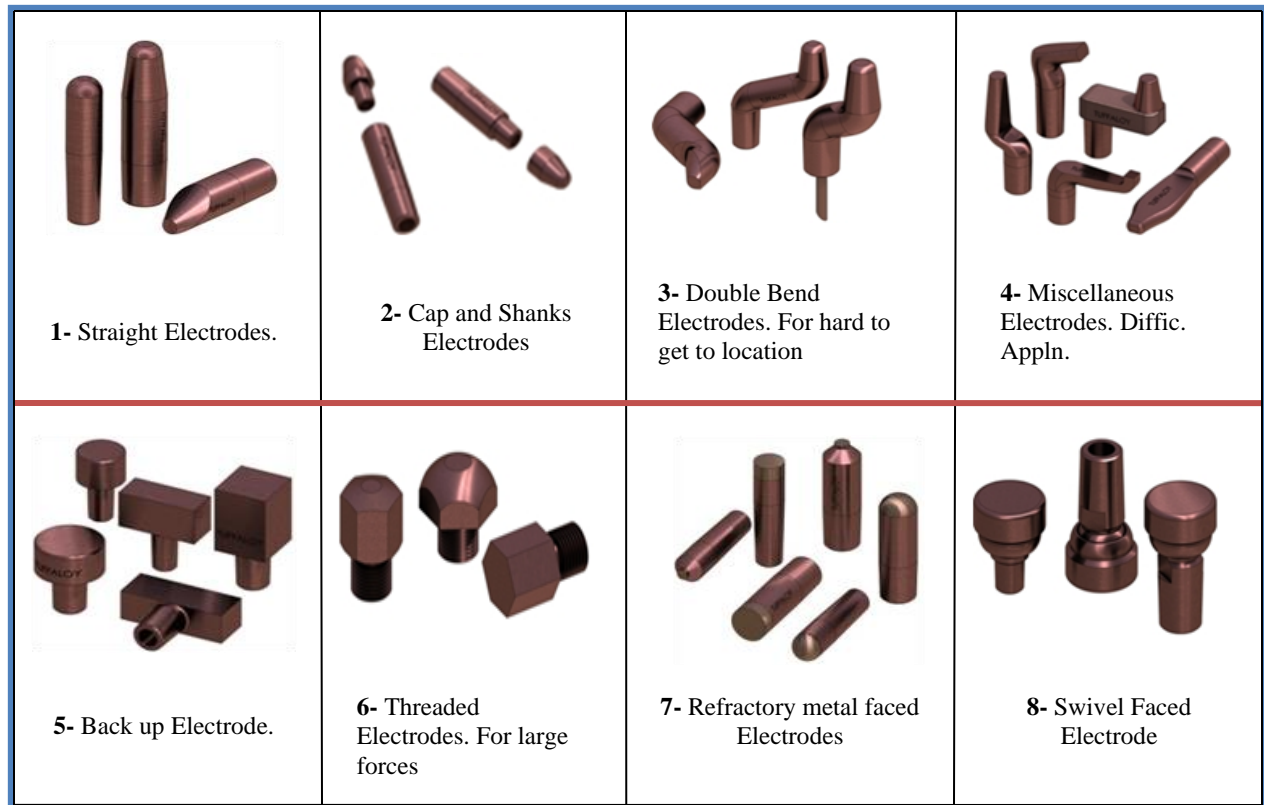


Figure 2.11 Electrode designs in various configurations 1- 8 (www.tuffaloy.com-catalog.html)

The electrodes, usually wear out during the resistance spot welding resulting into weld joints with weak fusion or a symmetrical nugget formation. The corrosion of the electrode tip contact areas tend to increase during RSW process which prohibits the attainment of sufficient current densities. Such welds have poor quality welds. Hence it is important to maximize electrode life to consistently achieve acceptable welds.

Bowers, R.J. *et al*, 1990, while studying the relationship between the electrode geometry, current distribution and the electrode life, noted that higher angles of electrode-workpiece interface resulted into more uniform current distribution at the electrode tip surface. Therefore equal current distribution at the electrode tip yielded even wear, although higher angles are known to rapidly facilitate mushrooming of the tip. They further asserted that electrode – workpiece interface angles approaching 90 degree facilitate more equal current distribution at the electrode tip, electrode geometry affect wear and life as result of its influence on the local current distribution, the electrode geometry tends to shift the position

of the welding lobe, and lastly efficient electrode design must provide for a thermal and mechanical strength, as well as maintain uniform current distribution.

2.3.3 Classification of RSW electrode materials

The most important function of the spot welding electrode is to conduct electric current, to squeeze the sheets together and cool the weld joint. Therefore, electric conductivity, compressive strength and hardness are important factors in finding an appropriate electrode material. The material that fits the demands best is copper and copper-based alloys, as described in the standard ISO 5182:2008 Standard. The most common electrode material is a copper-chromium- zirconium alloy, while higher resistance alloys of nickel, beryllium and/or cobalt may be used for higher strength steels and stainless steels

The electrodes are one of the most important factors in the resistance welding process but often the most neglected. It is important to consider the electrode material, shape, size, tip profile and cooling. Electrode materials are covered by ISO 5182, 1999 Standard. These are mainly copper alloys with a small percentage of alloying element to improve hardness, while maintaining good conductivity. The most common electrode materials are Class 2 (e.g. copper/chromium or copper/chromium/zirconium) and mostly for welding low carbon and high strength steels in general. Higher conductivity alloys, such as copper/zirconium and dispersion strengthened copper electrodes, exhibit some benefits when welding coated steels as they provide less surface heating because of their low contact resistance.

However, welding harder sheet materials such as stainless steels require much higher electrode forces are required with lower welding current, ISO 5182, 1999. These materials are better welded with the harder Class 3 electrodes such as copper/nickel/silicon. This is replacing the superior copper/cobalt/beryllium alloy because of the potential beryllium hazard (mainly as a dust from machining or dressing operations).

Refractory electrode materials, such as tungsten/copper, tungsten, or molybdenum are used for applications such as projection welding inserts, where the electrode contact area is at least

three times the weld size. These materials have higher hardness but lower conductivity than the Class 2 electrodes. They are unsuitable for spot welding as they suffer localized heating at the tip contact, which can lead to cracking of the electrode. The exception is for joining high conductivity metals such as copper wire or foil, where heat is generated mainly within the refractory electrode tip and conducted into the materials to be joined. Therefore knowledge of the resistance spot welding electrode materials and properties is significant in achieving quality resistance spot weld joints. In this particular research study, copper based electrodes were specified to suit the 1mm steel based materials identified to be used in the study.

2.4.0 Classification of RSW Materials

The resistance spot welding materials are classified into stainless steel, mild steel, and carbon steel of varying gauges ranging from 14 to 18. With reference to the introductory note contained in this document, the commonly used material in the resistance spot welding is Ferritic Stainless Steel (FSS) which accounts for nearly half of the AISI 400 series stainless steels, Mohandas, T, *et al*, 2005. The characteristic feature of this material is that it does not contain nickel and hence are considered as cheaper substitutes to austenitic stainless steels. In the contemporary world, ferritic stainless steels are widely used for structural applications in metal fabrications, automobile and rail coaches manufacturing, Pouranvari, M, *et al*, 2015.

Stainless steel constitutes a group of high alloy steels based on the Fe-Cr, Fe-Cr-C and Fe-Cr-Ni systems. Stainless steel derives its unique characteristics from the presence of 10.56 wt % chromium which according to Lippold, C. John and Kotecki, J. Damian, 2005, while studying “New welding metallurgy and weldability of stainless steel”, form passive layer on the surface of the material inhibiting oxidation and subsequent decaying of the underlying metal. Stainless steels are widely used for body structural applications in automotive, rail cars, and domestic appliance industries. There are many obvious advantages of using stainless steels, such as weight reduction, improved corrosion resistance and recyclability. Stainless steels also have excellent manufacturing and fire-resistant properties. Stainless steel exhibits

high energy retention capacity under impact loads as discussed by Pouranvari, M and Marashi, S. P. H, 2012. In the contemporary world, ferritic stainless steels are commonly employed for the manufacture of the structural parts of vehicles, rail coaches and aerospace Pouranvari, M, *et al*, 2015. The ferritic grade steels as observed by Amuda, M.O.H. and Mridha, S., 2010, contain very small amount or no nickel, and hence they are cheaper compared to the austenitic grade steels

2.5.0 Characterization of Mechanical Properties of RSW Joints

A key mechanical property of the material can be defined by its stress strain curve figure 2.12, which is generated from a uniaxial tension test. Many of the defining characteristics features of a material, like strength, ductility, and toughness can be taken from key features of its unique curve. Deformation of a metallic material can be elastic or plastic. Elastic deformation occurs as very small strains and can be completely recovered upon unloading. Plastic deformation is permanent and occurs when the strain cannot be linearly related to the stress based on Hooke's law H. Zhang and J. Senkara, 2011. The stress at which deformation changes from elastic to plastic is desirable to know and usually used as a maximum in the design of structures. The exact transition point is difficult to accurately pin-point and can be estimated by measuring the 0.2% offset, commonly referred to as the yield strength. After yielding, the stress needed to continue plastically deforming the material increases until it reaches a maximum. The maximum stress a material can endure is also known as its tensile strength. For steels, the tensile strength is proportional to the hardness and a materials ability to withstand plastic deformation. At this point, necking begins and deformation is subjected only to the necking region where final failure occurs.

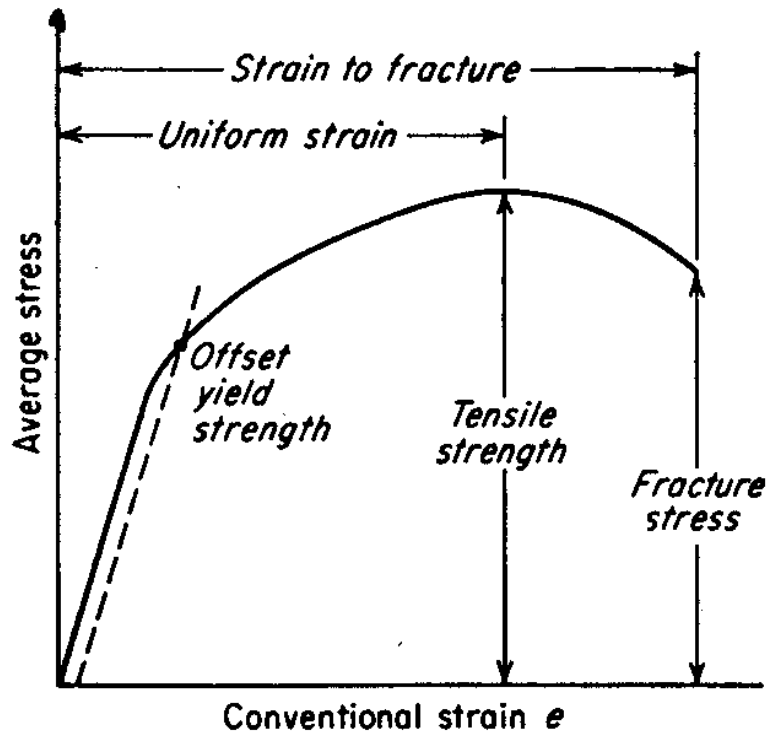


Figure 2.12 Example stress versus strain curve of a metallic material, pointing out characteristic features

The degree of plastic deformation at failure is referred to as ductility. A material that can endure severe deformation is known as ductile, while a material that cannot is known as brittle. Ductility is an important trait of a material from a design perspective, giving insight of the degree of plastic deformation before fracture. For fabrication of sheet metal, it is often used to determine the allowable deformation during forming.

For static testing conditions, the area encompassed under the curve can be described as the toughness of the material. For a metallic material to be tough, it must display both strength and ductility. Toughness represents the amount of plastic deformation and energy a material can absorb prior to fracture. However, according to W. D. Callister and D. G. Rethwisch, 2010, the term toughness can also be used to categorically explain a materials resistance to fracture when a pre-existing stress concentration or flaw is present.

2.5.1 Testing methods used in RSW

There are various methods employed in the testing of the RSW joints, depending on the functional requirements. They are categorized in to two main branches, namely; Non destructive and the destructive test. Standards are in place for these two categories for ease of application. In this particular research both categories were used in testing the integrity of the RSW joints under the conventional electrodes and those under annular recessed electrodes.

The functionality requirements for a resistance spot welded joint for a given application determine the needed performance level. The performance of the joint is often related to the weld nugget diameter, but Y.J. Chao, 2003 and S. Dancette *et al*, 2011, observed that the chemical and micro-structural composition of the material, thermal profile, inhomogeneous material properties, residual stresses, and specific loading conditions can alter the performance behavior. Prior knowledge of the base metal microstructure facilitate the determination of the strength of the material, but upon welding of the same, the microstructure is usually altered severely at the weld nugget and heat affected region, K. Easterling, 2013. The direct relationship between the applied load and subsequent deformation or response observed on the material was best explained by W. D. Callister and D.G. Rethwich, 2010. This relationship is severely altered during welding; therefore, it is important to use mechanical testing methods to determine qualitative and quantitative weldability characteristics of resistance spot welds that meet the requirements of a specific application, Andrea Jane Peer, 2017.

Testing of resistance spot welded samples is different from testing uniform material samples because of the geometry. According to H. Zhang and J. Senkara, 2011, spot welded joints are typically considered a singular unit and the strength and elongation is displayed in force and displacement, respectively. The unit of a spot weld consists of the weldment and the surrounding heat affected zone region. Therefore, the measurement of strength is not solely determined by the weld nugget, but is also influenced by the HAZ and base material. It is always necessary to provide information on the base material when discussing the strength of spot welded joints. However, according to AWS Standards, 2007, the design criteria, of the

resistance spot welded joints must exceed the strength of the weakest base metal being joined.

The methodologies used to replicate different loading conditions that could be seen in application. In the case of RSW for automotive use, testing parameters employ combinations of various loading rates and directions to mimic the crash analyses used. The test results are typically displayed as failure mode, weld button size, and weld strength H. Zhang and J. Senkara, 2011. The failure mode is a qualitative measure of weld quality and can give information on whether the failure was brittle or ductile in nature. The weld button size is a measure of the size of the button-like material that remains joined after destructive testing. An example of how the button measurement is taken is shown in figure 2.13. The weld strength can be quantitatively measured in many ways. The peak load is the maximum force endured by the weld prior to failure. The ductility gives insight on the energy that can be absorbed by the joint prior to failure. The fatigue limit measures the number of cyclical cycles to failure in a specific loading condition.

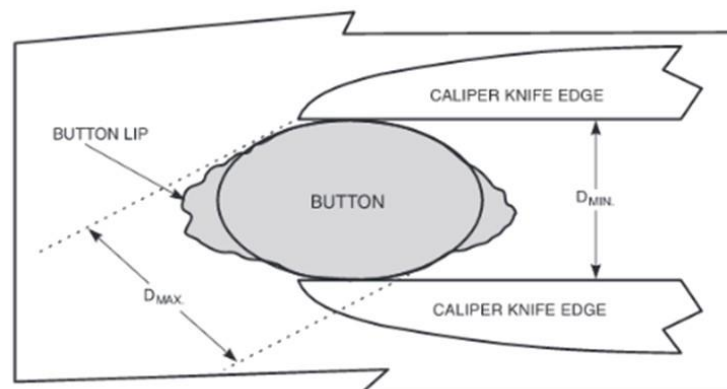


Figure 2.13 Example of how to measure the weld button size post destructive testing (AWS Standards, 2007)

Procedures for common mechanical tests are described in standards to define a consistency between organization and different market sectors. There are a wide variety of standards available which may have slight modifications but in general address a similar set of guidelines eg. ISO Standard 18278-2, 2004 and AWS, *D8.1M*, 2007. Due to the geometry of the spot weld, testing procedures and specimen preparation are necessary to minimize the

bending of the specimen. The stress concentration, or notch-like feature, of the weldment at the interface of the workpieces plays a large role in the deformation and fracture. From standardized testing methods, it is easy to obtain results that can be used to quantify the weld quality. Each manufacturer has unique joint design and quality control that can alter the acceptance levels of spot welds subjected to different loading conditions. If bending occurs, the original loading mode is not maintained during the entire test. The naming of the tests describes the original loading mode that is used in the procedure.

2.5.2 Tensile Shear Testing

One of the most common testing methods used for RSW joints in industry and research is the tensile shear test. Unlike cross tension testing, the exact location of the weld is less significant to the results. The test can be conducted at a quasi-static or dynamic loading rate. According to M. Khan, 2013, dynamic loading conditions require specialized equipment and are not very reliable and repeatable, often quantified with trends in data. Therefore, H. Zhang and J. Senkara, 2011, emphasized that to evaluate the weldability of new materials and joint configurations, static tensile shear tests are often used.

The test specimens are welded in a lap configuration, as shown in figure 2.14. Shims are often used in the set-up to minimize bending that would deviate the loading mode from shear. The amount of deformation and rotation that is often seen in testing is dependent on the thickness and size of the weldment. Upon deformation, the nugget begins pulling from the base plate creating a moment. Tensile shear testing provides information on the ultimate strength and failure mode of RSW joints. Failure is primarily a factor of weld diameter, but can also be influenced by expulsion, defects, and heterogeneous microstructures.

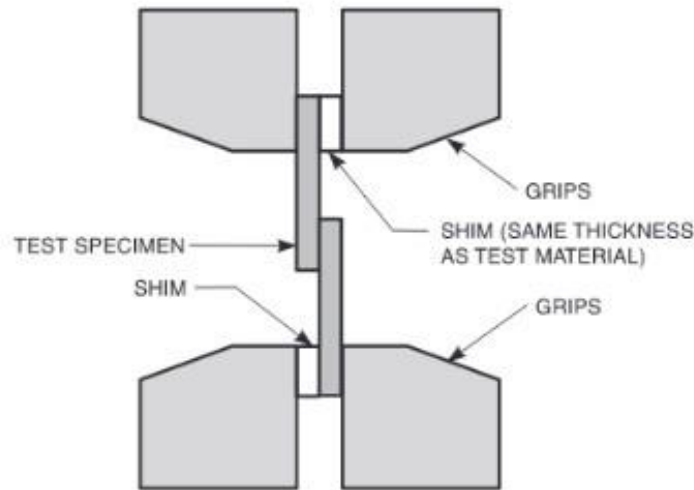


Figure 2.14 Loading configurations for tensile shear testing (AWS D8.1M, 2007)

Although the tensile shear test gives good indication of the welds strength and deformation behavior, it cannot completely simulate the loading conditions seen during crash testing. The tensile shear specimen is easy to fabricate, requires little fixturing, and exhibits much less experimental variability, which are why this test is commonly used to validate RSW joints.

Figure 2.15 shows the load versus elongation, typical tensile shear testing output, of single steel spot welds. The higher strength materials have less elongation. Currently, new materials are being researched and developed to increase the ductility while still maintaining the high strengths. While strength is important, without ductility, the failure mode is typically brittle which correlates to very little energy absorption at failure.

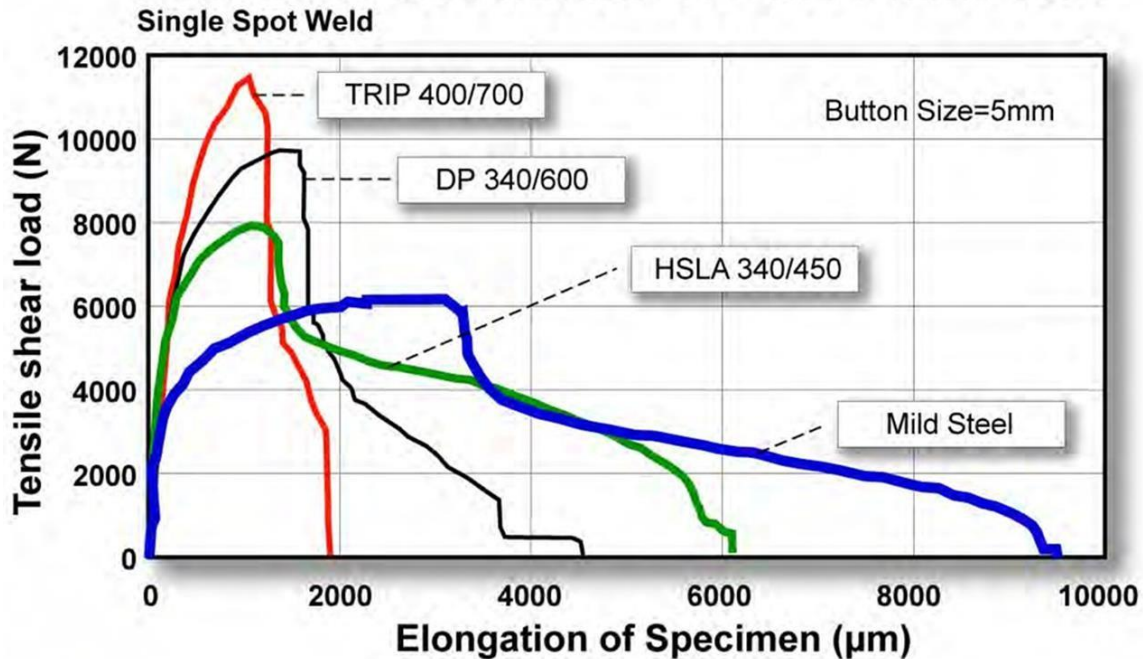


Figure 2.15, Loading versus elongation of single spot weld steel specimens subjected to tensile shear loading (World AutoSteel)

Y.J. Chao, 2003, has shown that while the lap-shear test specimen is subjected to a shear load globally, the failure mechanism of the weld at the micro-structural level is tensile. He has also shown that the cross-tension test is subjected to a normal load but the failure mechanism seen is shearing. This explains why the cross-tension test often sees a lower overall load than the tensile-shear test for the same given weldment and base material.

2.5.3 Mechanical Performance of RSW joints

The mechanical performances of RSW joints are crucial for the quality, safety and durability design of a vehicle. According to Peterson, W. *et al*, 2000, many of the RSW joints are used in structural assemblies that are involved in transferring loads through the body frame (e.g. Car body frames) during a crash event, and may act as fold initiation sites to manage impact energy. Donders, S. *et al*, 2005, stated that the integrity and mechanical properties of spot welded joints also affect their fatigue and fracture resistance and, thus the overall performance of a car body frame in terms of vibrations, noise and harshness.

Research revealed that mechanical performance of a resistance spot welded joint is commonly evaluated by the tensile shear test. Zhang, H. and Senkara, 2006, in this context defined tensile shear test as being simple and arguably the most widely used test for assessing the spot weld mechanical performance. The parameters commonly derived from the load - displacement graph is significant in the assessment of mechanical performance of RSW weld joints; they are; peak load, displacement at the peak load and lastly failure energy at the peak load.

Pouranvari, M. and Marashi, S. P. H., 2010, also observed that the Peak load, obtained from the tensile shear test is widely used to describe the mechanical performance of the spot weld. However, other quality attributes with the exception of the peak load is failure energy or the energy absorption capacity of the weld. It is known to be a function of peak load and the displacement value. Failure energy indicates the energy absorption capability of the weld and the reliability of a weld joint during an accident. The higher the failure energy value, the better the weld performance reliability against impact loads as in the case of crush accident Pouranvari, M. and Marashi, S. P. H., 2010. According to Pouranvari, M. and Ranjbamooodeh, E. 2011, failure energy is a function of the load-displacement curve. Zhang, H. and Senkara, 2006, stressed that failure energy is calculated up to peak load point and not up to the failure point because both displacement and failure energy cannot maintain their uniqueness after the peak load point.

2.6.0 Evaluating Failure modes in RSW

Failure modes in resistance spot welding as recorded by Chao, Y. J., 2003, and Pouranvari,, M., 2011, is measure of its mechanical performance. According to Maryra, M. and gayden, X.D., 2005 and Chao, Y. J., 2003, spot welded joints may fail in two different ways, namely; pull out failure and interfacial mode.

The interfacial failure (IF) mode is known to exhibit fracture propagation through the fusion zone. In-depth analysis of interfacial failure mechanism has been linked to primarily weak joints that greatly affect the crashworthiness of a vehicle, Pouranvari, M. and Marashi,

S.P.H., 2012. On the other hand, pullout failure (PF) mode, exhibit cracks development and propagation along the periphery of the weld nugget formed. Destructive tests such as tensile shear strength test, cross tensile shear test and peel test provide the primary means to reveal the two types of RSW failure mode. During the peel test, the nugget from one sheet metal comes out in the form of a button, creating a hole in the other sheet metal piece as shown in figure 2.16. During pull out failure mode, initiation of fracture tends to commence in either the base metal (BM), heat affected zone (HAZ) or fusion zone (FZ) as a result of the mechanical, microstructure, geometrical properties of the weld joint or the loading conditions as stated by Pouranvari, M. and Marashi, S.P.H, 2010 while studying “Factors affecting mechanical properties of resistance spot welds.”

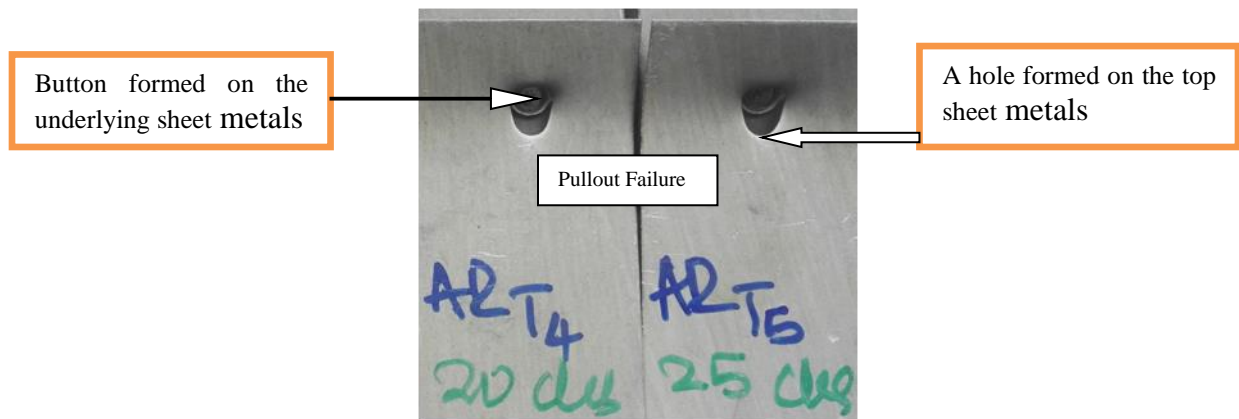


Figure 2.16 Pullout failure mode during Peel Test

Pullout failure mode is the most desirable mode as it is associated with better mechanical performance. Failure mode according to Pouranvari, M. and Marashi, S.P.H., 2010 and 2013 affects the peak load value and failure energy of the joint in resistance spot welding. The high load and energy absorbing capacities of the resistance spot welded joints during crash conditions are linked to pullout failure of the RSW joints. Thus Pouranvari, M., et al, 2008 and Marashi, S.P.H., *et al*, 2008, recommended skillful synchronization of input parameters during resistance spot welding.

However, Pouranvari, M., *et al*, 2008, in their study suggested two distinctive criteria that govern pullout failure mode namely; one, the ratio of fusion zone (FZ) hardness to failure

location hardness and the others were volume fraction of velocity and the thickness of the sheet. While Radakovic, D.K. and Tumuluru, M., 2008, in their study on RSW of advanced high strength steel, echoed that RSW failure mode alone should not be used as a criterion to judge the quality of spot welds. They categorically pointed out that, pullout failure mode may occur even at low peak load, and further stressed that there is a critical sheet thickness above which, the transition from the pullout failure mode to interfacial failure mode manifest itself.

RSW Failure modes in the automotive industry are classified into the eight descriptions as shown in figure 2.17 that explicitly expose fracture modes at the joint level.

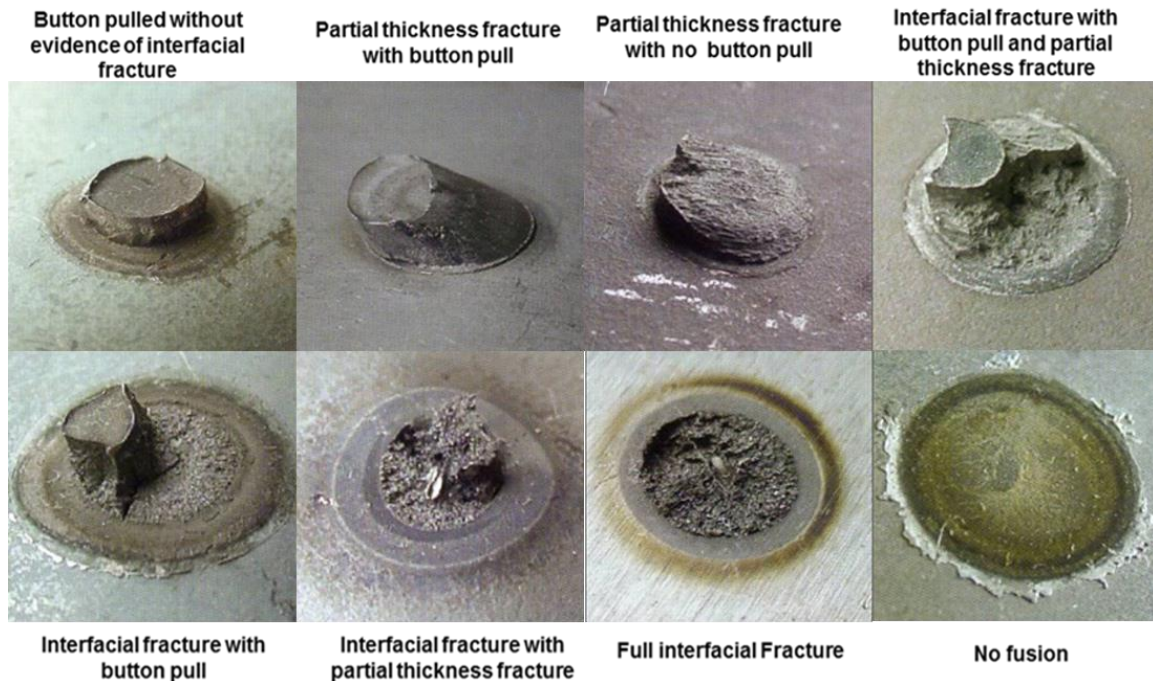


Figure 2.17 Common fracture modes seen in the automotive industry (worldautosteel)

Button pull out fracture as earlier discussed occurs when the joint itself does not fail, but the HAZ or base material (BM) at the border of the joint fails. Usually the joint around the HAZ is weakened during the resistance welding processes by tempering the microstructure or excessive growth around the region. However, Andrea Jane Peer, 2017, observed that failure

in the base metal occurs when the welding processes reinforced the weld joint well above the base metal strength. The partial button pullout fracture failure occurs when the RSW joint cannot support the load fully and thus partially fractures. The crack due to fractures propagates through a portion of the nugget. There are many different variations depending on the path of the crack, figure 2.17, but these are usually lumped together as partial button fracture. Interfacial fracture occurs when failure is in a straight line along the interface of the workpieces, Andrea Jane Peer, 2017.

Button pullout fracture as earlier mentioned is deemed an acceptable failure mode and gives evidence that the welding process did not affect the materials' ability to withstand loading. There is often more part deformation, indicating more energy absorption at failure, and areas of fracture commencement where less energy is seen to be less absorbed when button pullout is the fracture mode. At the material level, this failure is considered ductile in nature and exhibits localized necking of the material surrounding the nugget.

Partial button pull out fracture is indicative of the welding process altering the materials ability to endure a load. The joint is the weakest link and a crack propagates partially through the solidified weld nugget. There are many different factors that can contribute to partial button pull out and it is often deemed an unacceptable fracture mode for production, Andrea Jane Peer, 2017. N.Williams and J. Parker, 2004, on the other hand observed that brittle martensitic weld nuggets and partial button pull-out can be deemed acceptable in situations where a maximum load is reached prior to failure for advanced high strength steel.

Interfacial fracture does not provide warning signs before complete propagation along the weld centerline in a brittle fashion. There is often no part deformation at failure, indicating very low energy absorption. In the past, interfacial fracture was always deemed unacceptable, but like partial button pullout has been qualified as acceptable for some advanced high strength materials.

However, H. Zhang and J. Senkara, 2011, while studying “Resistance Welding: Fundamentals and Applications,” observed a strong relationship between RSW failure modes and the weld size, which although relevant but not stipulated in the common RSW specification used by welders. This relationship according to the available literature is simply stated as “smaller welds tend to fail as interfacial while the large welds tend to fail as button pullout.” The degree between small and large welds continuously changes based on material thickness and strength.

In an ideal situation, the RSW joint would never fail and material properties could be used to define failure of the unaffected base metal besides the weld parameters which equally play important role in determining the weld joint failure mode. S. Zuniga and S.D. Shepard, 1997, while studying “Resistance spot weld failure loads and failure modes in overload conditions,” observed a significant challenge in determining the failure mode or location of the failure in advance, especially while analyzing the inter-relationship among the type of loads; weld joint geometry and material properties.

CHAPTER THREE

This chapter covered the step by step procedures used in achieving the three specific objectives stated in chapter one and the collection of the data from experiments and tests.

3.0 METHODOLOGY

This study was empirical in nature and the research design was qualitative. Data collection methods were by experiments. The experiments were conducted on an 18 gauge (1mm) sample metal sheet material extracted from written off motor vehicle. The sample metal sheet material was composed of the same thickness throughout the span.

To meet objective one, the Ø16mm conventional electrode, Ø6mm face, shape and size was studied, the mounting position on the upper and lower system (tool post) were also studied on the resistance spot welding machine. The depth of the cooling hole in the lower and upper electrodes was equally studied. The noble idea of creating the annular recess hole at of the centre the tip 45⁰ truncated electrode Ø6mm face, 2.5mm and 4mm depth was conceived and initial designs were made using a computer software. The manufacturing sections were contacted for advice on the possibility of machining the component at minimum costs. The final design was made; the mass property and manufacturing costs were also generated automatically by the computer software. The new electrode (annular recess electrode was machined to spec.

3.1.0 Types of Materials

Gauge 18 (1mm) sample metal sheet material, measuring about 500mm by 1000mm were used. However, gauges 28-30 were not used in the experiment because such gauges are too thin to withstand high welding current and long weld time

3.2.0 Determination of the mechanical properties of the 1mm Sample Metal Sheet (SMS).

The 3 sample metal sheets 1mm thick were prepared into a 50mm by 175mm each. The 3 pieces of the sample material were further prepared to gauge length of 40mm by 20mm width with curvature angle of 35° . The ends of the prepared piece were supported alternately to the jaws of the tensile testing machine using spacers. The machine was set to a maximum load of 25KN and the scale zeroed. The specimens were subjected to maximum peak load and their results recorded. The Universal tensile testing machine used is as shown in figure 3.1



Figure 3.1 Universal Tensile Testing machine (KYU, 2018)

3.2.1 Determination of surface hardness of the 1mm Sample Metal Sheet

A sample space of 3 pieces each measuring 50mm by 50mm were prepared for the Rockwell hardness test. Five random readings were taken from each piece and recorded. The equipment used is as shown in figure 3.2

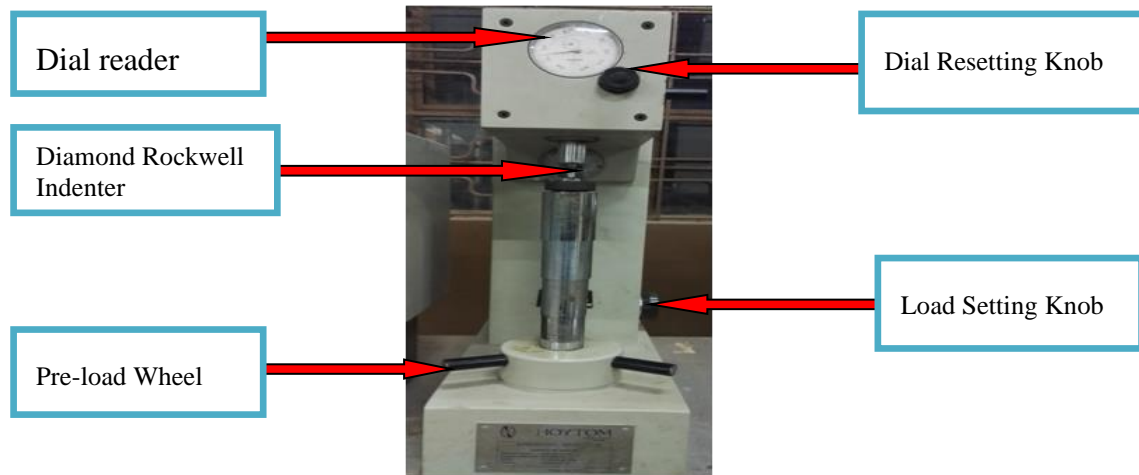


Figure 3.2 Hardness testing machine, Supper Rockwell-Duplex 713-SR, Maquina. No.1233/94 (KYU, 2018)

HRC – Cono 120⁰, indenter was selected on Supper Rockwell-Duplex 713-SR, Maquina **No.1233/94**. The diamond indenter was tested on a standard block with HRC 63.5 and found satisfactory. A pre load of 10kg was set and maximum load of 150kg was also set. The 3 sample specimens as mentioned above were tested at 5 different random points on each specimen surfaces and the best averages recorded. ISO 14271:2011 Standard for resistance spot welding and seam welding was followed

3.2.2 Determination of the chemical composition of the sample metal sheets

A sample space of 5 pieces (Kp1, Kp2, Kp3, Kp4 and Kp5) each measuring about 40mm by 40mm were prepared for the chemical composition test using atomic emission spark spectrometry machine. The results were obtained and the average values calculated.

3.2.3 Determination of the chemical composition of the sample copper electrodes.

A sample space of six pieces (KC1 (1), KC1 (2), KC2 (1), KC2 (2), KC3 (1) and KC3 (2)) measuring Ø16mm by 30mm height each were prepared for the composition test using the atomic emission spark spectrometry machine. Results were equally obtained and the average values determined.

3.3.0 Welding Parameters

To meet objectives II and III the following independent RSW process parameters (a)-(c) below were varied under two categories namely; welding schedule under conventional electrode application and welding schedule under annular recessed electrodes application respectively. The process parameter (d) was varied from the conventional $\varnothing 6\text{mm}$ face, 45° truncated cone electrode to annular recess $<\varnothing 6\text{mm}$ face, $\varnothing 2.5\text{mm}$ annular recess hole, 4mm depth electrode. A sample space of 5 pairs of split sample metal sheet material was chosen for each of the independent process parameters (a) – (d) for the two categories of the schedules.

- a) Welding current
- b) Weld time
- c) Electrode force and
- d) Electrode tip geometry

The tables 3.1-3.6 briefly detail the welding parameters that were varied under the two categories of the welding schedule mentioned above.

Table 3.1 Welding Schedules for Conventional Electrode – under varied welding current; 1cycle = 0.02seconds, 50HZ

Welding Schedule No.	Welding Current (KA)	Welding Times (cycles)	Electrode Force (KN)	Hold time (Cycles)	Squeeze time (Cycles)	Electrode tip size (mm)
1	6	15	4	20	40	6
2	7	15	4	20	40	6
3	8	15	4	20	40	6
4	9	15	4	20	40	6
5	10	15	4	20	40	6

Table 3.1 Welding Schedule for Conventional Electrode – under varied Welding time; 1cycle = 0.02seconds, 50HZ

Welding Schedule No.	Welding Current (KA)	Welding Times (cycles)	Electrode Force (KN)	Hold time (Cycles)	Squeeze time (Cycles)	Electrode tip size (mm)
1	10	5	4	20	40	6
2	10	10	4	20	40	6
3	10	15	4	20	40	6
4	10	20	4	20	40	6
5	10	25	4	20	40	6

Table 3. 2 Welding Schedule for Conventional Electrode – under varied Electrode force; 1cycle = 0.02seconds, 50HZ

Welding Schedule No.	Welding Current (KA)	Welding Times (cycles)	Electrode Force (KN)	Hold time (Cycles)	Squeeze time (Cycles)	Electrode tip size (mm)
1	10	15	2.0	20	40	6
2	10	15	2.5	20	40	6
3	10	15	3.0	20	40	6
4	10	15	3.5	20	40	6
5	10	15	4.0	20	40	6

Table 3.3 Welding Schedule for Annular Recessed Electrode (6mm-2.5mm) – under varied Welding Current; 1cycle = 0.02seconds, 50HZ

Welding Schedule No.	Welding Current (KA)	Welding Times (cycles)	Electrode Force (KN)	Hold time (Cycles)	Squeeze time (Cycles)	Electrode tip size (mm)
1	6	15	4	20	40	3.5
2	7	15	4	20	40	3.5
3	8	15	4	20	40	3.5
4	9	15	4	20	40	3.5
5	10	15	4	20	40	3.5

Table 3.4 Welding Schedule for Annular Recessed Electrode (6mm-2.5mm) – under varied Welding Time; 1cycle = 0.02seconds, 50HZ

Welding Schedule No.	Welding Current (KA)	Welding Times (cycles)	Electrode Force (KN)	Hold time (Cycles)	Squeeze time (Cycles)	Electrode tip size (mm)
1	10	5	4	20	40	3.5
2	10	10	4	20	40	3.5
3	10	15	4	20	40	3.5
4	10	20	4	20	40	3.5
5	10	25	4	20	40	3.5

Table 3.5 Welding Schedule for Annular Recessed Electrode (6mm-2.5mm) – under varied Electrode Force; 1cycle = 0.02seconds, 50HZ

Welding Schedule No.	Welding Current (KA)	Welding Times (cycles)	Electrode Force (KN)	Hold time (Cycles)	Squeeze time (Cycles)	Electrode tip size (mm)
1	10	15	2.0	20	40	3.5
2	10	15	2.5	20	40	3.5
3	10	15	3.0	20	40	3.5
4	10	15	3.5	20	40	3.5
5	10	15	4.0	20	40	3.5

3.3.1 Surface Preparation

Connecting surfaces of the sample metal sheet materials were rendered free of contaminants such as scale, oil, and dirt, to ensure quality welds. Metal thickness is generally not a factor in determining good welds. The sketch drawings of the metal sheets prepared for resistance spot welding process is as shown in figure 3.3. The sample metal sheet material was split into small pieces of 50mm by 175mm making about 60 pairs ready for the two categories of the experimental schedules as detailed in table 3.1-3.6. A sample space grouping of 5pairs of sample metal sheet were chosen for each of the independent variables for the two categories of the schedules. The prepared pieces of the sample metal sheets can be as shown in figure 3.3

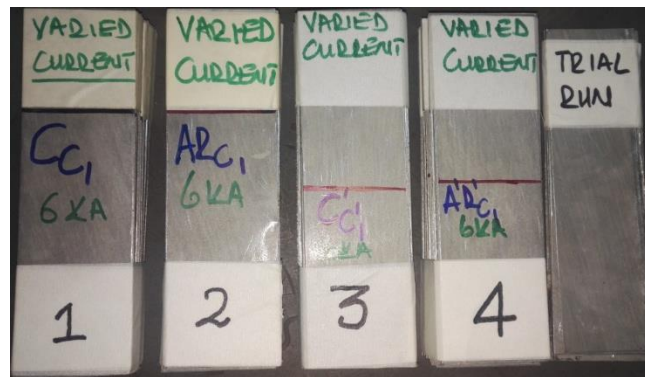


Figure 3.3 Sample Metal Sheet, 1mm thick, 50mm by 175mm, stacked to 5pairs each and 3 bundles per label 1- 4

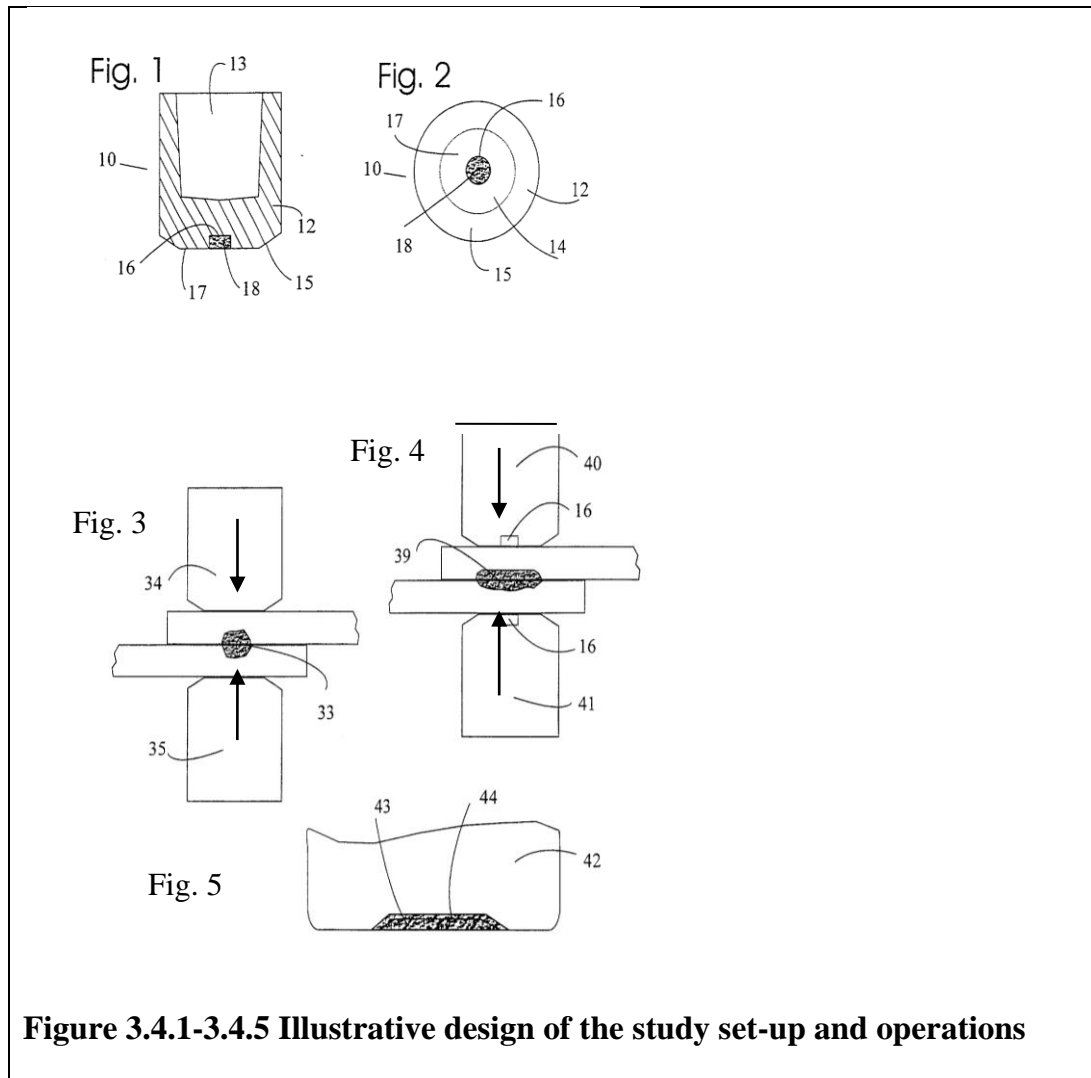
3.4.0 Experimental Features

The $\varnothing 16\text{mm}$ conventional $\varnothing 6\text{mm}$ face electrode was redesigned using a computer software to create annular recess electrode $< \varnothing 6\text{mm}$ face, $\varnothing 2.5\text{mm}$ annular recess hole, 4mm depth and machined to spec. The mass property and cost of manufacture of the new electrode per piece in US dollars were generated and results recorded.

The study was described further, by way of example, with reference to the sketch drawings below, in which:

- i) Figure 3.4.1 is an axial section of a resistance welding electrode embodying the study
- ii) Figure 3.4.2 is an end view of the welding electrode of figure 3.4.1

- iii) Figure 3.4.4 shows a typical weld formed using conventional electrodes and displaying a lower aspect ratio weld nugget concentrated in an area less than that of the contact area of the electrodes
- iv) Figure 3.4.5 shows an alternative embodiment of the study



3.4.1 Detailed Description of the Drawings

Referring to figures 3.4.1 and 3.4.2, a resistance welding electrode 10 comprises a cylindrical body 12 formed with a mounting recess 13 to enable the electrode to be assembled on a weld probe (not shown) of a resistance welding machine (not shown) for spot welding of sheet metal workpieces.

The electrode has a tip 14 for contacting a workpiece. The tip is formed with a chamfered rim 15. In accordance with the study, the tip has a disc shaped recess 16 centered on the axis of the electrode and forming an annular contact surface 17. The recess 15 is filled with an insulating material 18. The material 18 was cemented kaolin mix with clay into the tip or may be formed by ceramic cement applied to the recess 16 and finished flush with the annular contact surface 17.

Figure 3.4.4 shows a symmetrical weld nugget 39, achieved using recessed upper and lower electrodes 40 and 41.

The area of the recess 16 as a proportion of the working area of the tip 14 may be between 25 and 35%, preferably about 35% and the depth is of the order of 4mm.

A further embodiment of the Study is shown in figure 3.4.5 A resistance welding electrode 42 is formed with a shallow central recess 43 of depth about 1mm. Compared to the embodiments described above the recess has a lower aspect ratio. Recess 43 is left unfilled but it is coated, as shown as 44 with an insulating material such as aluminum oxide.

3.5.0 Equipment for the Welding

The equipment (UTO Spot Welder, model S1-6-354, Serial No. 21563, 35KVA rated capacity, 50HZ rated frequency, 6l/min water supply and 255kgf) was used in the spot welding process consisted of tool holders and electrodes as shown in figure 3.5 (a), (b), and (c). The tool holders function as a mechanism to hold the electrodes firmly in place and also support optional water hoses that cool the electrodes during welding. Generally, the basic spot welder consists of a power supply, an energy storage unit (e.g., a capacitor bank), a switch, a welding transformer, and the welding electrodes. In other words, SHOTBOLT, 1988, recounted the minimum requirement for the resistance sport welding equipment as follows;

1. A suitable electric current; this means a good transformer to step down the mains voltage and increase the current flowing.

2. A method of applying pressure between the electrodes either by pneumatics or hydraulic pressure, although spring-loaded mechanism can be used but not common in the contemporary world.
3. A suitable timing device to give the correct sequence and length of events during the RSW

The equipment used in the experiment met the minimum requirement for the RSW as outlined above. Figure 3.5 provide a detailed view of the equipment used in the experiment.

Lower Electrode Post

Dial meter
for reading
force exerted



(a)



(b)



(c)

Figure 3.5 (a) Electrode force control Unit, (b) UTO Spot Welder, and (C) Weld Current and time control unit respectively (Nakawa Voc. Inst., 2018).

The energy storage element allows the welder to deliver high instantaneous power levels. If the power demands are not high, then the energy storage element isn't needed. The switch causes the stored energy to be dumped into the welding transformer. The welding transformer steps down the voltage and steps up the current. An important feature of the transformer is that it reduces the proposed level that the switch must handle. The welding electrodes are part of the transformer's secondary circuit. There is also a control box that manages the switch and may monitor the welding electrode voltage or proposed.

3.5.1 Welding Operations

The welding experiment was performed at Nakawa Vocational Institute. Resistance spot welding operations follows Ohm's law. Principally it comprised of two conductive electrodes, power transformer and the mechanism for pressing the work-pieces together for proper weld joining as illustrated in figure 1. The Ø16mm conventional electrodes Ø6mm face, 45° truncated cone were fitted on the upper and lower electrode mounting posts. The sample metal sheets 1mm thick, measuring 50mm by 175mm were paired and lapped 50mm as shown in figure 3.5 (b) on each other and the first category of the welding schedules table 3.1- 3.3 were carried out and the results recorded.

After completion of the first category of welding operations, the conventional electrodes were dismantled from the tool posts, spot welder reset and the Ø16mm annular recess electrodes < Ø6mm face, 45° truncated cone, Ø2.5mm annular recess hole, 4mm depth were also mounted on the upper and lower electrode mounting posts. The sample metal sheets were prepared as in the first welding schedule and the second categories of the welding schedules table 3.4-3.6 were conducted and results recorded.

The equipment is designed and operates according to Ohm's law.

- i) **I** is the current in amperes, **E** is the voltage in volts, and **R** is the resistance of the material in ohms. The total energy is expressed by the formula:

$$\text{Energy} = \mathbf{I \times E \times T} \dots\dots\dots \mathbf{3.5.1(i)}$$

in which **T** is the time in seconds during which current flows in the circuit.

- ii) Combining these two equations gives **H** (heat energy) = **I² x R x T**.

For practical reasons a factor which relates to heat losses should be included; therefore, the actual resistance welding formula is

$$\mathbf{H=I^2 \times R \times T \times K} \dots\dots\dots \mathbf{3.5.1(ii)}$$

In this formula, **I** = current squared in amperes, **R** is the resistance of the work in ohms, **T** is the time of current flow in seconds, and **K** represents the heat losses through radiation and conduction.

3.6.0 Testing the Weld Strengths and Reliability

Non Destructive and Destructive tests were carried out respectively.

3.6.1 Non-destructive Testing of the Weld Nuggets Integrity

The Magnetic Particle Inspection (MPI) techniques were used during the testing process. It was the most suitable for the test due to its simplicity, and the small thickness of the sample material.

3.6.2 Information required prior to testing

During the execution of the non-destructive testing, the following procedures were adopted, namely;

- a) Specific testing procedure
- b) Extent of testing
- c) Testing plan
- d) Testing equipment
- e) Calibration of the equipment
- f) Calibration of blocks
- g) Acceptance level

As a rule of thumb, the following information below was retrieved from; the literature reviews. These are;

- a) Grade of the parent material was determined by composition tests of the sample metal sheet
- b) Welding parameters and conditions used to make the weld were, known as weld current, weld time, electrode force and the electrode geometry. Location and extent of welds to be tested
- c) Weld surface geometry- under conventional electrode and annular recessed electrode respectively.

This method involves testing of materials for surface or internal flaws or metallurgical condition, without interfering with the material or its suitability for service. These are the general rules on non-destructive testing of welds for metallic materials;

- i) BS EN ISO 17635 Non-destructive testing of welds. General rules for metallic materials
- ii) BS EN ISO 17637 Non-destructive testing of welds. Visual inspection/testing of fusion-welded joints.

3.6.3 Magnetic Particle Inspection

Magnetic Particle Inspection (MPI) is a process for detecting surface and slightly subsurface discontinuities in ferromagnetic materials such as steel, nickel and other alloys. MPI can detect imperfections just below the surface, but its sensitivity tends to diminish with depth. The MPI was carried out at Buhimba Technical College – Hoima district. In a sample space of 5, 3 pieces were selected from each of the group based on the independent variables identified in of the two categories of the weld schedules (under conventional electrodes and annular recess electrodes respectively). Magnetic Yoke (Magnaflux, Model Y-7 AC/DC, 220v-50HZ - 1PH, Max 2.5A) was used figure 3.6. Standard pre-test verification was done as shown in figure 3.7.

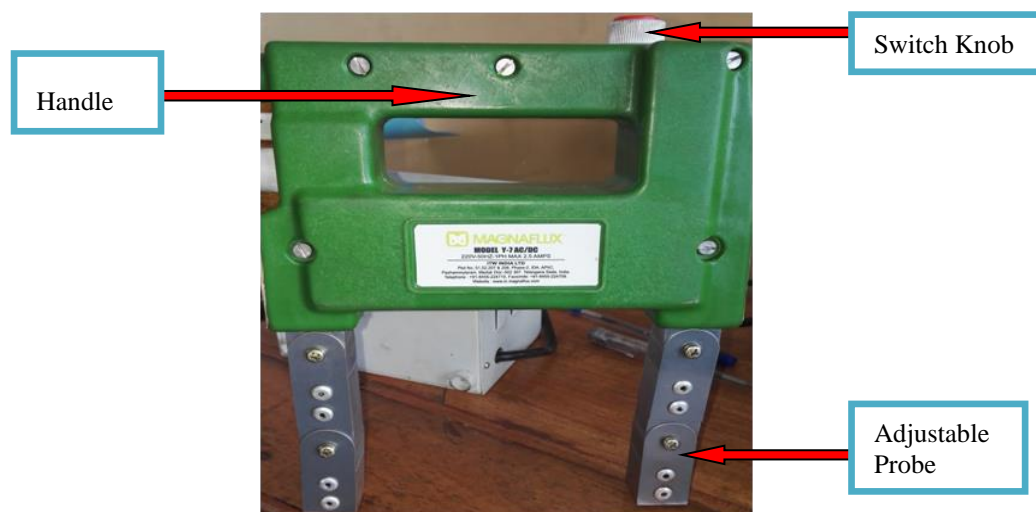


Figure 3.6 Magnetic Yoke, Y-7 AC/DC (Buhimba Tech. Col., 2018)

The magnetic yoke in figure 3.6 is equipped with articulated legs capable of being adjusted inwards or outwards depending on the point to be inspected, although it has a range of about 25- 150mm

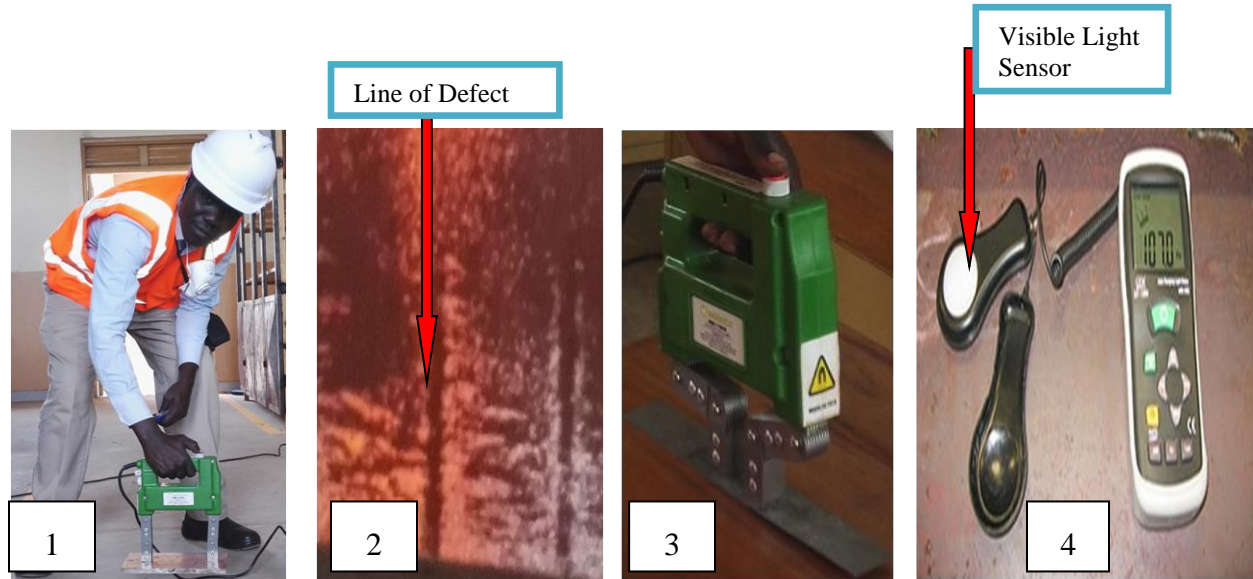


Figure 3.7 Magnetic Strength Tests (1), Magnetic Flux Strength Test (2), Magnetic Test of Sample (3), Minimum Light Intensity Test (4) (Buhimba Tech. Col., 2018)

The magnetic pull force was tested on a standard 5kg plate in AC mode and was capable of lifting as seen in figure 3.7, (1). The magnetic flux was spread across a standard piece of metal strip with line flaws beneath the surface and subsequently powered in AC mode and the magnetic flux was observe lining according to the flaws beneath the surface as seen in figure 3.7 (2). The articulated legs of the magnetic yoke were adjusted to about 25mm to enable concentration of the magnetic strength around the welded joint and powered in AC mode, and resulted into the lifting of the sample material being indicative of a ferromagnetic material as seen in figure 3.7 (3). Lastly the minimum light intensity was also tested on the surface of the sample material and an intensity of over 1000lux (visible light) was observed, indicative of enough light in the room as seen in figure 3.7 (4). Three welded samples under the varied current, weld time and electrode force from each of the two categories of schedules were selected for the test.

On the completion of pre-test requirement for the equipment, the tests were carried out according to the standard procedures mention in (i) and (ii) below;

- i)* BS EN ISO 17638 Non-destructive testing of welds. Magnetic particle testing
- ii)* BS EN ISO 23278 Non-destructive testing of welds. Magnetic Particle testing of welds. Acceptance levels.

Observations from the tests were recorded for further analysis..

3.6.4 Destructive Testing of the Weld Nugget Integrity

The Destructive Testing (DT) of the weld nugget integrity was carried out at Kyambogo University, Materials lab. DT is a cheaper method of inspecting the strength of the welded joints or nuggets in the case of resistance spot welding (RSW). In this method the tests were performed in compliance with:

- i)* BS EN ISO 5173 Destructive tests on welds in metallic materials, Bend Tests
- ii)* BS EN ISO 9015 parts 1 & 2 Destructive tests on welds in metallic materials. Hardness Testing
- iii)* BS EN ISO 9018 Destructive tests on welds in metallic materials. Tensile test on Cruciform and tapped joints
- iv)* BS EN ISO 1764 1-2 Destructive tests on welds in metallic materials. Hot cracking tests for weldments, i.e. Self-Restraint Tests

3.6.5 Determination of tensile shear strength of the welded joints under the two welding schedules.

This test was conducted to assess the strength and ductility of the spot welded joint formed as a result of using conventional and annular recess electrodes respectively. In the tensile shear test, a spot welded joint in lap joint configuration was pulled apart in tension on a universal tensile testing machine (UTM), figure 3.1. Figure 3.8 and 3.9 illustrates the sketch drawings of the sheet metals preparation and lap joining ready for the spot welding and tensile shear test respectively. 15 welded specimens from the each welding schedules. The welded pieces measuring 50mm wide by 300mm long (figure 3.8) were then each subjected

to tensile shear pull between the jaws of the tensile machine (figure 3.1) and maximum load recorded for each category of the welding schedules. The results were tabulated for analysis.

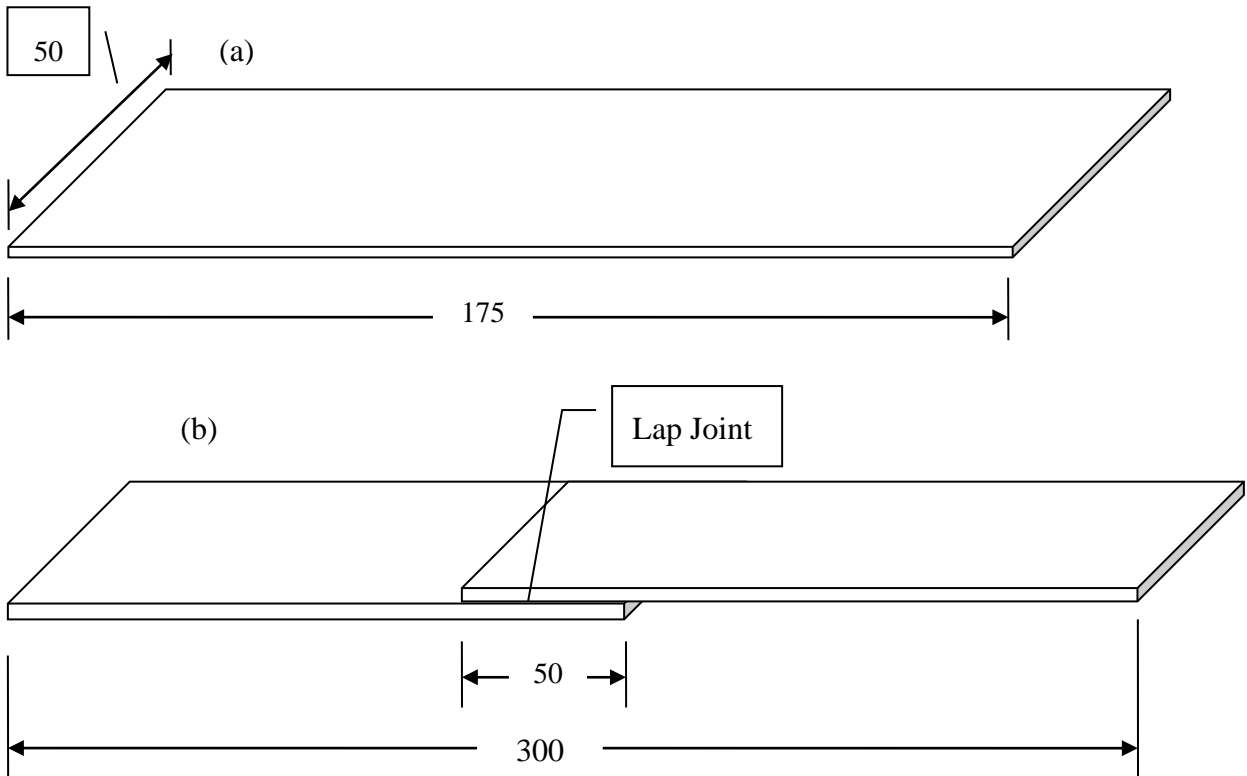


Figure 3.8 Preparation of the metal sheets (a) to form lap joint (b) ready for RSW

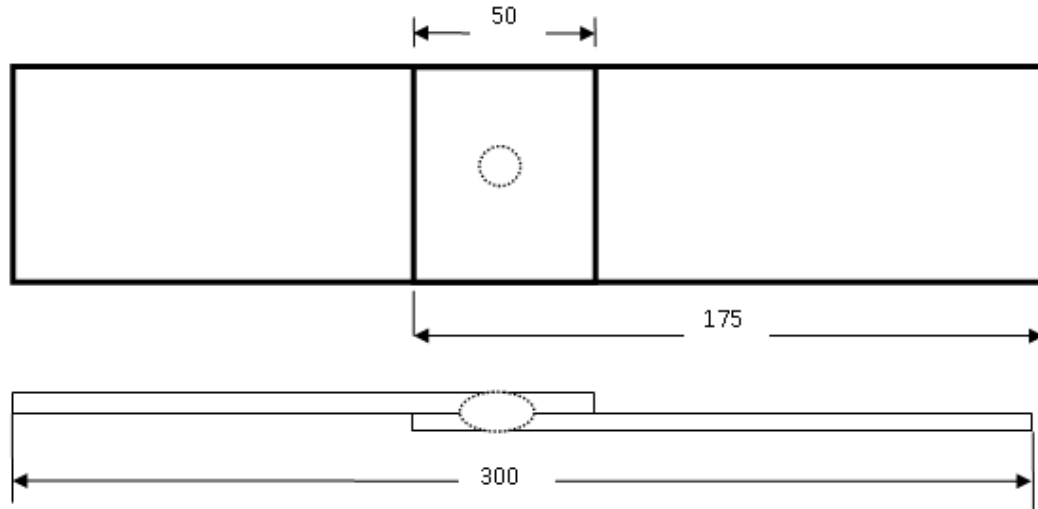


Figure 3.9 Specimen descriptions for the tensile shear test.

3.6.6 Peel Test for welded joints under conventional and annular recess electrodes.

Peel test was performed on the shop floor to determine mainly qualitative information about the strength of the joint as well as the size of the nugget formed (Hernandez, 2008, Zhang and Senkara, 2006). The process of peel testing was facilitated by using a manually fabricated roller similar to the one in figure 3.10. The minor and major button diameter of the peeled samples measured to attain an average button diameter as shown in figure 3.11. Specimen dimensions and procedures followed were as per ISO 14270: 2000 and ISO 10447: 2006 Standards.

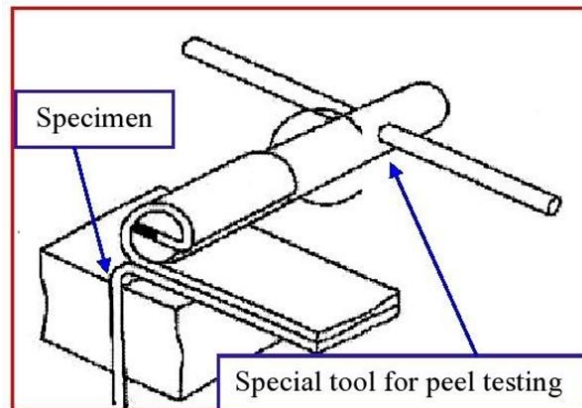


Figure 3.10 Peel Testing Process (Zhang,H.and Senkara,J., 2006)

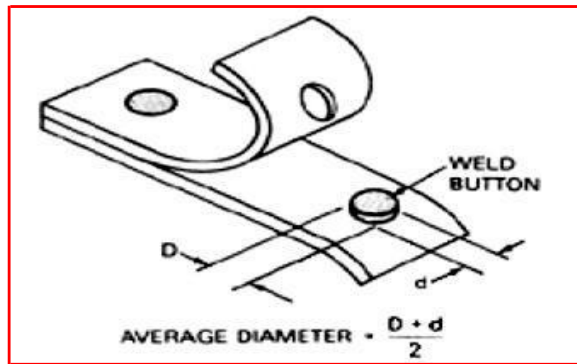


Figure 3.11 Measurement of nugget diameter after peel test (Zhang,H.and Senkara,J., 2006)

Three samples were selected from each category of the welded metal sheets. The samples were each cut cross sectional to expose the joints. The cross section joints were each extracted rendering 10mm by 25mm pieces. The pieces were then polished in sequence on a grinder polisher equipped with No. 120, 320, 480 sanding papers respectively and finally polished of micro-cloth d with 0.05μ Gama Alumina powder applied on. The polisher grinder was powered between the ranges of 100-450rpm. The polish surfaces were then etched in a solution of 98% ethanol and 2% nitric acid. The etched surfaces were each viewed on metallurgical microscope with magnification of x100, x200, x400, x500, x600 and x800 and recorded. These processes were done at Kyambogo University, Materials Lab., with the assistance of a senior technician.

However, a second microstructure analyses on the same specimens were conducted at Makerere University, Materials Lab., and micrographs taken. Magnification ranges of x100, x200, x400, x500 and x800 were used. Figure 3.12 and 3.13 present the analysis carried out at the two institutions respectively.

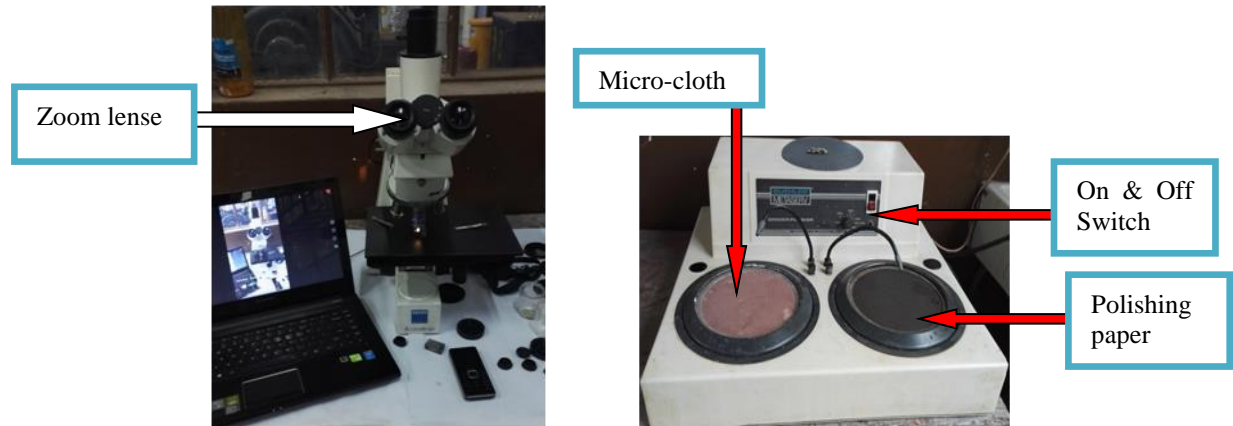


Figure 3.12 Metallurgical Microscopes (a) and Grinder Polisher (b) (KYU, 2018)



Figure 3.13 Metallurgical Microscopes (MUK, 2018)

The application of Solver in Excel for the Analysis of Variance (ANOVA) was effected. Excel Solver, a statistical software package was used for linear regressions analysis to determine the correlation that exists between the predictor variable and the response variable. Statistical Regression analysis provides an equation that explains the nature and relationship between the predictor variables (independent variable) and the response variable (dependent variable). The linear regression takes form;

$$Y = aX + b \dots \dots \dots 3.7 (i)$$

Using the DRYMIX acronym (Carlson Robert, 2006) to define equation 3.7 (i) above,

D= the dependent variable,

R = the responding variable,

Y = the axis on which the dependent or responding variable is graphed (the vertical axis), and

M = the manipulated variable or the one that is changed in an experiment,

I = the independent variable, and

X = the axis on which the independent or manipulated variable is graphed (the horizontal axis).

a = coefficient,

b = constant.

In this particular research study, dependent variables (tensile shear strength and nugget diameter) were graphed on to the independent variables (weld current, weld time, electrode force) for both the conventional and annular recess electrodes for purposes of performance analysis and comparison between the old tool (conventional electrode) and the new proposed tool (annular recess electrode) as guided by the DRYMIX acronym (Carlson Robert, 2006, Dodge, Y. 2003, and Everitt, B.S. 2002).

From the linear regression analysis, some of the inferences were drawn based on the output of p-values and coefficients. The p-values helped to determine whether the relationships that were observed in the sample also existed in the larger population.

The p-value for each independent variable tests the null hypothesis that the variable has no correlation with the dependent variable. If there is no correlation, there is no association between the changes in the independent variable and the shifts in the dependent variable. In Therefore, there is insufficient evidence to conclude that there is effect at the population level. However, if the p-value for a variable is less than the significance level (0.05), the sample data provide enough evidence to reject the null hypothesis for the entire population. The data thus, favor the hypothesis that there is a non-zero correlation. This means, changes in the independent variable are associated with changes in the response at the population level. This therefore leads us to infer that the variable is statistically significant and probably a worthwhile addition to the regression model at hand. On the other hand, a p-value that is greater than the significance level (0.05) indicates that there is insufficient evidence in the sample to conclude that a non-zero correlation exists.

The correlation coefficient **r** is defined as a measure of the degree of linear correlation existing between the dependent variable Y and the independent variable X. The coefficient **r** is mathematically written as;

$$r = \frac{\sum_{i=1}^n (X_i - \bar{X})(Y_i - \bar{Y})}{(n-1)S_X S_Y} \dots\dots\dots 3.7 \text{ (ii)}$$

$$r = \frac{\overline{XY} - \bar{X}\bar{Y}}{\sqrt{(\bar{X}^2 - \bar{X}^2)(\bar{Y}^2 - \bar{Y}^2)}} \dots\dots\dots 3.7 \text{ (iii)}$$

$$r = a S_X / S_Y \dots\dots\dots 3.7 \text{ (iv)}$$

The coefficient of determination **r²** is given mathematically as;

$$r^2 = \frac{\text{variation due to regression}}{\text{total variation}} \dots\dots\dots 3.7 \text{ (v)}$$

$$r^2 = \frac{SSR}{SST} \dots\dots\dots 3.7 \text{ (vi)}$$

The value of r lies between -1 and +1, thus a positive coefficient indicates that as the value of the independent variable increases, the mean of the dependent variable also tends to increase while a negative coefficient suggests that as the independent variable increases, the dependent variable tends to decrease. Hence analysis of the data in this research study was based on the p-value, coefficient of determination **r²** and using confidence level of 95%

CHAPTER FOUR

This chapter discussed the outcome of the experiments and tests that were conducted to meet the specific objectives set in chapter one and provided logical scientific interpretation to all the observations made using excel solver, a software in the excel spread sheet.

4.0 RESULTS AND DISCUSSION

This section covered the outputs from the preliminary tests (tensile, hardness, and chemical composition) on the 1mm sample metal sheet, chemical composition of Ø16mm sample copper rods, and design and manufacture of the annular recess electrode respectively, followed by outputs from experiments -RSW operations, Non destructive tests (i.e. magnetic particle inspections (MPI)) ,and lastly the destructive tests (tensile shear test, peel test and microstructure analysis of the welded joints using the conventional electrodes and annular recess electrodes) and analysis of each category.

4.1 Mechanical Properties of the 1mm Sample Metal Sheet (SMS)

The mechanical properties of the 1mm sample metal sheet were calculated from the average values obtained from the 3 sample category prepared for both the tensile test and hardness tests respectively. The properties considered in the two tests were ultimate tensile strength (UTS), percentage elongation and hardness. The values of the selected mechanical properties are as shown in table 4.1

Table 4.1 Mechanical Properties of the 1mm Sample Sheet Metal

S/N	Ultimate Tensile Strength (KN)	Percentage Elongation (%)	Vickers Hardness
1	2400	32	HRC88.3

The 1mm sample metal sheet yielded calculated values of ultimate strength of 2400KN, percentage elongation of 32% and the hardness value of HRC88.3 which is indicative of a ductile material.

4.2 Chemical Composition of 1mm Sample Metal Sheet (SMS)

The chemical composition of the N0.5, 1mm sample metal sheets (KP1-KP5) were determined using the spark emission spectrometry and the calculated average results are as displayed in table 4.2.

Table 4.2 Chemical Composition of the 1mm Sample Sheet Metal (wt %)

C	Si	Mn	P	S	Cr	Mo	Ni	Al	Co	Cu	Nb
0.0305	0.0110	0.213	0.0114	0.0111	0.0460	0.0010	0.0015	0.0388	0.0033	0.0472	0.0019
Ti	V	W	Pb	Sn	AS	Zr	Bi	Ca	Ce	Sb	Se
0.0002	0.0052	0.0050	0.0018	0.0032	0.0076	0.0018	0.0010	0.0001	0.0060	0.0012	0.0035
Te	Ta	B	Zn	La	N	Fe	CEQ				
0.0017	0.0070	0.0013	0.0029	0.0003	0.0024	99.5	0.0797				

The chemical composition of the 1mm sample metal sheet by weight as observed from table 4.2 is majorly 99.5%wt Fe and 0.213%wtMn. This confirmed that the 1mm sample metal sheet as alloy ferrite steel with ferromagnetic properties. Detailed results for each of the selected samples KP1-KP5 tested appendix 1-5

4.3 Chemical Composition of the 3 Ø16mm Sample Copper Rods (SCR)

The chemical composition of the No. 3, Ø16mm sample copper rods, each bearing No. 2 samples (KC1(1), KC1(2), KC2(1), KC(2), KC3(1) and KC3(2)) were determined using the

spark emission spectrometry and the average results of all the samples (KC1(1), KC1(2), KC2(1), KC(2), KC3(1) and KC3(2)) were equally displayed as shown in table 4.3.

Table 4.3 Chemical Composition of the Sample Copper rod (w %)

C	Si	Mn	P	S	Cr	Mo	Ni	Al	Co	Cu	Nb
0.0458	0.0122	0.0141	0.0166	0.0099	0.0052	0.0890	0.0520	0.0021	0.0742	>8.0	0.0408
Ti	V	W	Pb	Sn	Mg	As	Zr	Bi	Ca	Ce	Sb
0.0333	0.0047	0.0617	0.0261	0.0097	0.0069	0.0110	0.0033	0.0040	0.0007	0.0131	0.151
Se	Te	Ta	B	Zn	La	N					
0.0010	0.0800	>0.760	0.0015	>0.045	0.0043	0.302					

The chemical composition of the 3 Ø16mm sample copper rods by weight as observed from table 4.3 is majorly >8.0%wt Cu and >0.7600%wt Ta. This confirmed that the 3 Ø16mm sample copper rods as copper alloy with the greatest percent being copper and highly thermo-conductive. Detailed results for each of the selected samples (KC1 (1), KC1 (2), KC2 (1), KC (2), KC3 (1) and KC3 (2)) tested are shown in appendix 6-11

4.4.0 Design of Annular Recess Electrode

The design of the new novel electrode was accomplished with the use of a computer modeling software (solidworks 2015). The 3D model and longitudinal 3D sectional views of the annular recess electrode was generated as showed in figure 4.1(a) and (b) Detailed part drawing that enabled machining to spec. as is shown in appendix 12. The associated mass properties of the new novel electrode were also generated automatically to provide in-depth description on the physical properties based on the design specification.

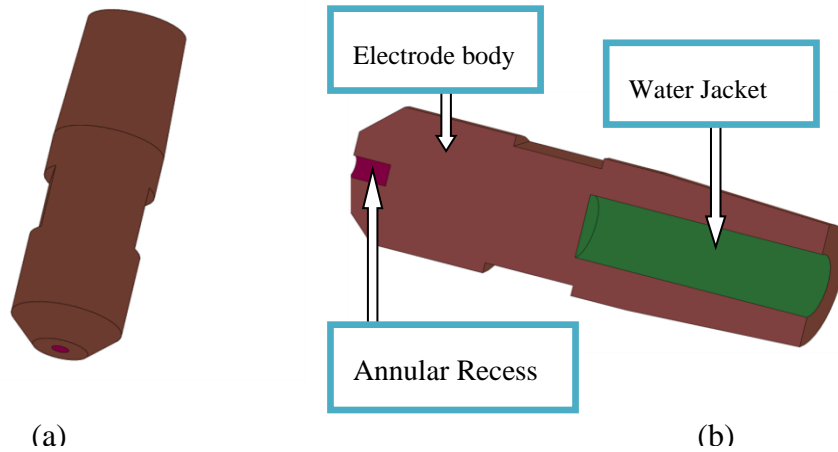


Figure 4.13 (a) 3D view of Annular Recess Electrode, (b) cross sectional view

The mass property of this new electrode was generated as described below;

4.4.1 Mass Properties of Annular Recess Electrode Material

Mass properties of ELECTRODE DESIGN

Configuration: Default

Coordinate system: -- default --

Density = 0.0089 grams per cubic millimeter

Mass = 72.2 grams

Volume = 8.12e+003 cubic millimeters

Surface area = 3.31e+003 square millimeters

Center of mass: (millimeters)

X = -6.08

Y = 0

Z = 0

Principal axes of inertia and principal moments of inertia: (grams * square millimeters)

Taken at the center of mass.

$I_x = (1, 0, 0)$ $P_x = 2.39e+003$

$I_y = (0, 0, -1)$ $P_y = 1.46e+004$

$I_z = (0, 1, 0)$ $P_z = 1.47e+004$

Moments of inertia: (grams * square millimeters)

Taken at the center of mass and aligned with the output coordinate system.

$$\begin{array}{lll} L_{xx} = 2.39e+003 & L_{xy} = 0 & L_{xz} = 0 \\ L_{yx} = 0 & L_{yy} = 1.47e+004 & L_{yz} = 0 \\ L_{zx} = 0 & L_{zy} = 0 & L_{zz} = 1.46e+004 \end{array}$$

Moments of inertia: (grams * square millimeters)

Taken at the output coordinate system.

$$\begin{array}{lll} I_{xx} = 2.39e+003 & I_{xy} = 0 & I_{xz} = 0 \\ I_{yx} = 0 & I_{yy} = 1.73e+004 & I_{yz} = 0 \\ I_{zx} = 0 & I_{zy} = 0 & I_{zz} = 1.73e+004 \end{array}$$

4.4.2 The Costing Report for the Manufacture of the New Novel Electrode

The costs report in US dollars, associated with the manufacture of this new annular recess electrode per piece was generated automatically by the design software, from the design and is detailed in appendix 13. However, this cost may vary from one manufacturer to the other or from one country to another.

4.5.0 Machining to Spec. the New Novel Electrode.

The detailed part drawing in appendix12 was used. EachØ16mmcopper rod was set on a three jaw lathe machine and the machining was done to the spec. followed by drilling of the annular recess hole centrally on a Ø6mm face tip. The manufactured new novel electrode is Ø16mmmain diameter, 45⁰ truncated Ø6mmface tips, Ø2.5mm annular recess hole, 4mm depth as shown in figure 4.2. No. 4 pieces were produced.

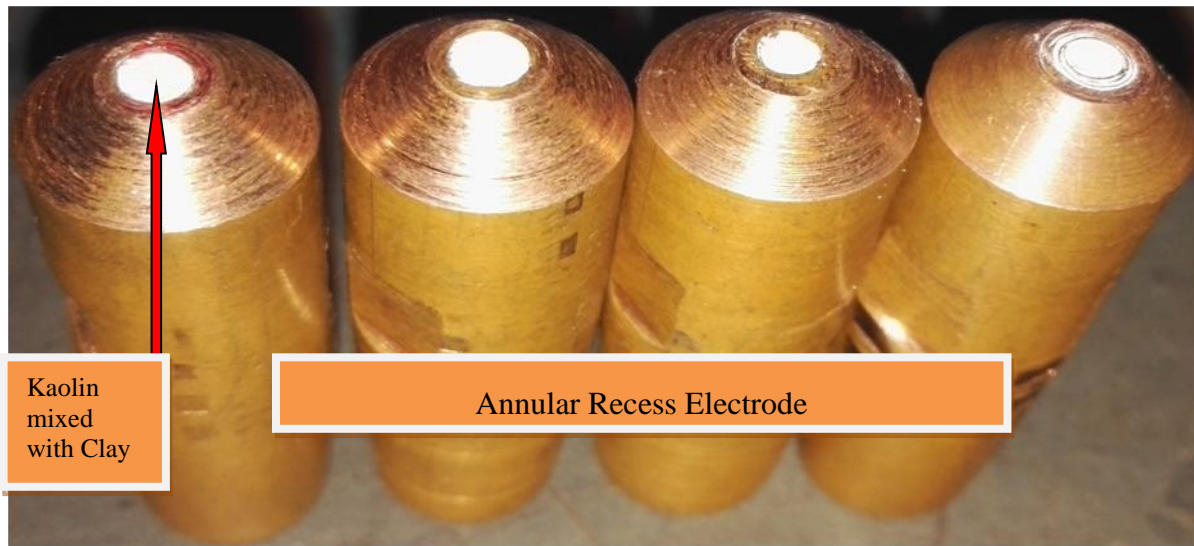


Figure 4.2 Annular Recess Electrode, filled with kaolin and mixed with clay

4.5.1 Machining to Spec. the Conventional Electrode.

The machining to spec. of the conventional electrode was tailored from the design of the annular recess electrode with the exclusion of the drilling operations. No. 4 pieces were also produced as shown in figure 4.3; ready for RSW research operations.

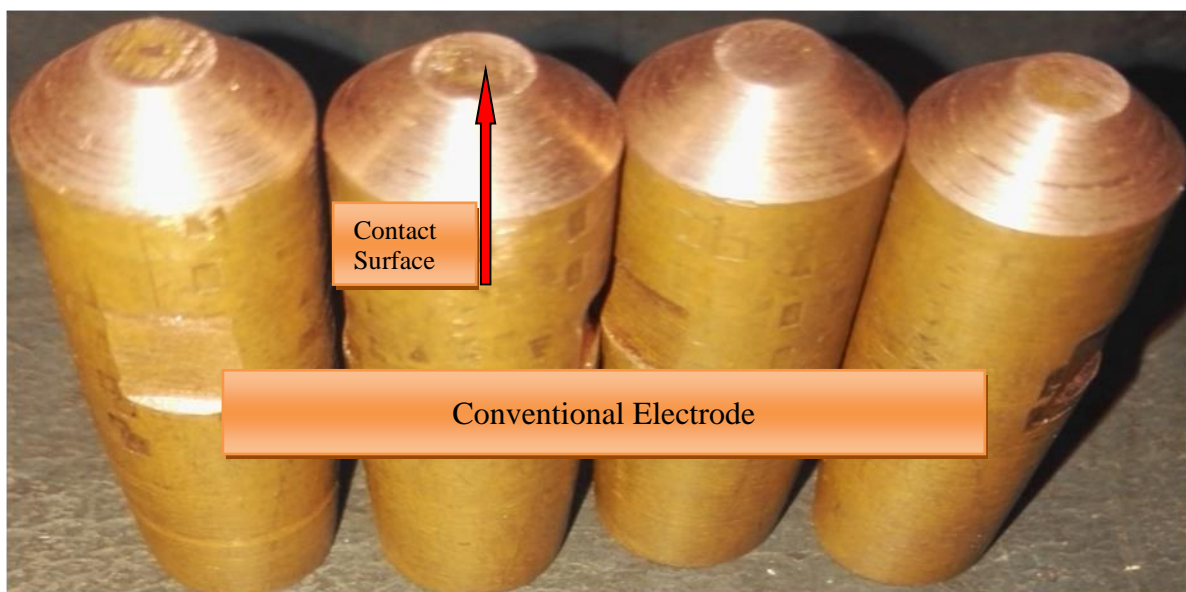
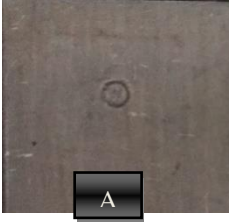

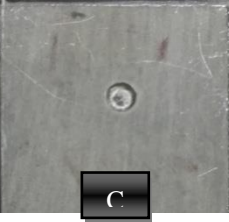


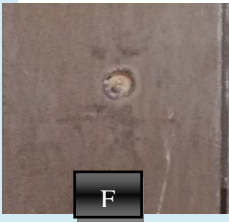

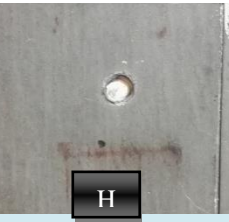

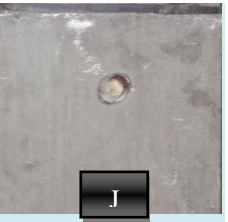
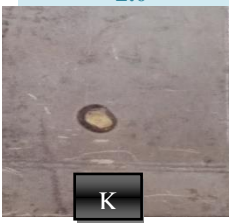




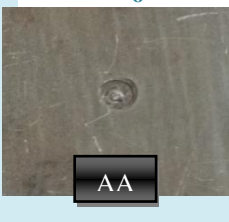
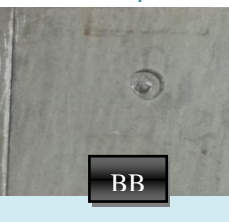






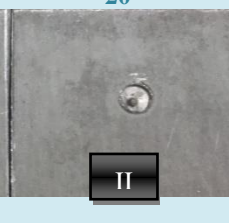




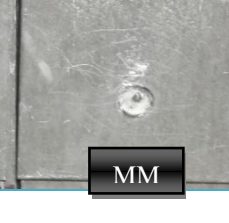
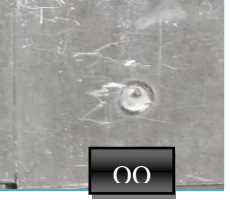


Figure 4.3 Conventional Electrodes

4.6 Results of RSW Experiments with Conventional Electrodes and Annular Recess Electrodes.

The outcomes of the RSW experiments with both the conventional and annular recess electrodes were recorded as shown in table 4.4;

Table 4.4 RSW Results when Conventional and Annular Recess Electrodes were used respectively.

Outcome of both Conventional and Annular Recess Electrodes application					
Weld Current(KA)	6	7	8	9	10
Conventional Electrodes used					
	A	B	C	D	E
Weld Time (CYCLES)	5	10	15	20	25
Conventional Electrodes used					
	F	G	H	I	J
Electrode Force (KN)	2.0	2.5	3.0	3.5	4.0
Conventional Electrodes used					
	K	L	N	M	O
Weld Current(KA)	6	7	8	9	10
Annular Recess Electrodes used					
	AA	BB	CC	DD	EE
Weld Time (CYCLES)	5	10	15	20	25
Annular Recess Electrodes used					
	FF	GG	HH	II	JJ
Electrode Force (KN)	2.0	2.5	3.0	3.5	4.0
Annular Recess Electrodes used					
	KK	LL	NN	MM	OO

4.7 Analysis of RSW Results when Conventional and Annular Recess Electrodes were used respectively.



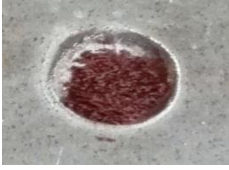
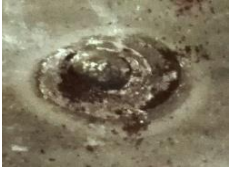
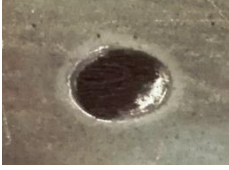



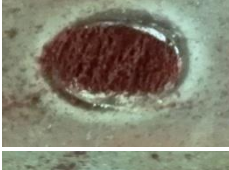
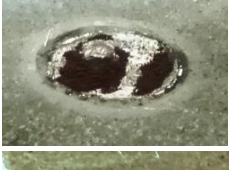

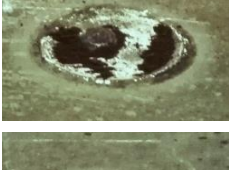

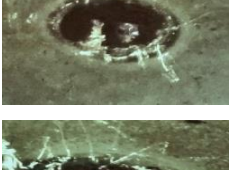
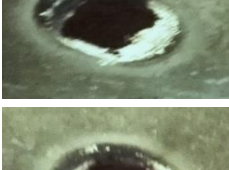
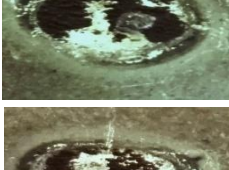
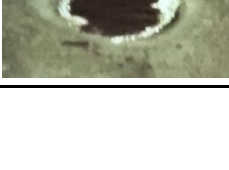

From table 4.4 (A – O), conventional electrodes were used for joining them under the three parameters of weld current, weld time and electrode force. Expulsions were observed when current increased to 9KA and 10KA as showed in table 4.4 (D and E respectively) while the weld time and electrode force were kept constant at 15Cycles and 4KN respectively causing high indentation. This trend was further observed in the subsequent weld operations as current and weld time were maintained at 10KA and 15Cycles as shown in table 4.4 (F – O).

However, on the other hand, no expulsions were observed when the new novel electrodes were used in the weld operations as shown in table 4.4 (AA – NN) except minor expulsions were noticed at electrode force of 3.5KN and 4KN respectively as shown in table 4.4 (MM – OO) with low level of indentation. Furthermore, due to the introduction of the annular recess on the electrode face diameter, and due to the weak bonding of a mixture of Kaolin and clay with the electrode material, approximately 0.65mm noodle shaped like weld beads were formed nearly at the centre of the RSW joints side by sides for all the samples that were welded using the new novel electrodes. This is clearly indicative of the stress relieving at the weld joints taking the shape of the annular recess on the face of the novel electrode table 4.4 (AA – OO).

4.8 Results of Magnetic Particle Inspection

The welded joints made under conventional electrodes and annular recess electrodes were investigated respectively for the joint integrity using the magnetic yoke and magnetic iron fillings. The results of this test were displayed as shown in table 4.5

Table 4.5 Photographic Magnetic Test (MT) results for Conventional and Annular Recess Electrodes respectively

Variable Parameters		Conventional Electrodes	Spread %	Annular Recess Electrodes	Spread %
Weld Current (KA)	6		75		45
	7		80		5
	8		85		4
Weld Time (Cycles)	5		70		55
	10		85		35
	15		60		25
Electrode Force (KN)	2.0		55		45
	2.5		40		30
	3.0		65		10

4.9 Analysis of the Magnetic Particle Inspection Test Results

From table 4.5, when the welded joints made under varied current, and annular recess electrode were tested for the weld integrity using the magnetic particle inspection, the magnetic particles were observed spread more at the edge of the joint than at the centre of the weld joints, and further more the particles concentration reduced drastically as current increased from 6KA to 8KA for the selected sample sheet. On the other hand the welded joints made under varied current and conventional electrode, showed more intense magnetic particle concentration both at the edges of the joint and centre-wise covering $\frac{3}{4}$ of the weld joint areas. The concentration of the magnetic particles around the joints increased as current varied from 6KA to 8KA for the selected samples. From the principle of magnetism, presence of magnetic particles on a surface during the test when the magnetic yoke is powered is indicative of a surface flaws causing opposite magnetic poles and thus reversing the magnetic field at that point. The shape and size of the flaws may vary from one article to the other and therefore the configuration formed by the magnetic particles on the test piece surface takes the shape and the form of the defects. However, multiple voids and crack concentration within a test piece area being tested may present intricate shapes and thus the magnetic particles tend to adopt the defect shape once the test piece is powered on a magnetic yoke. Absence of the magnetic particles on a surface being tested on the other hand is indicative of a sound (continuous joint/uniform material flow) weld joint although it is not a warranty for strength of the weld joint either.

From the analysis above, the presence of high concentration of the magnetic particles around that centers and edges of the welded joint made under conventional electrode confirms the presence of defects around the centers and edges of the weld joint. The low concentration of magnetic particles around the edges of the welded joint made under annular recess electrode indicates a shift of the defect line from the centre of the weld joint to the edge which tends to diminish as the current increased from 6KA to 8KA. By way of comparison, the welded joint made under the annular recess electrode presented a more sound joint integrity than the joint welded using the conventional electrode as noted in the analysis above. Destructive tests of

the welded joints under the two schedules were carried out to further characterize the property of the weld joints with a view that one of them may perform better.

4.9.1 Results of the Tensile Shear Strength of Welded Joints made under Conventional and Annular Recess Electrode

With the increasing load, the nugget will have a tendency to rotate. When sufficient value of load is reached, fracture initiates at one point near the nugget, and then starts propagating around the nugget, till the joint is separated. Tensile shear testing provides information on the ultimate strength and failure mode of RSW joints. Failure is primarily a factor of weld diameter, but can also be influenced by expulsion, defects, and heterogeneous microstructures. The results of the test were presented as shown in table 4.6

Table 4.6 Results of Tensile Shear Strength of Welded Joint Vs Weld Current

Max. Load (KN) - Using Conventional Electrodes	Max. Load (KN) - Using Annular Recess Electrodes	Current (KA)
3	3.1	6
4.9	3.3	7
4.8	4	8
4.6	4.1	9
3.3	4.4	10

4.9.2 Analysis of Effect of Weld Current on Tensile Shear Strength for Weld Joint made using Conventional and Annular Recess Electrodes respectively

From table 4.6, the tensile shear strength of the weld joints made using annular recess electrode increased from 3.1KN to 4.4KN with corresponding increase in the weld current from 6KA to 10KA. However, the weld joints made using the conventional electrode showed a marked decrease in the tensile strength from 4.9KN to 3.3KN with corresponding increase in the weld current from 6KN to 10KN. Figure 4.4 provide the graphical analysis of the characteristic behavior of the weld joints under the two schedules of the conventional and annular recess electrodes respectively. This observation may further be explained by the fact as the current intensity increase from 6KA to 10KA, the work being joint using the

conventional electrodes melts to the extent possible to allow joining but due to the absence of the room to relieving the stress during the application of the fusion force, part of the material is lost in the expulsion and indentation leading to the formation of a weak joint at higher current intensity. The provision of a annular recess hole on the electrode face, yielded rooms at the faying interfaces for the stress to be absorbed and the heat energy dissipated to the annular recess geometry thus forming weld nugget of bigger diameter, hence improving strength welded joints. The trend therefore shows progressive improvement on the weld joint strength using the new novel electrodes.

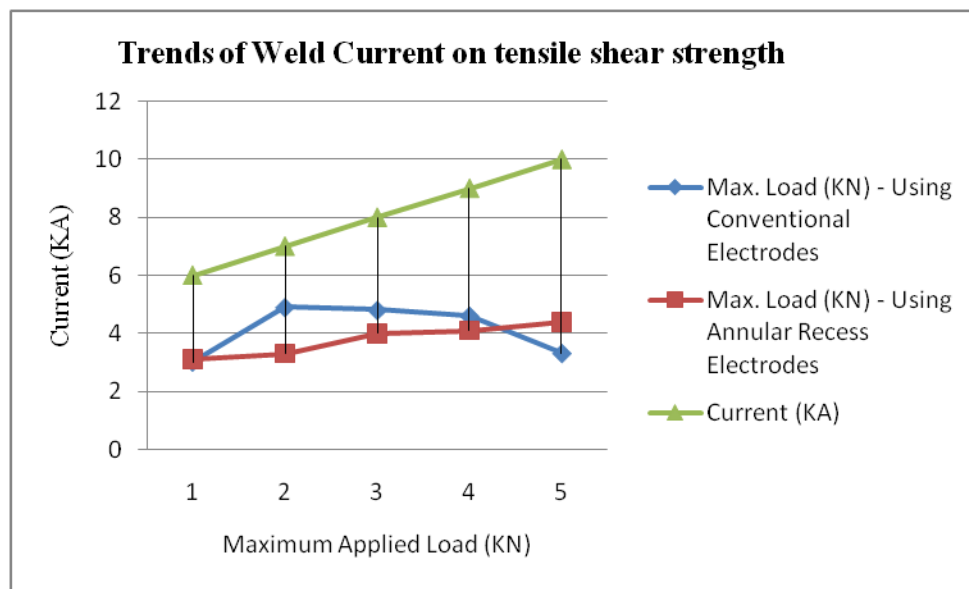


Figure 4.4 Analysis of Effect of Weld Current on Tensile Shear Strength

Table 4.7 Regression Analysis of Weld Current Vs Tensile Shear Strength of RSW joint - when Conventional and Annular Recess Electrodes were used respectively.

Statistical Analysis	Regression Coefficient				
	a	b	r^2	p-value	95%Confidence Level
Conventional Electrodes application	0.03	3.80	0.0028	0.9328	-1.0125 - 1.0725
Annular Recess Electrodes application	0.34	1.06	0.9414	0.0061	0.1841 - 0.4959

The p-value = 0.93 under the conventional electrode application in table 4.7 above is greater than the significant level of 0.05. Therefore it indicates the fact that there is insufficient evidence in the sample dependent variable to conclude that a non – zero correlation exists between the weld current and the tensile shear strength. This can further be explained by the fact that only 0.28% of the tensile shear strength sample data can be explained by the linear relationship between the weld current and tensile shear strength. In other words, the tensile shear, under the application of the conventional electrodes, in this particular case was not statistically significant because it's P-value = 0.93 > significant level of 0.05. However, the p-value = 0.0061 under the new novel electrodes (annular recess electrodes) application, is less than the significant level of 0.05. This means that the sample data provide enough evidence to reject the null hypothesis for the entire population. Therefore the sample data favors the hypothesis that there is a non-zero correlation between the tensile shear strength and the weld current under the annular recess electrode application. Thus the changes in the weld current are associated with tensile shear strength change, which requires further research. This is further strengthened by the fact that 94% of the variables in the dependent variable can be explained by the linear relationship between the weld current and tensile shear strength. Details of this regression analysis is in appendix 14 and 15

Table 4.8 Results of Tensile Shear Strength of Welded Joint Vs Weld Time

Max. Load (KN) - Using Conventional electrodes	Max. Load (KN) - Using Annular Recess Electrodes	Weld Time (Cycles)
5.5	5.2	5
5.2	6.1	10
5.5	6	15
3.1	6.3	20
3.2	6.1	25

4.9.3 Analysis of Effect of Weld Time on Tensile Shear Strength for Weld Joint made using Conventional and Annular Recess Electrodes respectively.

Weld time was measured in cycles in the ranges 5Cycles to 25Cycles at intervals of 5Cycles. As weld time increased from 5 cycles to 25 cycles, the peak load oscillated between 5.2KN and 6.3KN for the joints welded using the annular recess electrodes as shown in table 4.8.

While the peak load for the weld joints made using the conventional electrodes oscillated between 5.2KN and 5.5KN as the weld time increased from 5cycles to 15 cycles, but dropped drastically to 3.1KN and 3.2KN for the weld time of 20cycles and 25cycles respectively. This can further be explained graphically by the trends shown in figure 4.5. In a nut shell, the weld joints made under annular recess electrode performed better compared to the conventional electrodes. However, further statistical analysis may reveal otherwise this characteristic behavior displayed between the two variables.

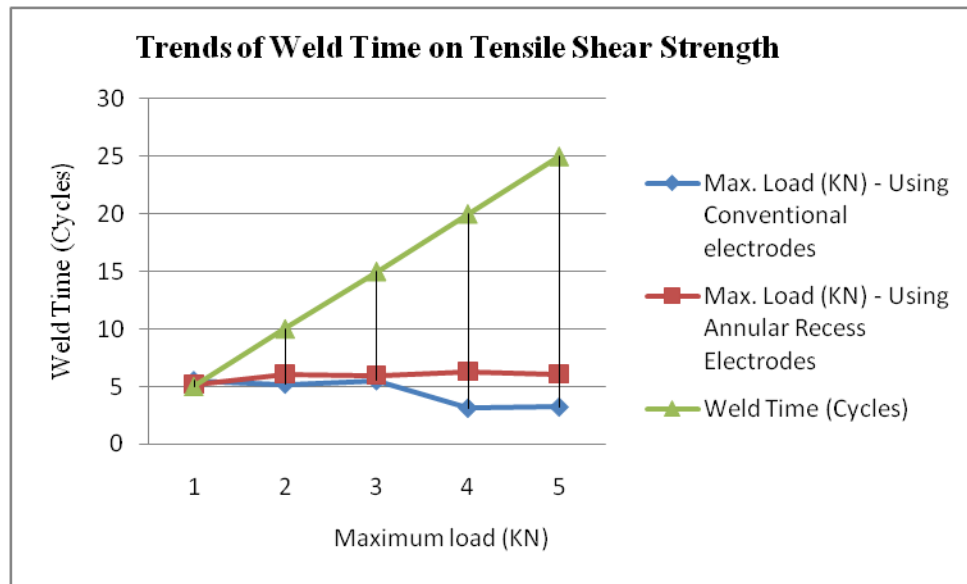


Figure 4.5 Analysis of Effect of Weld Time on Tensile Shear Strength

Table 4.9 Regression Analysis of Weld time Vs Tensile Shear Strength of RSW joint - when Conventional and Annular Recess Electrodes were used respectively.

Statistical Analysis	Regression Coefficient				
	a	b	r^2	p-value	95% Confidence Level
Conventional Electrodes application	-0.13	6.51	0.7311	0.0648	-0.2833 – 0.01531
Annular Recess Electrodes application	0.04	5.34	0.5464	0.1534	-0.0270 – 0.1070

Unlike in the previous regression analysis in table 4.7, the P-value in table 4.9 for both variables under the conventional and annular recess electrodes are 0.065 and 0.153

respectively, and are greater than the significant level of 0.05. This affirms that the fact there is insufficient evidence to adduce non - zero relationship in both variables under the conventional and annular recess electrodes respectively. Although coefficient of determination, r^2 , for both variables are above 50%, the coefficient of linear regression ‘a’ is negative (-0.13) under the conventional electrode application, and this reveal a fact that as the weld time increases, the peak load under the same condition decreases. Therefore 95% confident that the peak load value will reduce between -0.28 – 0.02 as shown in table 4.8

However, the coefficient of linear regression ‘a’ for the annular recess electrodes application is positive 0.04, meaning that as the weld time increases, the corresponding peak load under the same condition increases and we are 95% confident that peak will increase between - 0.027 – 0.11. Thus, where the peak load required for breaking the weld joints under conventional electrodes stopped, is where the peak loads required for breaking the weld joints under annular recess electrodes begin. This is revealed in table 4.8. Details of this regression analysis is in appendix 16 and 17

Table 4.10 Results of Tensile Shear Strength of Welded Joint Vs Electrode Force

Max. Load (KN) - Using Conventional Electrodes	Max. Load (KN) - Using Annular Recess Electrodes	Electrode Force (KN)
4.3	3.5	2
5.7	6	2.5
3.9	4.6	3
4.9	5.8	3.5
2.2	11.4	4

4.9.4 Analysis of Effect of Electrode Force on Tensile Shear Strength of Weld Joint using Conventional and Annular Recess Electrodes respectively.

The electrode force was varied in the ranges 2KN to 4KN at the intervals of 0.5KN as shown in table 4.10. The peak load meant to fracture the weld joints made under annular recess electrode varied from 3.5KN to 11.4KN as the electrode force increased from 2KN to 4KN as compared to the peak load required for breaking the weld joints made under the conventional electrodes varied from 5.7KN to 2.2KN as the electrode force increased from 2KN to 4KN respectively. The annular recess electrode improved the joint strength by 11.4KN, approximately 2 times the conventional electrode. This puts application of 2

annular recess electrodes for upper and lower electrodes to exhibit better performance compared to the single one used the G. Watanabe, *et al*, 2015 study. This trend is further explained graphically as shown in figure 4.6. The performance of the annular recess electrodes as compared to the conventional one is far better under all the varied parameters of weld current, weld time and electrode force respectively.

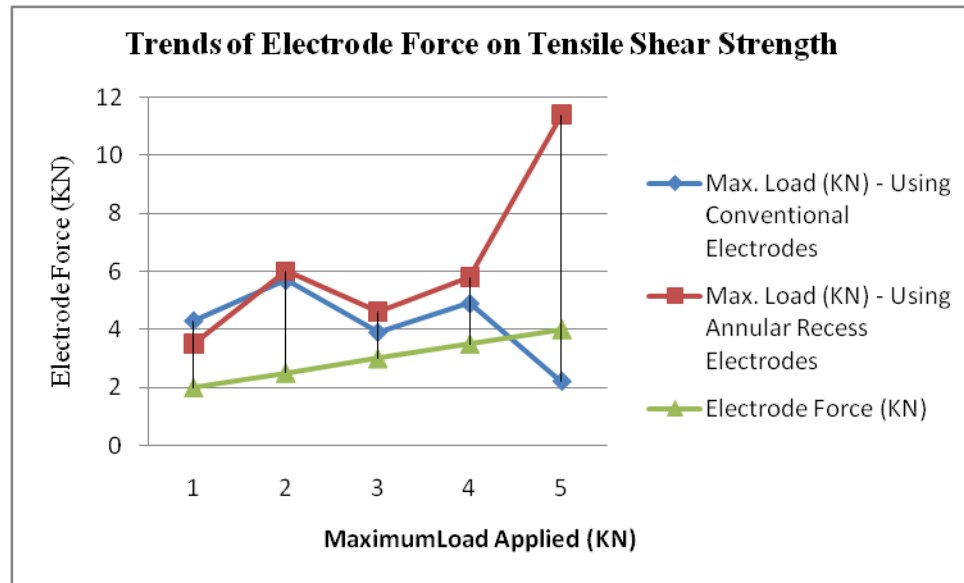


Figure 4.6 Analysis of Effect of Electrode Force on Tensile Shear Strength

Table 4.11 Regression Analysis of Electrode Force Vs Tensile Shear Strength of RSW joint - when Conventional and Annular Recess Electrodes were used respectively.

Statistical Analysis	Regression Coefficient				
	A	b	r^2	p-value	95% Confidence Level
Conventional Electrodes application	-1.00	7.20	0.3655	0.2801	-3.4209 – 1.4209
Annular Recess Electrodes application	3.12	-3.10	0.6564	0.0964	-1.0271 – 7.2671

The P-values for both weld joints made under the conventional and annular recess electrodes are above the significant level of 0.05 (table 4.11). This same scenarios were observe in table 4.8. This therefore affirms that the fact there is insufficient evidence to adduce non - zero relationship in both variables under the conventional and annular recess electrodes respectively. The coefficient of determination r^2 is 65.6% with a linear regression coefficient

‘a’ of positive value 3.12 for the dependent variable under annular recess electrodes. This therefore means that 65.6% of the variables in dependent variable can be explained by the linear relationship between the electrode force and the peak load and the positive 3.12 means that as the electrode force increases, the corresponding tensile shear strength also increases. However, the coefficient of determination r^2 , and linear regression coefficient ‘a’ are 36.6% and -1 only respectively. This is indicative of a negative gradient and it explains the fact as the electrode force increases, the corresponding tensile shear strength decreases. The highest peak load attained during the tensile shear test of welded joints using the annular recess electrodes was 11.4KN while the highest peak load attained during the tensile shear test of welded joints using the conventional electrodes was 5.7KN. Therefore the peak load attained when the annular recess electrodes was 2 times the one attained using the conventional electrodes. This puts the new novel electrode at a better performance level over the conventional one, besides other factors. Details of this regression analysis are in appendix 18 and 19.

Table 4.12 Results of Nugget Diameter of Welded Joint Vs Weld Current

Nugget Diameter (mm)- Using Conventional Electrodes	Nugget Diameter (mm)- Using Annular Recessed Electrodes	Current (KA)
5.9	7.3	6
7.5	5.8	7
7	7.4	8
7.1	7.6	9
7	7.9	10

4.9.4 Analysis of Effect of Weld Current on Nugget Diameter of Weld Joint using Conventional and Annular Recess Electrodes respectively.

The weld current was varied between the 6KA to 10KA with a consecutive interval of 1KA (table 4.12). The nugget diameter formed when the annular recess electrodes were used varied between 5.8mm to 7.9mm as the current varied from 6KA to 10KA. Well on the other hand the nugget diameter formed when the conventional electrodes were used oscillated between 5.9mm to 7.5mm with a consistent value of 7mm, 7.1mm and 7mm with the corresponding current of 8KA, 9KA and 10KA respectively. The nugget diameter formed

for current ranges of 8KA, 9KA and 10KA under the annular recess electrodes were 7.4mm, 7.6mm and 7.9mm respectively. This clearly shows that nugget diameter formed under the new novel electrodes increased with the increased in the weld current. This trend can be further explained graphically as shown in figure 4.7. The nugget diameter formed by annular recess electrode application is larger compared to the nugget diameter for the conventional one.

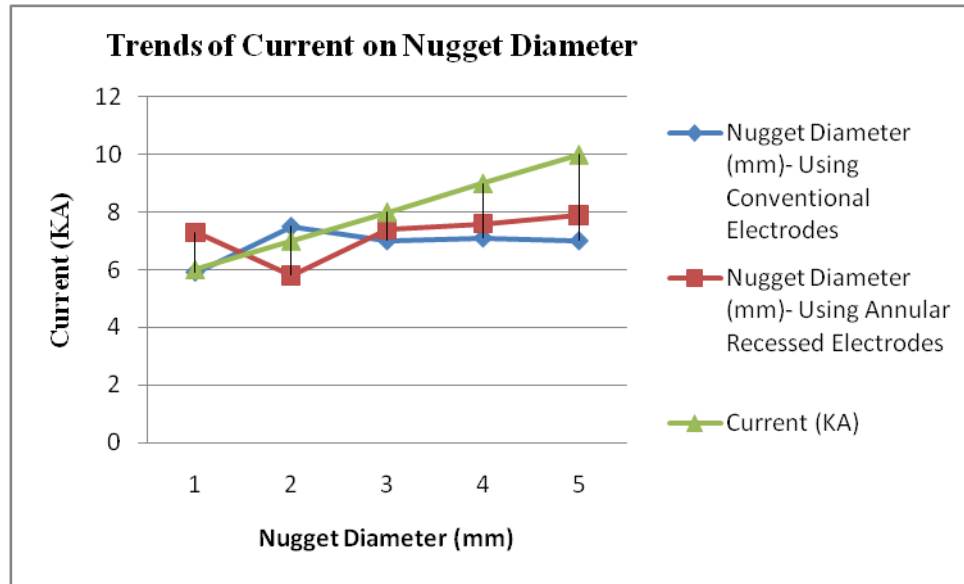


Figure 4.7 Analysis of Weld Current on Nugget Diameter

Table 4.13 Regression Analysis of Weld Current Vs Nugget Diameter of RSW joint - when Conventional and Annular Recess Electrodes were used respectively.

Statistical Analysis	Regression Coefficient				
	a	B	r^2	p-value	95%Confidence Level
Conventional Electrodes application	0.18	5.46	0.2282	0.4158	-0.4283 – 0.7883
Annular Recess Electrodes application	0.30	4.80	0.3384	0.3036	-0.4708 – 1.0708

The p-value for both the nugget diameters formed by both the conventional and annular recess electrodes is above the significant level 0.05 (table 4.13). This means that the fact

there is insufficient evidence to adduce non - zero relationship between the weld current and the nugget diameters formed under the conventional and annular recess electrodes respectively. Although both variables bear positive gradients, the coefficient of determination r^2 , for both types of tools are far below 50%. This is indicative of a weak relationship between the weld current and the nugget diameter. Details of this regression analysis are in appendix 20 and 21.

Table 4.14 Results of Nugget Diameter of Welded Joint Vs Weld Time

Nugget Diameter (mm) - Using Conventional Electrodes	Nugget Diameter (mm)- Using Annular Recess Electrodes	Weld Time (Cycles)
7.3	7.9	5
7.2	8.1	10
6.8	8	15
7.4	8.2	20
7.7	8.1	25

4.9.4 Analysis of Effect of Weld Time on Nugget Diameter of Weld Joint using Conventional and Annular Recess Electrodes respectively.

The weld time was equally varied from 5Cycles to 25Cycles at equal intervals of 5cycles. The weld current and electrode force was maintained at 10KA and 4KN respectively (table 4.14). The nugget diameter formed under the annular recess electrode oscillated between 7.9mm and 8.2mm for the weld time ranging from 5Cycles to 25Cycles. The nugget diameter formed under the conventional electrode also oscillated between 6.8mm and 7.7mm, but lower in value than the new novel electrode. Figure 4.8, attempts to explain the trend as the weld time varied.

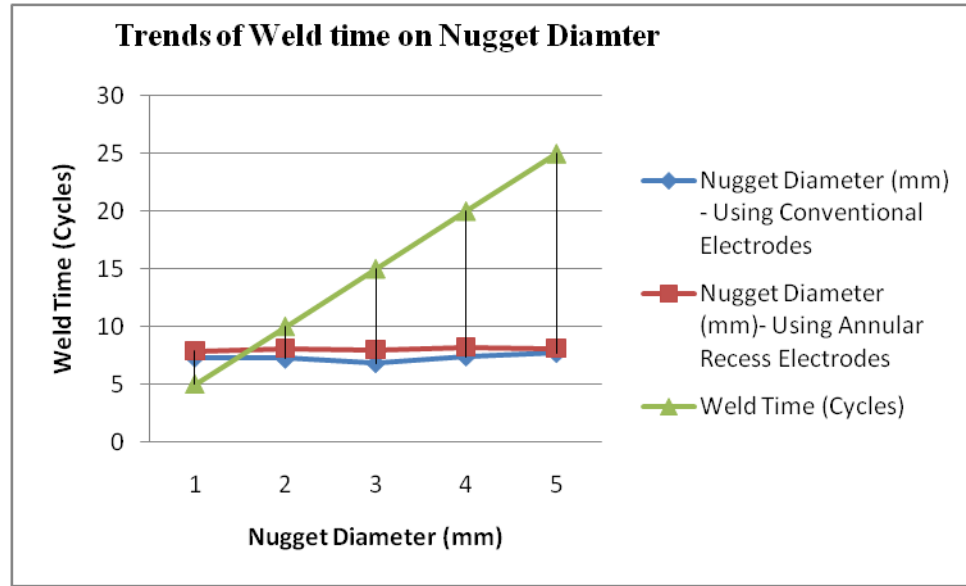


Figure 4.8 Analysis of Weld Time on Nugget Diameter

Table 4.15 Regression Analysis of Weld Time Vs Nugget Diameter of RSW joint - when Conventional and Annular Recess Electrodes were used respectively

Statistical Analysis	Regression Coefficient				
	a	B	r^2	p-value	95%Confidence Level
Conventional Electrodes application	0.02	6.98	0.2336	0.4094	-0.0466 – 0.0866
Annular Recess Electrodes application	0.01	7.91	0.4808	0.1942	-0.0091 – 0.0291

The p-value for both the nugget diameters formed under conventional and annular recess electrodes are 0.41 and 0.19 respectively table 4.15. They are both greater than the significant level of 0.05. This therefore, infers that there is insufficient evidence to adduce non - zero relationship between the weld time and the nugget diameters formed under the conventional and annular recess electrodes respectively. The coefficient of determination r^2 , for the nugget diameter formed under annular recess electrodes is 48% compared to the other at 23%. This means that 48% of the dependent variables can be explained by the linear relationship between the weld time and the nugget diameter as compared to only 23% in the conventional electrodes. Details of this regression analysis is in appendix 22 and 23

Table 4.16 Results of Nugget Diameter Vs Electrode Force

Nugget Diameter (mm) - Using Conventional Electrodes	Nugget Diameter (mm) - Using Annular Recess Electrodes	Electrode Force (KN)
6.8	8.4	2
7.5	8.1	2.5
7	8.2	3
7.2	7.7	3.5
7.8	8.1	4

4.9.5 Analysis of Effect of Electrode Force on Nugget Diameter of Weld Joint using Conventional and Annular Recess Electrodes respectively.

The electrode force was varied from 2KN to 4KN at an equal interval of 0.5KN. The weld current and weld time were kept at 10KA and 15Cycles respectively table 4.16. The nugget diameter for weld joints made using the annular recess electrode oscillated between 8.4mm and 7.7mm showing a considerable reduction in the nugget diameter. The nugget diameter for the weld joints formed by application of the conventional electrodes on the other hand, oscillated between 6.5mm to 7.8mm. The graphical representation of the trend is as shown in figure 4.9. The new novel electrodes provided large nugget diameters and this probably explained the high tensile strength exhibited by weld joints made using annular recess electrodes. The provision of the annular recess configuration in the novel electrode contributed to the redistribution of the current density and thus aiding the expansion of the fusion zone during the weld processes.

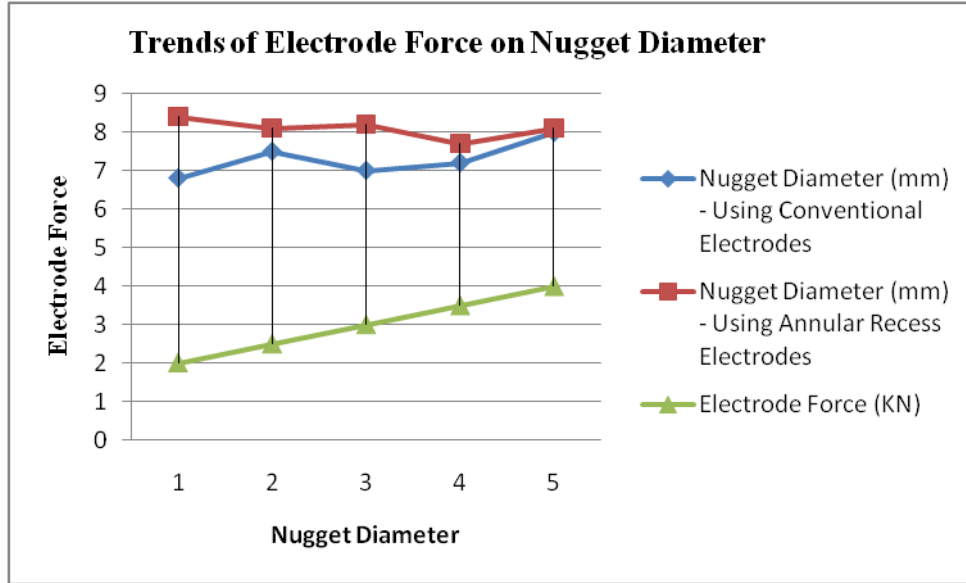


Figure 4.9 Analysis of Electrode Force on Nugget Diameter

Table 4.17 Regression Analysis of Electrode Force Vs Nugget Diameter of RSW joint - when Conventional and Annular Recess Electrodes were used respectively.



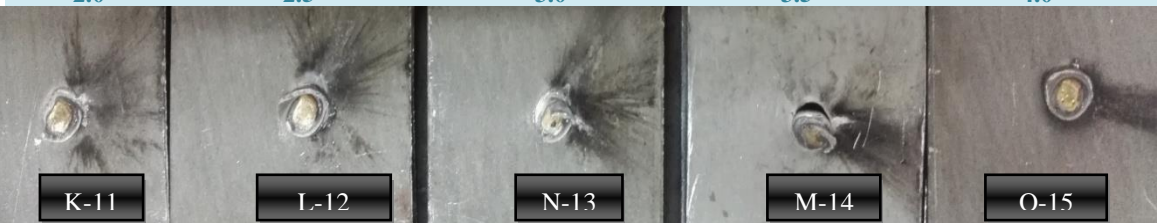


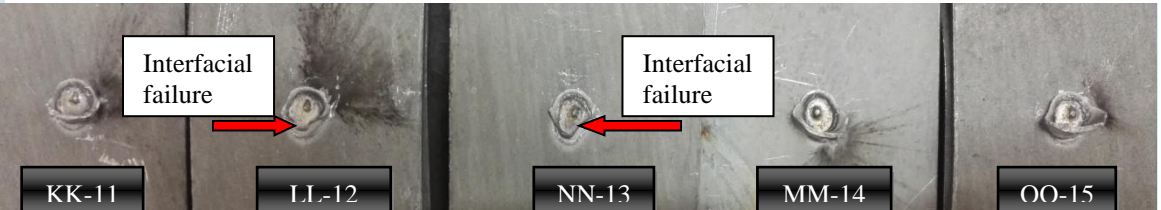
Statistical Analysis	Regression Coefficient				
	a	b	r^2	p-value	95% Confidence Level
Conventional Electrodes application	0.42	6.04	0.3348	0.1810	-0.3490 – 1.1900
Annular Recess Electrodes application	-0.20	8.70	0.3846	0.2644	-0.6648 – 0.2648

The p-value for both the nugget diameters formed under conventional and annular recess electrodes are 0.18 and 0.26 respectively table 4.17. They are both greater than the significant level of 0.05. This therefore, means that there is insufficient evidence to conclude that a non - zero relationship exists between the weld time and the nugget diameters formed under the conventional and annular recess electrodes respectively. The coefficient of determination r^2 , for both the nugget diameters formed under conventional and annular recess electrodes are below 50%. This therefore means that there is a very weak relationship between the electrode force and the nugget diameters for both types of the joint formed under conventional and annular recess electrodes. The variation of the nugget diameters for all the

samples tested with the three parameters of weld current, and weld time and electrode force gave p-values greater than the significant level of 0.05. This therefore leaves with no room, but to conclude that there are insufficient evidence to adduce that there exist a non-zero relationship between the weld parameters and the nugget diameter. The detail of this regression analysis is in appendix 24 and 25

4.9.6 Results on Peel Tests

Table 4.18 Failure Mode when Conventional and Annular Recess Electrodes were used

Weld		Failure Mode exhibited during Peel Test				
Current(KA)		6	7	8	9	10
Conventional Electrodes used						
Time (CYCLES)		5	10	15	20	25
Conventional Electrodes used						
Force (KN)		2.0	2.5	3.0	3.5	4.0
Conventional Electrodes used						
Weld Current(KA)		6	7	8	9	10
Annular Recess Electrodes used						
Weld Time (CYCLES)		5	10	15	20	25
Annular Recess Electrodes used						
Force (KN)		2.0	2.5	3.0	3.5	4.0
Annular Recess Electrodes used						

4.9.7 Analysis of Failure Mode observed on Peel Test

The failure mode is a qualitative measure of weld quality and can give information on whether the failure was brittle or ductile in nature. The weld button size is a measure of the size of the button-like material that remains joined after destructive testing.

Button pull out fracture usually occurs when the joint itself does not fail, but the HAZ or base material at the border of the joint fails. Failure in the HAZ occurs when the welding process has weakened the HAZ by tempering the microstructure or excessively growing the region. Failure in the base metal occurs when the welding process has strengthened the weld above the base metal strength. Partial button pull out fracture occur when the RSW joint cannot endure the load. Part of the weld nugget remains intact, but the crack propagates through a portion of the nugget. There are many different variations depending on the route of the crack, as seen in figure 2.1, but these are usually lumped together as partial button fracture. Interfacial fracture occurs when failure is in a straight line along the interface of the workpieces.

Button pull out fracture is deemed an acceptable failure mode and gives evidence that the welding process did not affect the materials' ability to withstand loading. There is often more part deformation, indicating more energy absorption at failure, when button pull out is the fracture mode. At a material level, failure is usually ductile in nature and exhibits localized necking of the material surrounding the nugget.

Partial button pull out fracture is indicative of the welding process altering the materials ability to endure a load. The joint is the weakest link and a crack propagates partially through the solidified weld nugget. There are many different factors that can contribute to partial button pull out and it is often deemed an unacceptable fracture mode for production. With the advancements of materials, and brittle martensitic weld nuggets, partial button pull-out can be deemed acceptable in situations where a maximum load is reached prior to failure.

Interfacial fracture leaves little to no warning signs before complete propagation along the weld centerline in a brittle fashion. There is often no part deformation at failure, indicating very low energy absorption. In the past, interfacial fracture was always deemed unacceptable, but like partial button pullout has been qualified as acceptable for some advanced high strength materials.

According to the observation made during the peel test, no failure occurred at the weld joints for the both weld joints made using the conventional and annular recess electrodes respectively. Partial interfacial failure modes were exhibited by some weld samples as seen in C-3, D-4, E-5 and G-7 for the current values 8KA, 9KA, and 10KA respectively table 4.9.5 for weld joints made under the conventional electrodes. However, on the other hand, partial interfacial failures were also observed on two weld pieces as shown in table 4.18, LL-12 and NN-13 respectively;

4.9.8 Results on Microstructure Test

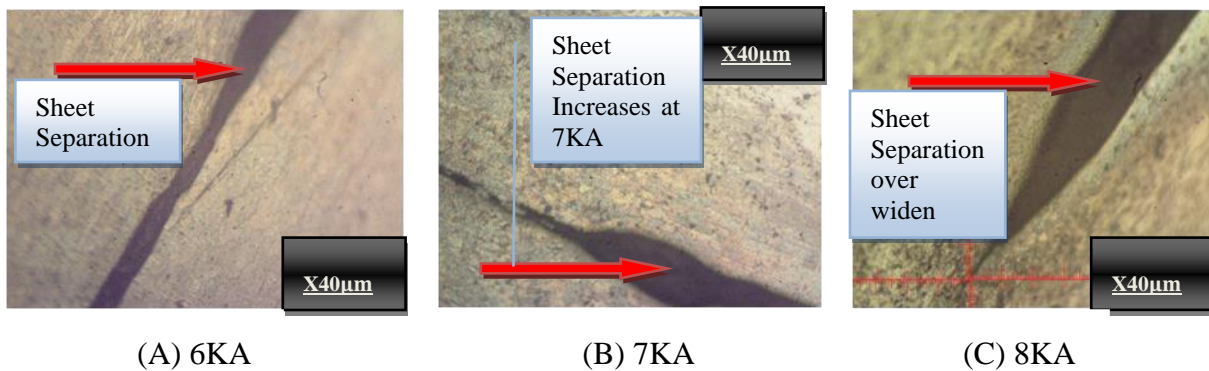


Figure 4.10 Large Sheet Separation, - using conventional electrodes

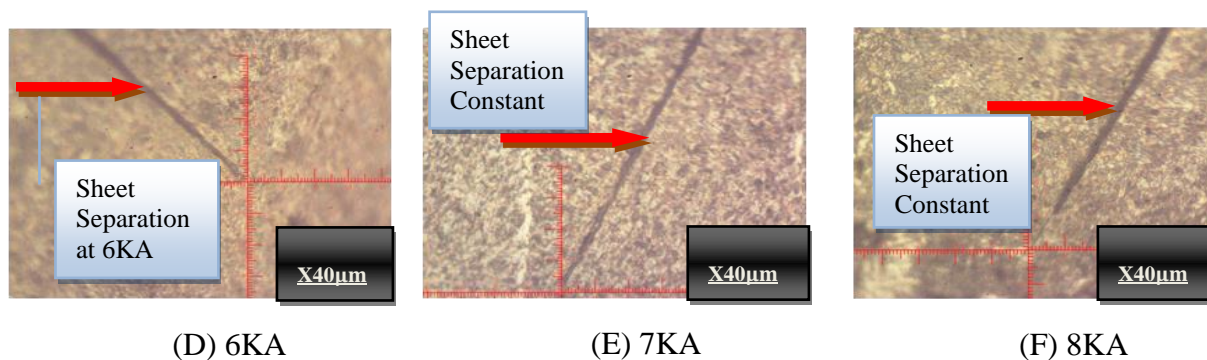


Figure 4.11 Small Sheet Separation, - using annular recess electrodes

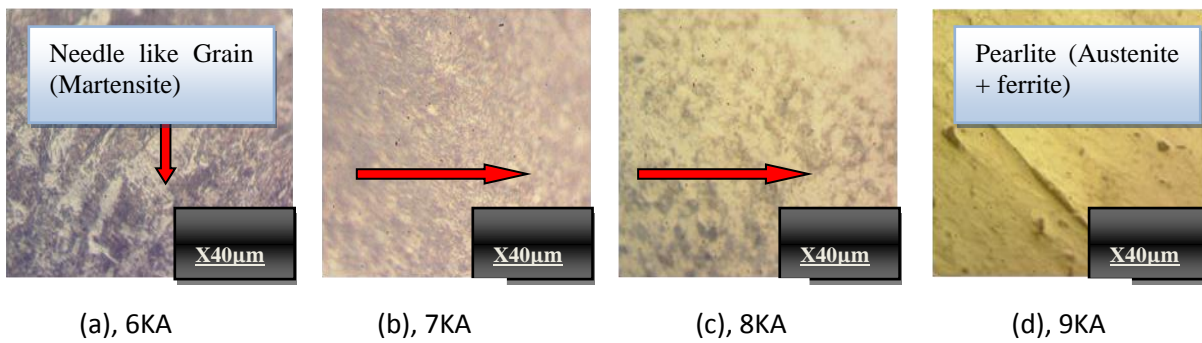


Figure 4.12 Weld joint microstructures, for joints welded using conventional electrodes

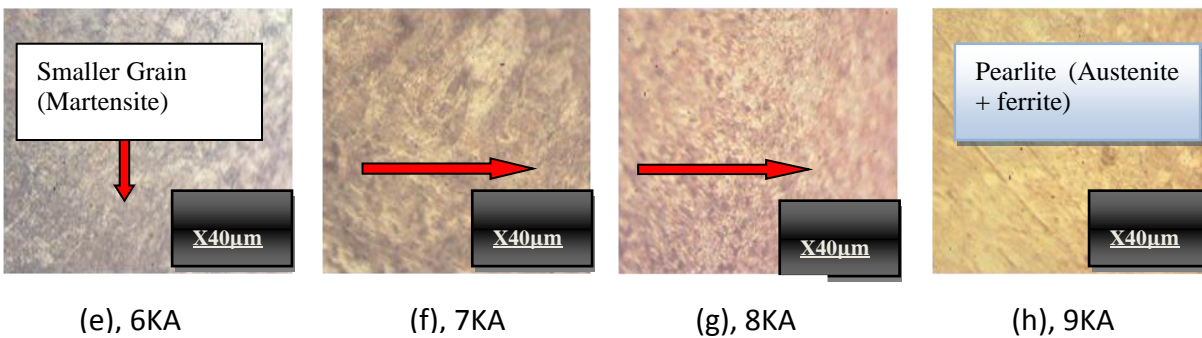


Figure 4.13 Weld joint microstructures, for joints welded using annular recess electrodes

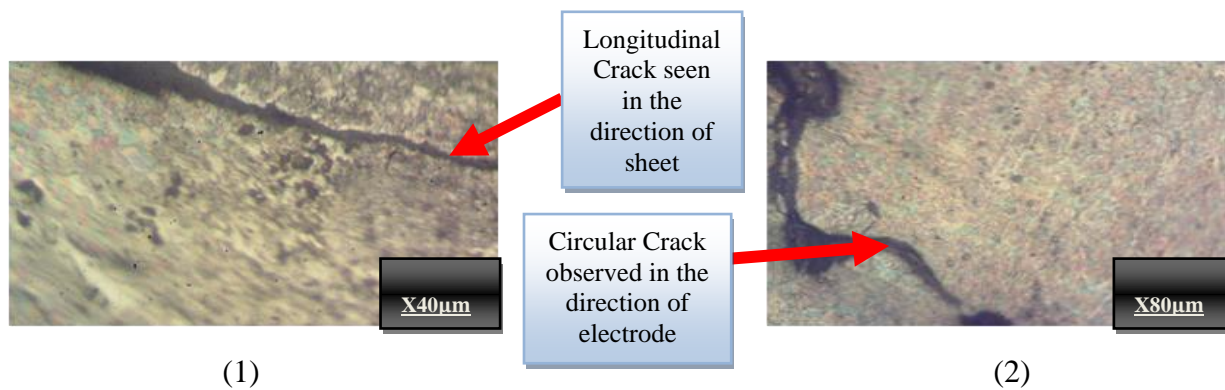


Figure 4.14 (1) Longitudinal joint cracks - under conventional electrodes, and (2) Circular joint cracks at the base of weld bead – under annular recess electrodes

4.9.9 Analysis of Micrographs obtained from Microstructure Test

During the microstructure study, emphasis was focused on the joint integrity at the center of the cross sections of the weld joints made under conventional electrode and annular recess electrode. Sheet separation was also checked for 3 samples from each categories welded under varied current ranging 6KA to 8KA. Weld defects resulting from the application of the two types of tools i.e., the conventional electrodes and the annular recess electrodes were also scrutinized.

From figure 4.10, increased sheet separations were observed at the weld joint cross section as current varied from 6KA to 8KA for weld joints made under the conventional electrode. The cross sectional weld joints, made under the annular recess electrodes exhibited small sheet separation that did not vary in shape at the same variable parameters (figure 4.11). This finding is in agreement with that of G. Watanabe, *et al*, 2015 while investigating the cross tension strength using concave electrode in RSW of High-Strength Steel Sheet (HSSS).

Resistance spot welding as earlier discussed in the literature review generate high temperatures in the range of over 1000⁰C at the faying workpiece interfaces causing the molten materials to transform from the ferrite state to the austenite state. As a result of short weld time and rapid cooling provided by the bulk water cooled electrodes, the austenite quickly transform to the martensite which is known to be hard, brittle and needle shape like. Figure 4.12 represents the cross sections of the weld joints made using the conventional electrode for the range current 6KA to 9KA. Closure observation of figure 4.12 (a) revealed needle like shape structures indicative of the martensite state of the weld joint. However, this needle like shape structures tend to diminished (figure 4.12 (b), (c) & (d)) as current increased from 7KA to 9KA, indicative of slower cooling processes and solidification into a state of austenite and ferrite called pearlite. However, on the other hand, cross sectional joints welded using annular recess electrode revealed finer grain structures which tended to the pearlite state as current varied from 6KA to 9KA (figure 4.13 (e), (f), (g) & (h)).

The crack propagation on the cross sectional weld joint made under conventional electrode as observed in figure 4.14 (1) is longitudinal in nature and along the direction of the sheet as opposed to the electrode direction. The same phenomenon occurred with Dulal Chandra Saha, *et al*, 2014, while investigating the heat - affect zone liquation cracks on resistance spot welded TWIP steel. The longitudinal crack may have aroused out of the differences in the solidification rates. There was a faster solidification rate in the electrode direction due to faster cooling rate facilitated by the bulk water cooled electrode as opposed to the balance of the molten liquid squeezed close to the faying workpiece interface because of the high electrode force experiencing lower cooling rate. Therefore the phase difference in the solidification rates caused the longitudinal crack. This crack usually reduces the nugget diameter rendering weak joint.

On the other hand, the crack propagation on the cross sectional joint made under annular recess electrode as observed in figure 4.14 (2) was circular in nature and along the direction of the electrode as opposed to the direction of the sheet. The shift in the direction of the crack from longitudinal to circular direction can be explained by the introduction of the annular recess configuration at the tip of both upper and lower electrodes face. Faster rate of solidification seemed to have occurred in the recess areas than the rate at the remaining face of the electrodes. The difference in this solidification rate shifted the crack direction from longitudinal to circular along the direction of the electrode. The provision of annular recess hole created low aspect ratio at the electrode face thus rendering greater surface area that facilitated very faster rate of cooling and hence solidification.

CHAPTER FIVE

This chapter discussed the conclusions to the study and drew recommendations to aspects that were discovered during the study but because of the limited time, those observations could not be investigated any further.

5.0 Conclusion and Recommendations

This research study has finally ended and all the specific objectives to the research study were successfully met and new observations that could not be handled during the scheduled time for the research were summed up as recommendations for further study.

The specific objectives were achieved in sequence as follows;

1) Objective I

The noble idea of creating the annular recess hole at the centre tip of 45⁰ truncated electrode Ø6mm face, 2.5mm and 4mm depth was conceived and initial designs were made using computer software. The mass property of a piece of annular recess electrode was determined at 72.2gm with the manufacturing costs of \$13.05. This new tool was much lighter in weight compared to the conventional electrode because of the creation of the annular recess on the contact surface of the conventional electrode. The manufacture of the annular recess electrode was achieved by machining to the specification as shown in the result. The annular recess configuration offered greater surface area with low aspect ratio. This therefore meant that there is faster and controlled cooling of the molten weld fusing towards the centre of the weld join and expanding outwards forming nugget of larger diameter when used in welding process. The new electrode was capable of welding the 1mm metal sheet with minimum expulsion when used on RSW machine.

2) Objective II

Much as the statistical analysis of the data showed a moderate relationship between the dependent variables (tensile shear strength and the nugget diameter) and the independent variables (weld current, weld time and electrode force), the performance

of the weld joints made by application of the annular recess electrodes rouse to a maximum at 11.4KN for the nugget diameter of 8.1mm compared to 5.7KN at the nugget diameter of 7.8mm. The annular recess electrode was therefore able to improve the weld joint strength by 2 times the performance of the conventional electrode. The performance offered by the new novel tool could be exploited in the automotive manufacturing industries. The application of two annular recess electrodes in the upper and lower tool post offered a better weld joint strength of 11.4KN and this support the findings of G. Watanabe, *et al*, 2015 when he used a single concave electrode while investigating the cross strength of HSSS. The statistical implication observed in some instances could have been as a result of inadequate sample space.

However, no expulsions were observed during the welding process using the new annular recess electrode as compared to the conventional one. The nugget diameter formed using the annular recess electrode varied from 5.8mm to 8.4mm which are larger compared to the one formed using the conventional electrode that varied from 5.9mm to 7.8mm. The statistical analysis on the other showed no apparent relationship between the independent variable and the dependent variable. This may be checked in the future by selecting big sample space for the review.

3) Objective III

Non destructive and destructive test were successfully carried. The Magnetic Particle Inspection test (MPI) was carried out as one of the non destructive tests (NDT) to detect weld defects on the weld joints made by the conventional electrode and the annular recess electrode. The weld joints made using annular recess electrode offered better sound joint integrity (minimum defects detect) compared to the weld joints made using conventional electrode which showed multiple defects configured by the spread of the magnetic particle. This was observed on the basis of the magnetic particle spread on the tested joints for the two schedules (conventional electrodes and annular recess electrodes).

Three destructive tests were carried out namely tensile shear strength test, peel test and microstructure test. The tensile shear strength test was conducted to determine the strength of the weld joints made by the two types of the electrode. It was observed that joints welded using annular recess electrode had peak load ranging from 3.1KN to 11.4KN compared to the weld joint made by the conventional electrode had peak load ranging from 3KN to 5.7KN. The annular recess electrode therefore offered better performance compared to the convention electrode. The peel test was used for determining the weld nugget diameter formed under the two welding schedules. As earlier stated the nugget diameters formed under the annular recess electrode were larger compared to the conventional (check results).

The microstructure test was carried out to expose the weld defects that were formed under the two welding schedules. The crack propagation for the weld joints made using annular recess electrode was observed circular in nature and is in the direction of the electrode as opposed to sheet direction. While the crack propagation for the weld joint made using the conventional electrode was observed longitudinal in nature and along the sheet direction. A longitudinal crack by visual inspection was found to reduce the nugget diameter and thus weaken the weld joint.

The occurrence of the longitudinal cracks in the direction of the sheet was in support of the findings of Dulal Chandra Saha, *et al*, 2014, while investigating the heat - affect zone liquation cracks on resistance spot welded TWIP steel. The longitudinal crack may have aroused out of the differences in the solidification rates. There was a faster solidification rate in the electrode direction due to faster cooling rate facilitated by the bulk water cooled electrode as opposed to the balance of the molten liquid squeezed close to the faying workpiece interface because of the high electrode force experiencing lower cooling rate. Therefore the phase difference in the solidification rates caused the longitudinal crack.

The shift in the direction of the crack from longitudinal to circular direction can be explained by the introduction of the annular recess configuration at the tip of both upper and lower electrodes face. Faster rate of solidification seemed to have occurred in the recess areas than the rate at the remaining face of the electrodes. The difference in this solidification rate shifted the crack direction from longitudinal to circular along the direction of the electrode. The provision of annular recess hole created low aspect ratio at the electrode face thus rendering greater surface area that facilitated very faster rate of cooling and hence solidification.

5.1 Recommendations

Due to limited time required to complete the study, some observations and results could not be investigated further. The researcher therefore recommends the following areas of interest observed during tests and experiments for further study.

- 1) Further destruction tests e.g., cross tension test for the joints welded using the new annular recess electrodes for different gauges of the sheet materials must be carried out.
- 2) In-depth analysis circular weld joint defects observed during this study.
- 3) The optimum weld parameters required to attain good weld joints while using the annular recess electrodes.
- 4) The rate of deformation/wear of the new electrode tip while handling bulk job.

References

1. Andrea Jane Peer, 2017, Performance Testing and Modeling of Ultra-High Strength Steel and Complex Stack-Up Resistance spot Welds, pp. 13-14.
2. C. Tsai *et al*, 1992, "Modeling of resistance spot weld nugget growth," *Welding Journal* (USA), vol. 71, pp.47.
3. S. Na and S. Park, 1996, "A theoretical study on electrical and thermal response in resistance spot welding," *Welding Journal-Including Welding Research Supplement*, vol.75, pp. 233-242.
4. H. Neid, 1984, "The finite element modeling of the resistance spot welding process," *Welding Journal*. 63(4), pp.123-s to 132-s.
5. Y. Cho and S. Rhee, 2003, "Experimental study of nugget formation in resistance spot welding," *Welding Journal*, vol.82, pp. 195-201.
6. Eisazadeh H., Hamedib M. and Halvae A, 2010, "New parametric study of nugget size in resistance spot welding process using finite element method," *Materials and Design* 31 149-157.
7. Watanabe G., Amago T., Ishii Y., Takao H., Yasui T., and Fukumoto M., 2016, "Improvement of Cross - Tension Strength Using Concave Electrode in Resistance Spot Welding of High – Strength Steel Sheets," *AIP Conference Proceedings* 1709, 020003; doi: 10.1063/1.4941202.
8. Zhang, H. and Senkara, J, 2006, Resistance Welding: Fundamentals and Applications, Taylor & Francis, New York.
9. Thakur, A. G. and Nandedkar, V. M. 2010, "Application of Taguchi method to determine resistance spot welding conditions of austenitic stainless steel AISI 304", *Journal of Scientific &Industrial Research*, Vol.69, pp.680-683.
10. Taban, E., Deleu, E., Dhooge, A. and Kaluc, E., 2008, "Evaluation of dissimilar welds between ferritic stainless steel modified 12% Cr and carbon steel S355", *Welding Journal*, Vol.87, pp.291s-297s.
11. Shanmugam, K., Lakshminarayanan, A. K. and Balasubramanian, V., 2009, "Tensile and impact properties of shielded metal arc welded AISI 409M ferritic stainless steel joints", *Journal of Material Science and Technology*, Vol.25, pp.181-186.

12. Pouranvari, M. and Ranjbarnood, E., 2012. "Effect of welding current on energy absorption of AISI 304 resistance spot welds", *Research Journal of Applied Sciences, Engineering and Technology*, Vol.4, pp. 2911-2914.
13. Pouranvari, M., Marashi, S. P. H. and Alizadehsh, M. , 2015, "Welding metallurgy of dissimilar AISI 430/DQSK steels resistance spot welds". *Welding Journal*, Vol.94, pp.203-210.
14. Pouranvari, M., Alizadeh-sh, M. and Marashi, S. P. H., 2015, "Welding metallurgy of stainless steel during resistance spot welding, part I: fusion zone", *Science and Technology of Welding & Joining*, Vol.20, No.6, pp.502-511.
15. Mohandas, T., Reddy, G. M. and Naveed, M., 1999, "A comparative evaluation of gas tungsten and shielded metal arc welds of a ferritic stainless steel", *Journal of Material Processing Technology*, Vol.94, Issue No.2-3, pp.133-140.
16. Hernandez, V. H. B., Panda, Sushanta Kumar, Okita, Yasuaki and Zhou, Y. Norman, 2010, "A Study on heat affected zone softening in resistance spot welded dual phase steel by nano indentation". *Journal of Material Science*, Vol. 45, pp.1638-1647.
17. Goodarzi, M., Marashi, S. P. H. and Pouranvari, M. , 2009, "Dependence of overload performance on weld attributes for resistance spot welded galvanized low carbon steel", *Journal of Material Processing Technology*, Vol. 209, Issue No.9, pp. 4379–4384.
18. Feng, J. C, Wang, Y. R. and Zhang, Z. D., 2006, "Nugget growth characteristic for AZ31B magnesium alloy during resistance spot welding". *Science and Technology of Welding and Joining*, Vol.11, Issue No.2, pp.154-162.
19. Charde, Nachimani and Rajkumar, Rajprasaad, 2013 "Investigating spot weld growth on 304 austenitic stainless steel (2mm) sheets", *Journal of Engineering Science and Technology*, Vol.8, pp.69 - 76.
20. Chao, Y. J., 2003, "Failure mode of resistance spot welds: interfacial versus pullout", *Science and Technology of Welding and Joining*, Vol.8, pp.133-137.
21. Zuniga, S. M., 1994, Predicting overload pull-out failures in resistance spot welds, Ph.D. thesis, Stanford University.

22. Pouranvari, M. and Marashi, S. P. H., 2011, "Failure mode transition in AHSS resistance spot welds. Part I. Controlling factors", *Material Science and Engineering: A*, Vol.528, pp.8337-8343.
23. Pouranvari, M., Abedi, A., Marashi, S. P. H. and Goodarzi, M., 2008, "Effect of f on peak load and energy absorption of low carbon resistance spot welds", *Science Technology Welding Joining*, Vol.13, Issue No.1, pp.39-43.
24. Pouranvari, M., 2017 "Fracture toughness of martensitic stainless steel resistance spot welds", *Material science & Engineering A*, Vol.680, pp.97-107.
25. Donders, S., Brughmans, M., Hermans, L., Liefvooghe, C., Van der Auweraer, H. and Desmet, H., 2006, "The robustness of dynamic vehicle performance to spot weld failures". *Finite Elements in Analysis and Design*, Vol.42, Issue No.8-9, pp.670-682.
26. Specimen dimensions and procedure for shear testing resistance spot and embossed projection welds, ISO 14273:2000 Standard.
27. Peterson, W.; Borchelt, J. , 2000, "Maximizing cross tension impact properties of spot welds in 1.5 mm low carbon, dual-phase, and martensitic steels". *In SAE Technical Paper 2000-01-2680; SAE International: Warrendale, PA, USA.*
28. Donders, S.; Brughmans, M.; Hermans, L.; Tzannetakis, N.O. 2005, "The effect of spot weld failure on dynamic vehicle performance". *Sound Vibrat.* 39, pp16–25.
29. Habib, L., Abdelkader, Z., Habib, B. and Benallel, B. F., 2016, "Experimental study of tensile test in resistance spot welding process", *Latin American Journal of Solids and Structures*, Vol.13, pp.1228-1235.
30. Marashi, S. P. H., 2016 "Dissimilar spot welding of DQSK/DP600 steels: The weld-nugget growth", *Materials and Technology*, Vol.50, No.5, pp.761-765.
31. Shamsul, J. B. and Hisyam, M. M., 2007, "Study of spot welding of austenitic stainless steel type 304", *Journal of Applied Science Research*, Vol.3, pp.1494-1499.
32. Ozyurek, D., 2008, "An effect of weld current and weld atmosphere on the resistance spot weldability of 304L austenitic stainless steel". *Materials and Design*, Vol.29, Issue No.3, pp.597–603.

33. Pouranvari, M., Asgari, H. R., Mosarizadch, S. M., Marashi, S. P. H. and Goodarzi, M., 2007, "Effect of weld nugget size on overload failure mode of resistance spot welds". *Science and Technology of Welding and Joining*, Vol.12, Issue No.3, pp.217-225.
34. Pouranvari, M., 2011, "Effect of welding current on the mechanical response of resistance spot welds of unequal thickness steel sheets in tensile- shear loading condition", *International Journal of Multidisciplinary Sciences and Engineering*, Vol. 2, pp.63-67.
35. Pouranvari, M. and Marashi, S. P. H., 2013, "Critical review of automotive steels spot welding: Process, structure and properties", *Science and Technology of Welding and Joining*, Vol.18, Issue No.5, pp.361-403.
36. Aslanlar, S., 2006, "The effect of nucleus size on mechanical properties in electrical resistance spot welding of sheets used in automotive industry", *Materials and Design*, Vol.27, Issue No.2, pp.125-131.
37. Bowers, R.I, Sorensen C.D, and Eagar T.W. 1990, "Electrode Geometry in Resistance Spot Welding. *Welding Journal's*.
38. Friedman, L. M., and McCauley, R. C. 1969. Influence of metallurgical characteristics on resistance welding of galvanized steel. *Welding Journal* 48(10) pp. 454-462
39. Greenwood, S. 1961. Temperatures in spot welding. *British Welding journal*, 8(6), pp 316-322
40. Holm, R. 1967. Electrical Contact: Theory and Application, pp. 9-18, New York, Springer Verlag.
41. Kaiser, J. C, Dunn, G. I., and Eagar, T. W. 1982. The effect of electrical resistance on nugget formation during spot welding. *Welding Journal* 62(6):164-s to 174-s.
42. Lane, C. T., Sorensen, C. D., Hunter, G. B., Gedeon, S. A., and Eagar, T. W. 1987. Cinematography of resistance spot welding of galvanized steel. *Welding Journal* 66(9), pp.2-60
43. Nadkarni, A. V., and Weber, E. P. 1977. A new dimension in resistance welding electrode materials. *Welding Journal* 56(11) pp. 331- 338
44. Simmons, W. P. 1967. Spot welding electrode life. *Welding Journal*, 46(11) pp 915-92

45. BS EN ISO 5173: Destructive tests on welds in metallic materials, Bend Tests
46. BS EN ISO 9015: parts 1 & 2 Destructive tests on welds in metallic materials. Hardness Testing.
47. BS EN ISO 9018: Destructive tests on welds in metallic materials. Tensile test on Cruciform and tapped joints.
48. BS EN ISO 1764 1-2: Destructive tests on welds in metallic materials. Hot cracking tests for weldments, i.e. Self-Restraint Tests.
49. BS EN ISO 17635: Non-destructive testing of welds. General rules for metallic materials.
50. BS EN ISO 17637: Non-destructive testing of welds. Visual inspection/testing of fusion-welded joints.
51. BS EN ISO 17638: Non-destructive testing of welds. Magnetic particle testing.
52. BS EN ISO 23278: Non-destructive testing of welds. Magnetic Particle testing of welds. Acceptance levels.
53. BS EN ISO 3059: Non-destructive testing. Penetrant and Magnetic particle testing viewing conditions.
54. BS DEN ISO 3452: Series 2013. Non-destructive testing Penetrant Testing.
55. BS EN ISO 23277:2015: Non-destructive testing of welds. Penetrant testing of welds. Acceptance Levels.
56. BS EN ISO 12718: Non-destructive testing. Eddy proposed testing. Vocabulary
57. BS EN ISO 15549: Non-destructive testing. Eddy proposed testing. General principles
58. C.R. SHOTBOLT, 1988, "Technician Manufacturing Technology". *Cassel Publisher Ltd, Vol.2, 2nd Edition, ISBN 0 304 31639 3, pp 27 – 31.*
59. Resistance Welder Manufacturers' Association, 1961. *Resistance Welding Manual.*
60. Karci, Feramuz, Kacar, Ramazan and Gunduz, Suleyman, 2009, "The effect of process parameter on the properties of spot welded cold deformed AISI304 grade austenitic stainless steel", *Journal of Materials Processing Technology, Vol.209, Issue No.8, pp.4011–4019.*

61. W. Li, D. Cerjanec and G.A. Grzadzinski, 2005, "A comparative study of single-phase AC and multiphase DC resistance spot welding", *Journal of Manufacturing Science and Engineering*, vol. 127, pp. 583-589.
62. K. Hofman *et al*, 2005, "AC or DC for resistance welding dual-phase 600?" *Welding Journal*, vol. 84, pp. 46-48.
63. W. Li *et al*, 2004, "Energy consumption in AC and MFDC resistance spot welding," *Proceedings of the Sheet Metal Welding Conference XI, Sterling Heights, Michigan*.
64. Z. Mikno, S. Kowieski and A. Pilarczyk, 2016, "Analysis of liquid metal expulsion from the weld nugget," *the 9th International Seminar and Conference on Advances in Resistance Spot Welding, Miami*.
65. N. Williams and J. Parker, 2004, "Review of resistance spot welding part 1 Modeling and Control of weld nugget formation," *International Materials Reviews*, vol. 49, pp. 45-75.
66. D. Dickinson, 1981, "Welding in the Automotive Industry; State of the Art," A Report. *Republic Steel Research Centre*.
67. W. Chuko and J. Gould, "Development of resistance welding practice for transformation-hardened steels," *American Iron and Steel Institute*, Pittsburgh, Tech. Rep. DE-FC07-97ID13554.
68. Pouranvari, M. and Ranjbarnooodeh, E., 2013 "Effect of electrode force on fracture type of DQSK steel resistance spot welds", *Acta Metallurgica Slovaca*, Vol. 19, Issue No.2, pp.149-153.
69. M. Khan, 2007, "Spot Welding of Advanced High Strength Steels (AHSS)." UWSpace.
70. N.J. Deng Uuijl, 2015, "Resistance Spot Welding of Advance High Strength Steels." TU Delf, Delf University of Technology, Netherlands.
71. ISO 5182, 1999 Standard, "Materials for resistance welding electrodes and ancillary equipment," Second Edition.
72. ISO 5182, 2008 Standard, "Materials for resistance welding electrodes and ancillary equipment".

73. Amuda, M.O.H. and Mridha, S. 2010, "Grain refinement in ferritic stainless steel welds: the journey so far", *Advanced Materials Research*, Vol.83-86, pp.1165-1172.
74. Lippold, C. John and Kotecki, J. Damian, 2005, "New Welding metallurgy and weldability of stainless steel", *John Wiley & Sons, Inc., Hoboken Jersey*.
75. Pouranvari, M. and Marashi, S. P. H. 2012, "Failure mode transition in AISI 304 resistance spot welds", *Welding Journal*, Vol.91, pp.303-308.
76. Marya, M. and Gayden, X. Q., 2005, "Development of requirements for resistance spot welding Dual-Phase (DP600) steels part 1 –The causes of interfacial fracture", *Welding Journal*, pp. 172 -182.
77. Pouranvari, M. and Marashi, S. P. H., 2010, "Factors affecting mechanical properties of resistance spot welds", *Material Science and Technology*, Vol.26, Issue No.9, pp.1137-1144.
78. Pouranvari, M., 2011, "Effect of welding current on the mechanical response of resistance spot welds of unequal thickness steel sheets in tensile- shear loading condition", *International Journal of Multidisciplinary Sciences and Engineering*, Vol. 2, pp.63-67.
79. Marashi, S. P. H., Pouranvari, M., Amirabdollahian, S., Abedi, A. and Goodarzi, M., 2008 "Microstructure and failure behavior of dissimilar resistance spot welds between low carbon galvanized and austenitic stainless steels", *Materials Science and Engineering*, Vol.480, Issue No.1-2, pp.175–180.
80. WorldAutoSteel, "Advanced High-Strength Steels Application Guidelines," unpublished.
81. S. Zuniga and S. D. Sheppard, 1997, "Resistance spot weld failure loads and modes in overload conditions," in *Fatigue and Fracture Mechanics: 27th Volume* Anonymous ASTM International.
82. Peterson, W.; Borchelt, J., 2000, Maximizing cross tension impact properties of spot welds in 1.5 mm low carbon, dual-phase, and martensitic steels. In *SAE Technical Paper 2000-01-2680*; SAE International: Warrendale, PA, USA.
83. Donders, S.; Brughmans, M.; Hermans, L.; Tzannetakis, N.O., 2005, "The effect of spot welds failure on dynamic vehicle performance." *Sound Vibrat.* 39, 16–25.

84. Pouranvari, M. and Ranjbamoodeh, E., 2011, "Resistance spot welding characteristic of ferrite- martensite DP600 dual phase advanced high strength steel-Part III: mechanical properties", *World Applied Sciences Journal*, Vol.15, pp.1521-1526.
85. W. D. Callister and D. G., 2010. Rethwisch, *Materials Science and Engineering*. John Wiley & Sons NY.
86. S. Dancette *et al*, 2011, "Experimental and modeling investigation of the failure resistance of Advanced High Strength Steels spot welds," *Eng. Fract. Mech.*, vol. 78, pp. 2259-2272, 7.
87. K. Easterling, 2013, *Introduction to the Physical Metallurgy of Welding*. Elsevier.
88. WWW. *resistanceweldsupplies.com*
89. Hernandez, V. H. Balthazar, Kuntz, M. L., Khan, M. I. and Zhou, Y. , 2008 "Influence of microstructure and weld size on the mechanical behavior of dissimilar AHSS resistance spot welds" *Science and Technology of Welding and Joining*, Vol.13, Issue No.8, pp.769-776.
90. Resistance Welding - Peel and chisel testing of resistance spot and projection welds, ISO 10447:2006 Standard.
91. Resistance Welding-Vickers hardness testing (low force and micro hardness) of resistance spot, projection and seam, ISO 14271:2011Standard.
92. Specimen dimensions and procedure for mechanized testing resistance spot, seam and embossed projection welds, ISO 14270:2000Standard.
93. Carlson, Robert, 2006. A concrete introduction to real analysis. CRC Press. p.183.
94. Dodge, Y. 2003, *The Oxford Dictionary of Statistical Terms*, OUP. ISBN, 0-19-920613-9
95. Everitt, B. S. 2002. *The Cambridge Dictionary of Statistics*, (2nd Ed.). Cambridge UP. ISBN 0-521-81099-X
96. Dulal Chandra Saha, et al, 2014. Heat-affected zone Liquation Cracks on resistance spot welded TWIP steels. *MATERIALS CHARACTERIZATION* 93, 40 –51
97. M. Li, H. Shengsun, H. Bao, S. Jungi, W. Yonghi, 2014. Activating flux design for laser welding of ferritic stainless steel. *Trans. Tianjin Univ.* 20, 429-434

LIST OF APPENDICES.

APPENDICES.....	1
Appendix 1, Results for sample plate KP1	1
Appendix 2, Results for sample plate KP2	2
Appendix 3, Results for sample plate KP3	2
Appendix 4, Results for sample plate KP4	3
Appendix 5, Results for sample plate KP5	4
Appendix 6, Results for sample rod KC1 (1).....	4
Appendix 7, Results for sample rod KC1 (2).....	5
Appendix 8, Results for sample rod KC2 (1).....	5
Appendix 9, Results for sample rod KC2 (2).....	6
Appendix 10, Results for sample rod KC3 (1).....	6
Appendix 11, Results for sample rod KC3 (2).....	7
Appendix 12, Detailed Part Drawing of the Annular Recess Electrode	8
Appendix 13, Generated Manufacturing Cost Reports in US dollars, of Annular Recess Electrode.	9
Appendix 14, Regression Analysis of Effect of Current on Tensile Shear Strength of RSW joint - when Conventional Electrodes were used	12
Appendix 15, Regression Analysis of Effect of Current on Tensile Shear Strength of RSW joint - when Annular Recess Electrodes were used	13
Appendix 16, Regression Analysis of Effect of Weld Time on Tensile Shear Strength of RSW joint, when Conventional Electrodes were used	14
Appendix 17, Regression Analysis of Effect of Weld Time on Tensile Shear Strength of RSW joint, when Annular Recess Electrodes were Used.....	15
Appendix 18, Regression Analysis of Effect of Electrode Force on Tensile Shear Strength of RSW joint, when Conventional Electrodes were Used	16
Appendix 19, Regression Analysis of Effect of Electrode Force on Tensile Shear Strength of RSW joint, when Annular Recess Electrodes were Used.....	17
Appendix 20, Regression Analysis of Analysis of effect of Current on Nugget Diameter – when Conventional Electrodes were used	18
Appendix 21, Regression Analysis of Effect of Current on Nugget Diameter – when Annular Recess Electrodes were used.....	19
Appendix 22, Regression Analysis of Effect of Weld Time on Nugget Diameter – when Conventional Electrodes were used.....	20


Appendix 23, Regression Analysis of Effect of Weld Time on Nugget Diameter – when Annular
Recess Electrodes are used 21


Appendix 24, Regression Analysis of Effect of Electrode Force on Nugget Diameter - when
Conventional Electrodes were used 22

Appendix 25, Regression Analysis of Effect of Electrode Force on Nugget Diameter - when Annular
recess Electrodes were used..... 23

APPENDICES

Appendix 1, Results for sample plate KP1





STEEL & TUBE INDUSTRIES LTD.

Measure Date Time	Method Name	Type	Type Corr Sample Name							
10/2/2018 5:35:45 PM	Fe-10-M	Unknown								
Sample ID	Heat Number	Operator Name	Date	Grade ID						
SAMPLE PLATE	KP1	MUHAMMED	02/10/2018							
Meas.	C	Si	Mn	P	S	Cr	Mo	Ni	Al	Co
	%	%	%	%	%	%	%	%	%	%
1	0.0345	0.0110	0.211	0.0117	0.0109	0.0457	<0.0010	<0.0015	0.0384	0.0028
2	0.0330	0.0113	0.209	0.0113	0.0097	0.0464	<0.0010	<0.0015	0.0386	0.0032
<Q>	0.0337	0.0112	0.210	0.0115	0.0103	0.0460	<0.0010	<0.0015	0.0385	0.0030
Meas.	Cu	Nb	Ti	V	W	Pb	Sn	As	Zr	Bi
	%	%	%	%	%	%	%	%	%	%
1	0.0483	0.0026	<0.0002	0.0054	<0.0050	0.0013	0.0036	0.0103	0.0018	<0.0010
2	0.0471	0.0024	<0.0002	0.0055	<0.0050	0.0013	0.0035	0.0088	0.0019	<0.0010
<Q>	0.0477	0.0025	<0.0002	0.0055	<0.0050	0.0013	0.0035	0.0096	0.0018	<0.0010
Meas.	Ca	Ce	Sb	Se	Te	Ta	B	Zn	La	N
	%	%	%	%	%	%	%	%	%	%
1	0.0001	0.0056	<0.0010	0.0025	0.0015	<0.0070	0.0012	>0.0270	<0.0003	0.0068
2	<0.0001	0.0060	<0.0010	0.0028	0.0017	<0.0070	0.0011	>0.0270	<0.0003	0.0079
<Q>	0.0001	0.0058	<0.0010	0.0027	0.0016	<0.0070	0.0011	>0.0270	<0.0003	0.0074
Meas.	Fe	CEQ								
	%	%								
1	99.5	0.0834								
2	99.5	0.0817								
<Q>	99.5	0.0825								

Appendix 2, Results for sample plate KP2



STEEL & TUBE INDUSTRIES LTD.

Measure Date Time	Method Name	Type	Type Corr Sample Name							
10/2/2018 5:39:50 PM	Fe-10-M	Unknown								
Sample ID	Heat Number	Operator Name	Date	Grade ID						
SAMPLE PLATE	KP2	MUHAMMED	02/10/2018							
Meas.	C	Si	Mn	P	S	Cr	Mo	Ni	Al	Co
	%	%	%	%	%	%	%	%	%	%
1	0.0362	0.0113	0.212	0.0112	0.0108	0.0459	<0.0010	<0.0015	0.0384	0.0018
2	0.0367	0.0119	0.213	0.0116	0.0100	0.0463	<0.0010	<0.0015	0.0388	0.0025
<0>	0.0364	0.0116	0.213	0.0114	0.0104	0.0461	<0.0010	<0.0015	0.0386	0.0021
Meas.	Cu	Nb	Ti	V	W	Pb	Sn	As	Zr	Bi
	%	%	%	%	%	%	%	%	%	%
1	0.0475	0.0020	<0.0002	0.0052	<0.0050	0.0014	0.0035	0.0057	0.0016	<0.0010
2	0.0475	0.0022	<0.0002	0.0051	<0.0050	0.0014	0.0035	0.0069	0.0017	<0.0010
<0>	0.0475	0.0021	<0.0002	0.0052	<0.0050	0.0014	0.0035	0.0063	0.0017	<0.0010
Meas.	Ca	Ce	Sb	Se	Te	Ta	B	Zn	La	N
	%	%	%	%	%	%	%	%	%	%
1	0.0004	0.0061	0.0019	0.0033	0.0015	<0.0070	0.0013	0.0095	<0.0003	0.0104
2	0.0004	0.0058	0.0011	0.0034	0.0018	<0.0070	0.0013	0.0062	<0.0003	0.0114
<0>	0.0004	0.0060	0.0015	0.0034	0.0016	<0.0070	0.0013	0.0078	<0.0003	0.0109
Meas.	Fe	CEQ								
	%	%								
1	99.5	0.0852								
2	99.5	0.0859								
<0>	99.5	0.0856								

Appendix 3, Results for sample plate KP3

STEEL & TUBE INDUSTRIES LTD.										
Measure Date Time		Method Name		Type		Type Corr Sample Name				
10/2/2018 5:42:04 PM		Fe-10-M		Unknown						
Sample ID		Heat Number		Operator Name		Date		Grade ID		
SAMPLE PLATE		KP3		MUHAMMED		02/10/2018				
Meas.	C	Si	Mn	P	S	Cr	Mo	Ni	Al	Co
	%	%	%	%	%	%	%	%	%	%
1	0.0336	0.0116	0.213	0.0116	0.0102	0.0460	<0.0010	<0.0015	0.0388	0.0019
2	0.0338	0.0117	0.211	0.0118	0.0110	0.0460	<0.0010	<0.0015	0.0387	0.0034
<>	0.0337	0.0117	0.212	0.0117	0.0106	0.0460	<0.0010	<0.0015	0.0387	0.0026
Meas.	Cu	Nb	Ti	V	W	Pb	Sn	As	Zr	Bi
	%	%	%	%	%	%	%	%	%	%
1	0.0476	0.0023	<0.0002	0.0051	<0.0050	0.0016	0.0035	0.0081	0.0016	<0.0010
2	0.0475	0.0024	<0.0002	0.0055	<0.0050	0.0013	0.0034	0.0088	0.0017	<0.0010
<>	0.0476	0.0023	<0.0002	0.0053	<0.0050	0.0014	0.0034	0.0084	0.0017	<0.0010
Meas.	Ca	Ce	Sb	Se	Te	Ta	B	Zn	La	N
	%	%	%	%	%	%	%	%	%	%
1	<0.0001	0.0057	0.0019	0.0042	0.0021	<0.0070	0.0013	>0.0270	<0.0003	0.0037
2	0.0001	0.0055	<0.0010	0.0033	0.0014	<0.0070	0.0014	>0.0270	<0.0003	0.0041
<>	0.0001	0.0056	0.0014	0.0038	0.0017	<0.0070	0.0013	>0.0270	<0.0003	0.0039
Meas.	Fe	CEQ								
	%	%								
1	99.5	0.0828								
2	99.5	0.0827								
<>	99.5	0.0828								

Appendix 4, Results for sample plate KP4

STEEL & TUBE INDUSTRIES LTD.										
Measure Date Time		Method Name		Type		Type Corr Sample Name				
10/2/2018 5:44:27 PM		Fe-10-M		Unknown						
Sample ID		Heat Number		Operator Name		Date		Grade ID		
SAMPLE PLATE		KP4		MUHAMMED		02/10/2018				
Meas.	C	Si	Mn	P	S	Cr	Mo	Ni	Al	Co
	%	%	%	%	%	%	%	%	%	%
1	0.0305	0.0112	0.215	0.0111	0.0110	0.0459	<0.0010	<0.0015	0.0389	0.0031
2	0.0303	0.0109	0.212	0.0117	0.0111	0.0461	<0.0010	<0.0015	0.0388	0.0035
<>	0.0304	0.0110	0.213	0.0114	0.0111	0.0460	<0.0010	<0.0015	0.0388	0.0033
Meas.	Cu	Nb	Ti	V	W	Pb	Sn	As	Zr	Bi
	%	%	%	%	%	%	%	%	%	%
1	0.0473	0.0016	<0.0002	0.0051	<0.0050	0.0018	0.0031	0.0069	0.0017	<0.0010
2	0.0472	0.0022	<0.0002	0.0053	<0.0050	0.0018	0.0034	0.0083	0.0018	<0.0010
<>	0.0472	0.0019	<0.0002	0.0052	<0.0050	0.0018	0.0032	0.0076	0.0018	<0.0010
Meas.	Ca	Ce	Sb	Se	Te	Ta	B	Zn	La	N
	%	%	%	%	%	%	%	%	%	%
1	0.0001	0.0060	<0.0010	0.0039	0.0017	<0.0070	0.0014	0.0039	<0.0003	0.0021
2	0.0001	0.0061	0.0013	0.0032	0.0017	<0.0070	0.0013	0.0018	<0.0003	0.0028
<>	0.0001	0.0060	0.0012	0.0035	0.0017	<0.0070	0.0013	0.0029	<0.0003	0.0024
Meas.	Fe	CEQ								
	%	%								
1	99.5	0.0799								
2	99.5	0.0794								
<>	99.5	0.0797								

Appendix 5, Results for sample plate KP5

STEEL & TUBE INDUSTRIES LTD.										
Measure Date Time	Method Name	Type	Type Corr Sample Name							
10/2/2018 5:46:49 PM	Fe-10-M	Unknown								
Sample ID	Heat Number	Operator Name	Date	Grade ID						
SAMPLE PLATE	KP5	MUHAMMED	02/10/2018							
Meas.	C	Si	Mn	P	S	Cr	Mo	Ni	Al	Co
	%	%	%	%	%	%	%	%	%	%
1	0.0361	0.0108	0.210	0.0114	0.0103	0.0461	<0.0010	<0.0015	0.0382	0.0029
2	0.0365	0.0109	0.213	0.0115	0.0106	0.0464	<0.0010	<0.0015	0.0392	0.0024
<>	0.0363	0.0109	0.212	0.0114	0.0105	0.0462	<0.0010	<0.0015	0.0387	0.0026
Meas.	Cu	Nb	Ti	V	W	Pb	Sn	As	Zr	Bi
	%	%	%	%	%	%	%	%	%	%
1	0.0469	0.0022	<0.0002	0.0051	<0.0050	0.0015	0.0033	0.0067	0.0015	<0.0010
2	0.0471	0.0024	<0.0002	0.0051	<0.0050	0.0015	0.0033	0.0085	0.0015	<0.0010
<>	0.0470	0.0023	<0.0002	0.0051	<0.0050	0.0015	0.0033	0.0076	0.0015	<0.0010
Meas.	Ca	Ce	Sb	Se	Te	Ta	B	Zn	La	N
	%	%	%	%	%	%	%	%	%	%
1	0.0001	0.0064	<0.0010	0.0034	0.0020	<0.0070	0.0013	0.0052	<0.0003	0.0127
2	0.0002	0.0056	<0.0010	0.0034	0.0016	<0.0070	0.0012	>0.0270	<0.0003	0.0104
<>	0.0001	0.0060	<0.0010	0.0034	0.0018	<0.0070	0.0013	0.0161	<0.0003	0.0115
Meas.	Fe	CEQ								
	%	%								
1	99.5	0.0848								
2	99.5	0.0857								
<>	99.5	0.0853								

Appendix 6, Results for sample rod KC1 (1)

STEEL & TUBE INDUSTRIES LTD.										
Measure Date Time	Method Name	Type	Type Corr Sample Name							
10/2/2018 4:30:16 PM	Fe-01-M	Unknown								
Sample ID	Heat Number	Operator Name	Date	Grade ID						
SAMPLE ROD	KC1 (1)	MUHAMMED	02/10/2018							
Meas.	C	Si	Mn	P	S	Cr	Mo	Ni	Al	Co
	%	%	%	%	%	%	%	%	%	%
1	A 0.0731	A 0.0184	A 0.0221	A 0.0178	A 0.0144	A 0.0081	A 0.115	A 0.0814	A 0.0032	A 0.117
<>	A 0.0731	A 0.0184	A 0.0221	A 0.0178	A 0.0144	A 0.0081	A 0.115	A 0.0814	A 0.0032	A 0.117
Meas.	Cu	Nb	Ti	V	W	Pb	Sn	Mg	As	Zr
	%	%	%	%	%	%	%	%	%	%
1	A >8.00	A 0.0609	A 0.0434	A 0.0074	A 0.894	A 0.0353	0.0135	A 0.0102	A 0.0172	A 0.0056
<>	A >8.00	A 0.0609	A 0.0434	A 0.0074	A 0.894	A 0.0353	0.0135	A 0.0102	A 0.0172	A 0.0056
Meas.	Bi	Ca	Ce	Sb	Se	Te	Ta	B	Zn	La
	%	%	%	%	%	%	%	%	%	%
1	A 0.0064	A 0.0011	A 0.0192	A 0.239	A 0.0012	A >0.0800	A >0.760	0.0030	A >0.0450	A 0.0076
<>	A 0.0064	A 0.0011	A 0.0192	A 0.239	A 0.0012	A >0.0800	A >0.760	0.0030	A >0.0450	A 0.0076

Appendix 7, Results for sample rod KC1 (2)

SPECTRO										
AMETEK [®] MATERIALS ANALYSIS DIVISION										
STEEL & TUBE INDUSTRIES LTD.										
Measure Date Time	Method Name		Type	Type Corr Sample Name						
10/4/2018 8:21:55 PM	Fe-01-M		Unknown							
Sample ID	Heat Number	Operator Name		Date	Grade ID					
SAMPLE ROD	KC1 (2)	MUHAMMED		4/10/2018						
Meas.	C	Si	Mn	P	S	Cr	Mo	Ni	Al	Co
1	%	%	%	%	%	%	%	%	%	%
	A 0.0570	A 0.0122	A 0.0171	A 0.0144	A 0.0118	A 0.0057	A 0.0906	A 0.0595	A 0.0047	A 0.0856
	A 0.0570	A 0.0122	A 0.0171	A 0.0144	A 0.0118	A 0.0057	A 0.0906	A 0.0595	A 0.0047	A 0.0856
Meas.	Cu	Nb	Ti	V	W	Pb	Sn	Mg	As	Zr
1	%	%	%	%	%	%	%	%	%	%
	A >8.00	A 0.0467	A 0.0327	A 0.0053	A 0.0669	A 0.0267	0.0104	A 0.0076	A 0.0128	A 0.0041
	A >8.00	A 0.0467	A 0.0327	A 0.0053	A 0.0669	A 0.0267	0.0104	A 0.0076	A 0.0128	A 0.0041
Meas.	Bi	Ca	Ce	Sb	Se	Te	Ta	B	Zn	La
1	%	%	%	%	%	%	%	%	%	%
	A 0.0048	A 0.0013	A 0.0146	A 0.187	A <0.0010	A >0.0800	A >0.760	0.0025	A 0.0438	A 0.0060
	A 0.0048	A 0.0013	A 0.0146	A 0.187	A <0.0010	A >0.0800	A >0.760	0.0025	A 0.0438	A 0.0060

Appendix 8, Results for sample rod KC2 (1)

SPECTRO										
AMETEK [®] MATERIALS ANALYSIS DIVISION										
STEEL & TUBE INDUSTRIES LTD.										
Measure Date Time	Method Name		Type	Type Corr Sample Name						
10/4/2018 8:30:04 PM	Fe-01-M		Unknown							
Sample ID	Heat Number	Operator Name		Date	Grade ID					
SAMPLE ROD	KC2 (1)	MUHAMMED		4/10/2018						
Meas.	C	Si	Mn	P	S	Cr	Mo	Ni	Al	Co
1	%	%	%	%	%	%	%	%	%	%
	A 0.0906	A 0.0142	A 0.0168	A 0.0146	A 0.0105	A 0.0060	A 0.0969	A 0.0680	A 0.0038	A 0.0920
	A 0.0906	A 0.0142	A 0.0168	A 0.0146	A 0.0105	A 0.0060	A 0.0969	A 0.0680	A 0.0038	A 0.0920
Meas.	Cu	Nb	Ti	V	W	Pb	Sn	Mg	As	Zr
1	%	%	%	%	%	%	%	%	%	%
	A >8.00	A 0.0488	A 0.0384	A 0.0058	A 0.0693	A 0.0276	0.0103	A 0.0085	A 0.0131	A 0.0044
	A >8.00	A 0.0488	A 0.0384	A 0.0058	A 0.0693	A 0.0276	0.0103	A 0.0085	A 0.0131	A 0.0044
Meas.	Bi	Ca	Ce	Sb	Se	Te	Ta	B	Zn	La
1	%	%	%	%	%	%	%	%	%	%
	A 0.0047	A 0.0027	A 0.0152	A 0.190	A 0.0011	A >0.0800	A >0.760	0.0024	A >0.0450	A 0.0059
	A 0.0047	A 0.0027	A 0.0152	A 0.190	A 0.0011	A >0.0800	A >0.760	0.0024	A >0.0450	A 0.0059



Appendix 9, Results for sample rod KC2 (2)

SPECTRO										
AMETEK [®] MATERIALS ANALYSIS DIVISION										
STEEL & TUBE INDUSTRIES LTD.										
Measure Date Time	Method Name		Type	Type Corr Sample Name						
10/4/2018 8:32:00 PM	Fe-01-M		Unknown							
Sample ID	Heat Number	Operator Name		Date	Grade ID					
SAMPLE ROD	KC2 (2)	MUHAMMED		4/10/2018						
Meas.	C	Si	Mn	P	S	Cr	Mo	Ni	Al	Co
1	%	%	%	%	%	%	%	%	%	%
1	A 0.112	A 0.0127	A 0.0171	A 0.0143	A 0.0101	A 0.0057	A 0.0915	A 0.0587	A 0.0028	A 0.0869
1	A 0.112	A 0.0127	A 0.0171	A 0.0143	A 0.0101	A 0.0057	A 0.0915	A 0.0587	A 0.0028	A 0.0869
Meas.	Cu	Nb	Ti	V	W	Pb	Sn	Mg	As	Zr
1	%	%	%	%	%	%	%	%	%	%
1	A >8.00	A 0.0450	A 0.0335	A 0.0056	A 0.0660	A 0.0269	0.0098	A 0.0077	A 0.0124	A 0.0043
1	A >8.00	A 0.0450	A 0.0335	A 0.0056	A 0.0660	A 0.0269	0.0098	A 0.0077	A 0.0124	A 0.0043
Meas.	Bi	Ca	Ce	Sb	Se	Te	Ta	B	Zn	La
1	%	%	%	%	%	%	%	%	%	%
1	A 0.0045	A 0.0033	A 0.0146	A 0.190	A 0.0011	A >0.0800	A >0.760	0.0024	A 0.0435	A 0.0057
1	A 0.0045	A 0.0033	A 0.0146	A 0.190	A 0.0011	A >0.0800	A >0.760	0.0024	A 0.0435	A 0.0057

Appendix 10, Results for sample rod KC3 (1)

SPECTRO										
AMETEK [®] MATERIALS ANALYSIS DIVISION										
STEEL & TUBE INDUSTRIES LTD.										
Measure Date Time	Method Name		Type	Type Corr Sample Name						
10/4/2018 8:25:25 PM	Fe-01-M		Unknown							
Sample ID	Heat Number	Operator Name		Date	Grade ID					
SAMPLE ROD	KC3 (1)	MUHAMMED		4/10/2018						
Meas.	C	Si	Mn	P	S	Cr	Mo	Ni	Al	Co
1	%	%	%	%	%	%	%	%	%	%
1	A 0.0765	A 0.0119	A 0.0149	A 0.0209	A 0.0110	A 0.0054	A 0.0903	A 0.0589	A 0.0027	A 0.0747
1	A 0.0765	A 0.0119	A 0.0149	A 0.0209	A 0.0110	A 0.0054	A 0.0903	A 0.0589	A 0.0027	A 0.0747
Meas.	Cu	Nb	Ti	V	W	Pb	Sn	Mg	As	Zr
1	%	%	%	%	%	%	%	%	%	%
1	A >8.00	A 0.0415	A 0.0373	A 0.0049	A 0.0626	A 0.0265	0.0101	A 0.0073	A 0.0113	A 0.0036
1	A >8.00	A 0.0415	A 0.0373	A 0.0049	A 0.0626	A 0.0265	0.0101	A 0.0073	A 0.0113	A 0.0036
Meas.	Bi	Ca	Ce	Sb	Se	Te	Ta	B	Zn	La
1	%	%	%	%	%	%	%	%	%	%
1	A 0.0042	A 0.0013	A 0.0134	A 0.155	A <0.0010	A >0.0800	A >0.760	0.0022	A >0.0450	A 0.0044
1	A 0.0042	A 0.0013	A 0.0134	A 0.155	A <0.0010	A >0.0800	A >0.760	0.0022	A >0.0450	A 0.0044

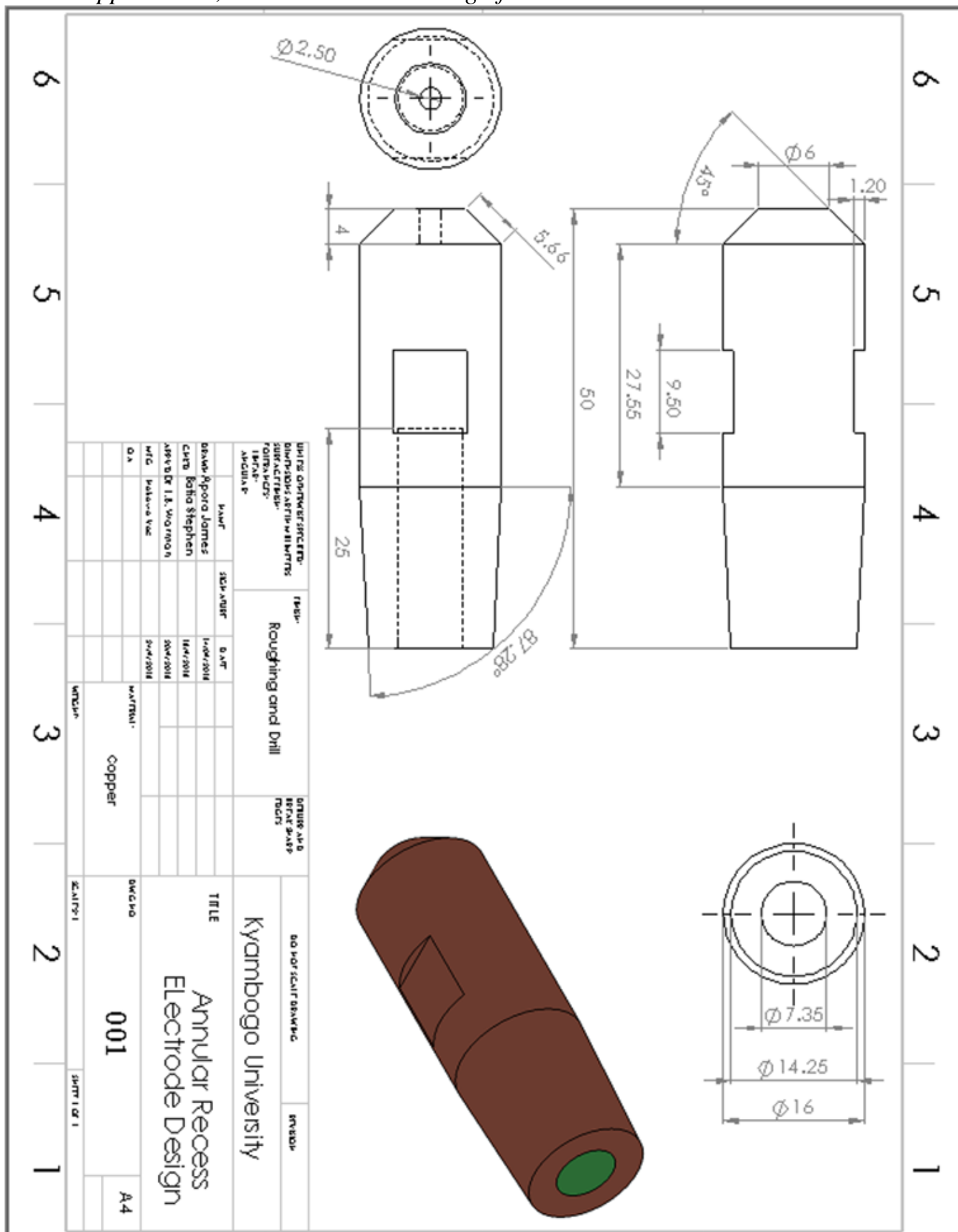
Appendix 11, Results for sample rod KC3 (2)

STEEL & TUBE INDUSTRIES LTD.

Measure Date Time	Method Name	Type	Type Corr Sample Name							
10/4/2018 8:27:44 PM	Fe-01-M	Unknown								
Sample ID	Heat Number	Operator Name	Date							
SAMPLE ROD	KC3 (2)	MUHAMMED	4/10/2018							
Grade ID										
Meas.	C	Si	Mn	P	S	Cr	Mo	Ni	Al	Co
	%	%	%	%	%	%	%	%	%	%
1	A 0.0458	A 0.0122	A 0.0141	A 0.0166	A 0.0096	A 0.0052	A 0.0890	A 0.0520	A 0.0021	A 0.0742
<>	A 0.0458	A 0.0122	A 0.0141	A 0.0166	A 0.0096	A 0.0052	A 0.0890	A 0.0520	A 0.0021	A 0.0742
Meas.	Cu	Nb	Ti	V	W	Pb	Sn	Mg	As	Zr
	%	%	%	%	%	%	%	%	%	%
1	A >8.00	A 0.0408	A 0.0333	A 0.0047	A 0.0617	A 0.0261	0.0097	A 0.0069	A 0.0110	A 0.0033
<>	A >8.00	A 0.0408	A 0.0333	A 0.0047	A 0.0617	A 0.0261	0.0097	A 0.0069	A 0.0110	A 0.0033
Meas.	Bi	Ca	Ce	Sb	Se	Te	Ta	B	Zn	La
	%	%	%	%	%	%	%	%	%	%
1	A 0.0040	A 0.0007	A 0.0131	A 0.151	A <0.0010	A >0.0800	A >0.760	0.0015	A >0.0450	A 0.0043
<>	A 0.0040	A 0.0007	A 0.0131	A 0.151	A <0.0010	A >0.0800	A >0.760	0.0015	A >0.0450	A 0.0043

Appendix 12, Detailed Part Drawing of the Annular Recess Electrode



*Appendix 13, Generated Manufacturing Cost Reports in US dollars, of
Annular Recess Electrode.*

Kyambogo University,

SOLIDWORKS Costing Report

Department of Mechanical & Production
Engineering,

Supervisors

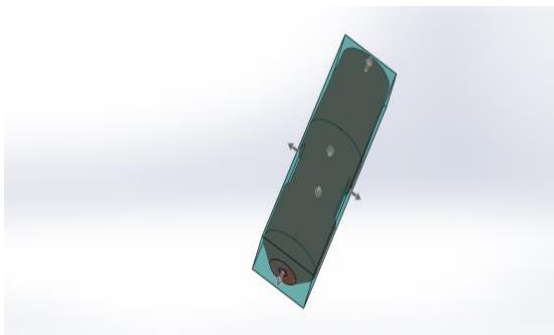
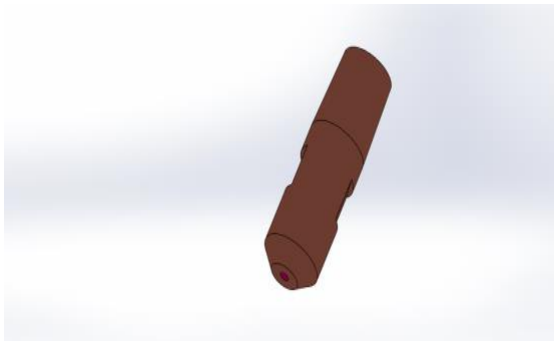
Dr. Catherine A. Wandera

Student: Apora James

Reg.No: 16/U/13977/GMEM/PE

Course: MSc. AMSEng, KYU

Dr. Titus B. Watmon



Model Name: ELECTRODE DESIGN

Date and time of report: 9/22/2018 1:53:16 PM

Manufacturing Method: Machining

Material: Copper

Stock weight: 0.25 lb

Stock Type: Block

Block Size: 1.97x0.63x0.63 in

Material cost/weight: 17.50 USD/lb

Shop Rate: N/A

Quantity to Produce

Total number of parts: 100

Lot size: 100

Estimated cost per part: 13.05 USD

Costing template used: Machining template default (English standard).sldctm

Costing mode used: Manufacturing Process Recognition

Comparison:

100%

Current 13.05 USD

Cost Breakdown

Material:	4.38 USD	34%
Manufacturing:	8.67 USD	66%
Markup:	0.00 USD	0%
Mold:	0.00 USD	0%

Estimated time per part: 00:17:20

Setups: 00:16:48

Operations: 00:00:32

Cost Report								
Model Name:	ELECTROD E DESIGN	Material:	Copper	Material cost:	4.38 USD	Total cost /part:	13.05 USD	
				Manufacturing cost:	8.67 USD	Total time /part:	00:17:20	
				Markup:	0.00 USD			
Manufacturing Cost Breakdown								
Operation Setups			Time (hh:mm:ss)		Cost (USD)			
Setup Operation 1			00:00:36		0.30			
Setup Operation 2			00:00:36		0.30			
Setup Operation 3			00:00:36		0.30			
Total			00:01:47		0.90			
Load and Unload Setups			Time (hh:mm:ss)		Cost (USD)			
Setup Operation 1			00:05:00		2.50			
Setup Operation 2			00:05:00		2.50			
Setup Operation 3			00:05:00		2.50			
Total			00:15:00		7.50			
Operation	Surface Finish	Volume Removed (in^3)	Time (hh:mm:ss)	Cost (USD)	Tooling	Cost-per-Volume (USD/in^3)		
Volume 1	Roughing	0.22	00:00:10	0.09	Flat End Mill	N/A		
Total		0.22	00:00:10	0.09				
Hole Operation	Surface Finish	Volume Removed (in^3)	Time (hh:mm:ss)	Cost (USD)	Tooling	Cost-per-Volume (USD/in^3)		
Hole 1	Drill	0.06	00:00:20	0.17	HSS Drill	N/A		
Hole 2	Drill	0.00	00:00:01	0.02	HSS Drill	N/A		
Total		0.07	00:00:21	0.18				

No Cost Features

Chamfer 1

Setup Operations

1. Setup Operation 1
 - a. Hole 1
2. Setup Operation 2
 - a. Hole 2
3. Setup Operation 3
 - a. Volume 1

Appendix 14, Regression Analysis of Effect of Current on Tensile Shear Strength of RSW joint - when Conventional Electrodes were used

□

SUMMARY OUTPUT

<i>Regression Statistics</i>	
Multiple R	0.052803
R Square	0.002788
Adjusted R Square	-0.32962
Standard Error	1.035857
Observations	5

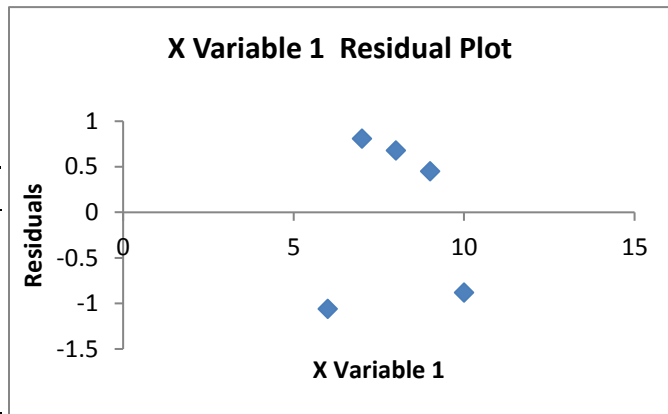
ANOVA

	<i>df</i>	<i>SS</i>	<i>MS</i>	<i>F</i>	<i>Significance F</i>
Regression (SSR)	1	0.009	0.009	0.008388	0.932801
Residual (SSE)	3	3.219	1.073		
Total (SST)	4	3.228			

	<i>Coefficient s</i>	<i>Standard Error</i>	<i>t Stat</i>	<i>P-value</i>	<i>Lower 95%</i>	<i>Upper 95%</i>
Intercept	3.88	2.661165	1.458008	0.240909	-4.58902	12.34902
X Variable 1	0.03	0.327567	0.091584	0.932801	-1.01246	1.072464

RESIDUAL OUTPUT

<i>Observation</i>	<i>Predicted Y</i>	<i>Residuals</i>
1	4.06	-1.06
2	4.09	0.81
3	4.12	0.68
4	4.15	0.45
5	4.18	-0.88



Appendix 15, Regression Analysis of Effect of Current on Tensile Shear Strength of RSW joint - when Annular Recess Electrodes were used

□

SUMMARY OUTPUT

<i>Regression Statistics</i>	
Multiple R	0.970241
R Square	0.941368
Adjusted R Square	0.921824
Standard Error	0.154919
Observations	5

ANOVA

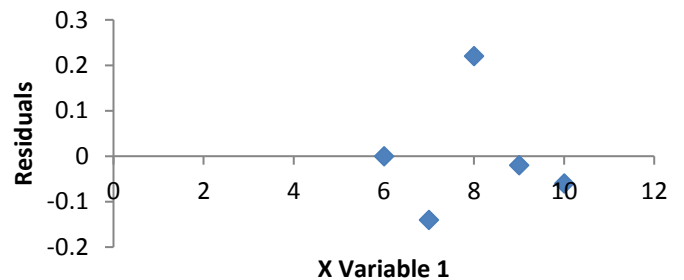
	<i>df</i>	<i>SS</i>	<i>MS</i>	<i>F</i>	<i>Significance F</i>
Regression	1	1.156	1.156	48.16667	0.006135
Residual	3	0.072	0.024		
Total	4	1.228			

	<i>Coefficients</i>	<i>Standard Error</i>	<i>t Stat</i>	<i>P-value</i>	<i>Lower 95%</i>	<i>Upper 95%</i>
Intercept	1.06	0.397995	2.66335	0.076121	-0.2066	2.326598
X Variable 1	0.34	0.04899	6.940221	0.006135	0.184093	0.495907

RESIDUAL OUTPUT

<i>Observation</i>	<i>Predicted Y</i>	<i>Residuals</i>
1	3.1	0
2	3.44	-0.14
3	3.78	0.22
4	4.12	-0.02
5	4.46	-0.06

X Variable 1 Residual Plot



Appendix 16, Regression Analysis of Effect of Weld Time on Tensile Shear Strength of RSW joint, when Conventional Electrodes were used

□

SUMMARY OUTPUT

<i>Regression Statistics</i>	
Multiple R	0.855048
R Square	0.731107
Adjusted R Square	0.641477
Standard Error	0.741845
Observations	5

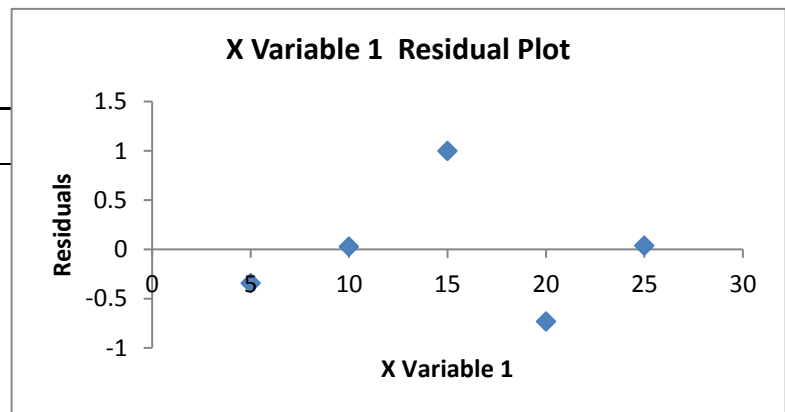
ANOVA

	<i>df</i>	<i>SS</i>	<i>MS</i>	<i>F</i>	<i>Significance F</i>
Regression (SSR)	1	4.489	4.489	8.156875	0.064788
Residual (SSE)	3	1.651	0.550333		
Total (SST)	4	6.14			

	<i>Coefficients</i>	<i>Standard Error</i>	<i>t Stat</i>	<i>P-value</i>	<i>Lower 95%</i>	<i>Upper 95%</i>
Intercept	6.51	0.778053	8.367038	0.00358	4.033888	8.986112
X Variable 1	-0.134	0.046918	-2.85602	0.064788	-0.28332	0.015315

RESIDUAL OUTPUT

<i>Observation</i>	<i>Predicted Y</i>	<i>Residuals</i>
1	5.84	-0.34
2	5.17	0.03
3	4.5	1
4	3.83	-0.73
5	3.16	0.04



Appendix 17, Regression Analysis of Effect of Weld Time on Tensile Shear Strength of RSW joint, when Annular Recess Electrodes were Used

□

**SUMMARY
OUTPUT**

<i>Regression Statistics</i>	
Multiple R	0.739221
R Square	0.546448
Adjusted R Square	0.395264
Standard Error	0.332666
Observations	5

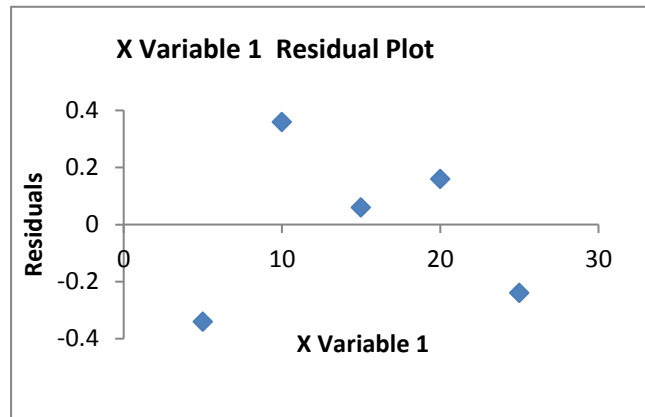
ANOVA

	<i>df</i>	<i>SS</i>	<i>MS</i>	<i>F</i>	<i>Significance F</i>
Regression (SSR)	1	0.4	0.4	3.614458	0.153454
Residual (SSE)	3	0.332	0.110667		
Total (SST)	4	0.732			

	<i>Coefficients</i>	<i>Standard Error</i>	<i>t Stat</i>	<i>P-value</i>	<i>Lower 95%</i>	<i>Upper 95%</i>
Intercept	5.34	0.348903	15.30511	0.000606	4.229635	6.450365
X Variable 1	0.04	0.02104	1.901173	0.153454	-0.02696	0.106958

RESIDUAL OUTPUT

<i>Observation</i>	<i>Predicted Y</i>	<i>Residuals</i>
1	5.54	-0.34
2	5.74	0.36
3	5.94	0.06
4	6.14	0.16
5	6.34	-0.24



Appendix 18, Regression Analysis of Effect of Electrode Force on Tensile Shear Strength of RSW joint, when Conventional Electrodes were Used

□

**SUMMARY
OUTPUT**

<i>Regression Statistics</i>	
Multiple R	0.604564
R Square	0.365497
Adjusted R Square	0.153996
Standard Error	1.202775
Observations	5

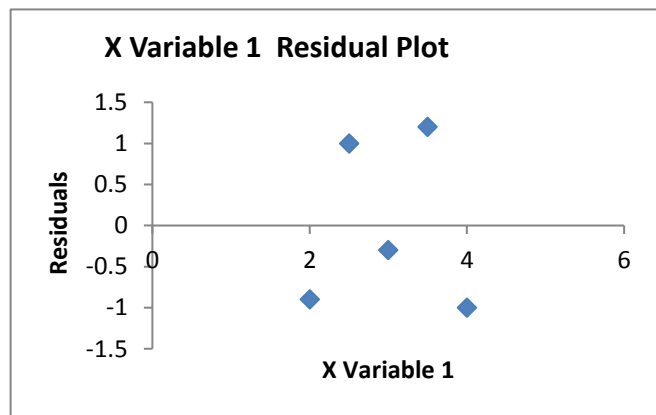
ANOVA

	<i>df</i>	<i>SS</i>	<i>MS</i>	<i>F</i>	<i>Significance F</i>
Regression (SSR)	1	2.5	2.5	1.728111	0.280119
Residual (SSE)	3	4.34	1.446667		
Total (SST)	4	6.84			

	<i>Coefficients</i>	<i>Standard Error</i>	<i>t Stat</i>	<i>P-value</i>	<i>Lower 95%</i>	<i>Upper 95%</i>
Intercept	7.2	2.344639	3.070835	0.054527	-0.26169	14.66169
X Variable 1	-1	0.760701	-1.31458	0.280119	-3.42089	1.420891

RESIDUAL OUTPUT

<i>Observation</i>	<i>Predicted Y</i>	<i>Residuals</i>
1	5.2	-0.9
2	4.7	1
3	4.2	-0.3
4	3.7	1.2
5	3.2	-1



Appendix 19, Regression Analysis of Effect of Electrode Force on Tensile Shear Strength of RSW joint, when Annular Recess Electrodes were Used

□

SUMMARY OUTPUT

<i>Regression Statistics</i>	
Multiple R	0.810217
R Square	0.656452
Adjusted R Square	0.541936
Standard Error	2.060421
Observations	5

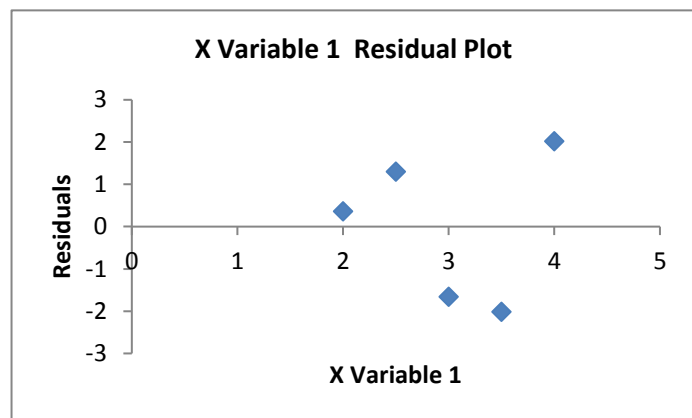
ANOVA

	<i>df</i>	<i>SS</i>	<i>MS</i>	<i>F</i>	<i>Significance F</i>
Regression (SSR)	1	24.336	24.336	5.732412	0.096372
Residual (SSE)	3	12.736	4.245333		
Total (SST)	4	37.072			

	<i>Coefficients</i>	<i>Standard Error</i>	<i>t Stat</i>	<i>P-value</i>	<i>Lower 95%</i>	<i>Upper 95%</i>
Intercept	-3.1	4.016499	-0.77182	0.496446	-15.8823	9.682293
X Variable 1	3.12	1.303124	2.394246	0.096372	-1.02712	7.267124

RESIDUAL OUTPUT

<i>Observation</i>	<i>Predicted Y</i>	<i>Residuals</i>
1	3.14	0.36
2	4.7	1.3
3	6.26	-1.66
4	7.82	-2.02
5	9.38	2.02



Appendix 20, Regression Analysis of Analysis of effect of Current on Nugget Diameter – when Conventional Electrodes were used

□

SUMMARY OUTPUT

<i>Regression Statistics</i>	
Multiple R	0.47767
R Square	0.228169
Adjusted R Square	-0.02911
Standard Error	0.604428
Observations	5

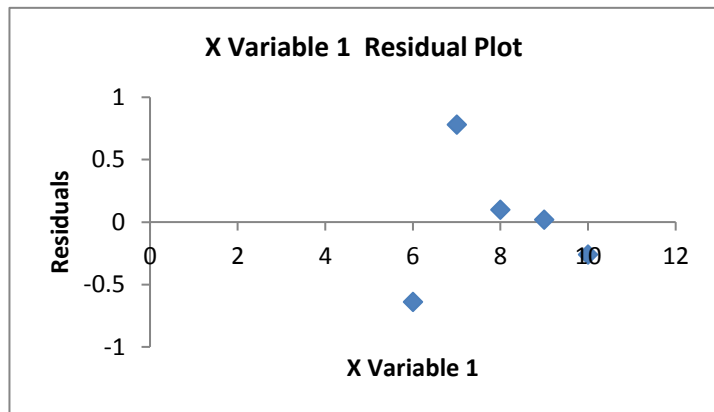
ANOVA

	<i>df</i>	<i>SS</i>	<i>MS</i>	<i>F</i>	<i>Significance F</i>
Regression (SSR)	1	0.324	0.324	0.886861	0.415804
Residual (SSE)	3	1.096	0.365333		
Total (SST)	4	1.42			

	<i>Coefficients</i>	<i>Standard Error</i>	<i>t Stat</i>	<i>P-value</i>	<i>Lower 95%</i>	<i>Upper 95%</i>
Intercept	5.46	1.552804	3.51622	0.039023	0.518285	10.40172
X Variable 1	0.18	0.191137	0.941733	0.415804	-0.42828	0.788283

RESIDUAL OUTPUT

<i>Observation</i>	<i>Predicted Y</i>	<i>Residuals</i>
1	6.54	-0.64
2	6.72	0.78
3	6.9	0.1
4	7.08	0.02
5	7.26	-0.26



*Appendix 21, Regression Analysis of Effect of Current on Nugget Diameter –
when Annular Recess Electrodes were used*

□

SUMMARY OUTPUT

<i>Regression Statistics</i>	
Multiple R	0.581675
R Square	0.338346
Adjusted R Square	0.117794
Standard Error	0.765942
Observations	5

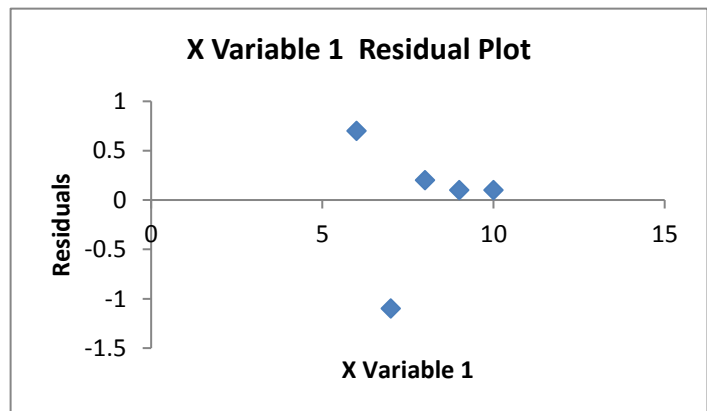
ANOVA

	<i>df</i>	<i>SS</i>	<i>MS</i>	<i>F</i>	<i>Significance F</i>
Regression (SSR)	1	0.9	0.9	1.534091	0.30358
Residual (SSE)	3	1.76	0.586667		
Total (SST)	4	2.66			

	<i>Coefficients</i>	<i>Standard Error</i>	<i>t Stat</i>	<i>P-value</i>	<i>Lower 95%</i>	<i>Upper 95%</i>
Intercept	4.8	1.96774	2.439347	0.092554	-1.46223	11.06223
X Variable 1	0.3	0.242212	1.238584	0.30358	-0.47083	1.070827

RESIDUAL OUTPUT

<i>Observation</i>	<i>Predicted Y</i>	<i>Residuals</i>
1	6.6	0.7
2	6.9	-1.1
3	7.2	0.2
4	7.5	0.1
5	7.8	0.1



Appendix 22, Regression Analysis of Effect of Weld Time on Nugget Diameter – when Conventional Electrodes were used

□

**SUMMARY
OUTPUT**

<i>Regression Statistics</i>	
Multiple R	0.483368
R Square	0.233645
Adjusted R Square	-0.02181
Standard Error	0.330656
Observations	5

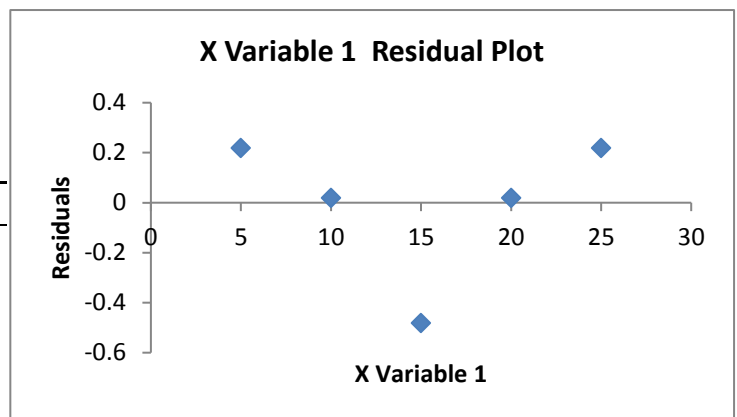
ANOVA

	<i>df</i>	<i>SS</i>	<i>MS</i>	<i>F</i>	<i>Significance F</i>
Regression (SSR)	1	0.1	0.1	0.914634	0.409442
Residual (SSE)	3	0.328	0.109333		
Total (SST)	4	0.428			

	<i>Coefficients</i>	<i>Standard Error</i>	<i>t Stat</i>	<i>P-value</i>	<i>Lower 95%</i>	<i>Upper 95%</i>
Intercept	6.98	0.346795	20.12717	0.000268	5.876344	8.083656
X Variable 1	0.02	0.020913	0.956365	0.409442	-0.04655	0.086553

RESIDUAL OUTPUT

<i>Observation</i>	<i>Predicted Y</i>	<i>Residuals</i>
1	7.08	0.22
2	7.18	0.02
3	7.28	-0.48
4	7.38	0.02
5	7.48	0.22



Appendix 23, Regression Analysis of Effect of Weld Time on Nugget Diameter – when Annular Recess Electrodes are used

□

**SUMMARY
OUTPUT**

<i>Regression Statistics</i>	
Multiple R	0.693375
R Square	0.480769
Adjusted R Square	0.307692
Standard Error	0.094868
Observations	5

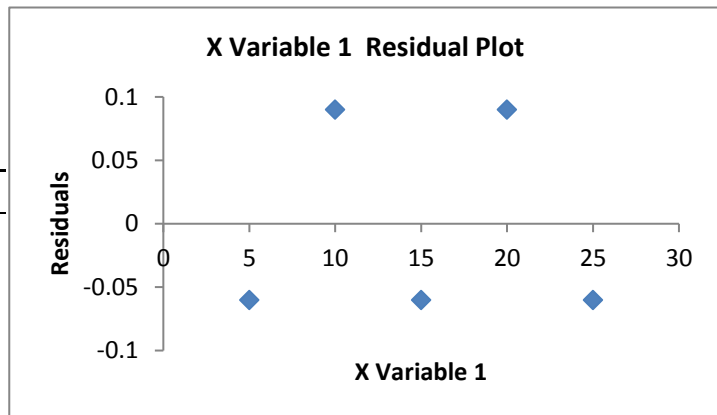
ANOVA

	<i>df</i>	<i>SS</i>	<i>MS</i>	<i>F</i>	<i>Significance F</i>
Regression (SSR)	1	0.025	0.025	2.777778	0.194171
Residual (SSE)	3	0.027	0.009		
Total (SST)	4	0.052			

	<i>Coefficients</i>	<i>Standard Error</i>	<i>t Stat</i>	<i>P-value</i>	<i>Lower 95%</i>	<i>Upper 95%</i>
Intercept	7.91	0.099499	79.49849	4.39E-06	7.593351	8.226649
X Variable 1	0.01	0.006	1.666667	0.194171	-0.00909	0.029095

RESIDUAL OUTPUT

<i>Observation</i>	<i>Predicted Y</i>	<i>Residuals</i>
1	7.96	-0.06
2	8.01	0.09
3	8.06	-0.06
4	8.11	0.09
5	8.16	-0.06



Appendix 24, Regression Analysis of Effect of Electrode Force on Nugget Diameter - when Conventional Electrodes were used

□

**SUMMARY
OUTPUT**

<i>Regression Statistics</i>	
Multiple R	0.70791
R Square	0.501136
Adjusted R Square	0.334848
Standard Error	0.382535
Observations	5

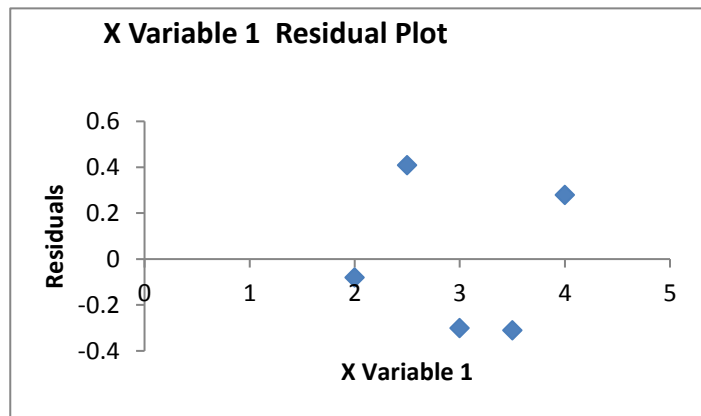
ANOVA

	<i>df</i>	<i>SS</i>	<i>MS</i>	<i>F</i>	<i>Significance F</i>
Regression (SSR)	1	0.441	0.441	3.013667	0.180968
Residual (SSE)	3	0.439	0.146333		
Total (SST)	4	0.88			

	<i>Coefficients</i>	<i>Standard Error</i>	<i>t Stat</i>	<i>P-value</i>	<i>Lower 95%</i>	<i>Upper 95%</i>
Intercept	6.04	0.745699	8.099785	0.003933	3.666854	8.413146
X Variable 1	0.42	0.241937	1.735992	0.180968	-0.34995	1.18995

RESIDUAL OUTPUT

<i>Observation</i>	<i>Predicted Y</i>	<i>Residuals</i>
1	6.88	-0.08
2	7.09	0.41
3	7.3	-0.3
4	7.51	-0.31
5	7.72	0.28



Appendix 25, Regression Analysis of Effect of Electrode Force on Nugget Diameter - when Annular recess Electrodes were used

□

**SUMMARY
OUTPUT**

<i>Regression Statistics</i>	
Multiple R	0.620174
R Square	0.384615
Adjusted R Square	0.179487
Standard Error	0.23094
Observations	5

ANOVA

	<i>df</i>	<i>SS</i>	<i>MS</i>	<i>F</i>	<i>Significance F</i>
Regression (SSR)	1	0.1	0.1	1.875	0.264406
Residual (SSE)	3	0.16	0.053333		
Total (SST)	4	0.26			

	<i>Coefficients</i>	<i>Standard Error</i>	<i>t Stat</i>	<i>P-value</i>	<i>Lower 95%</i>	<i>Upper 95%</i>
Intercept	8.7	0.450185	19.32538	0.000303	7.26731	10.13269
X Variable 1	-0.2	0.146059	-1.36931	0.264406	-0.66483	0.264826

RESIDUAL OUTPUT

<i>Observation</i>	<i>Predicted Y</i>	<i>Residuals</i>
1	8.3	0.1
2	8.2	-0.1
3	8.1	0.1
4	8	-0.3
5	7.9	0.2

